NASA TECHNICAL NOTE

NASA TN D-3460

NASA TN D-3460

EFFECT OF BODY NOSE BLUNTING, CONTROL PLANFORM AREA, AND LEADING-EDGE BLUNTNESS ON AERODYNAMIC CONTROL OF A 5° SEMIVERTEX CONE AT MACH NUMBER 6.9

by Jim A. Penland

Langley Research Center
Langley Station, Hampton, Va.

NATIONAL AERONAUTICS AND SPACE ADMINISTRATION • WASHINGTON, D. C. • JUNE 1966

EFFECT OF BODY NOSE BLUNTING, CONTROL PLANFORM AREA, AND LEADING-EDGE BLUNTNESS ON AERODYNAMIC CONTROL OF A 5° SEMIVERTEX CONE AT MACH NUMBER 6.9

By Jim A. Penland

Langley Research Center
Langley Station, Hampton, Va.

NATIONAL AERONAUTICS AND SPACE ADMINISTRATION

For sale by the Clearinghouse for Federal Scientific and Technical Information
Springfield, Virginia 22151 – Price $3.00

EFFECT OF BODY NOSE BLUNTING, CONTROL PLANFORM AREA, AND LEADING-EDGE BLUNTNESS ON AERODYNAMIC CONTROL OF A 5° SEMIVERTEX CONE AT MACH NUMBER 6.9

By Jim A. Penland
Langley Research Center

SUMMARY

An experimental investigation has been carried out to determine the longitudinal, lateral, and directional control characteristics of a conical configuration with a 5° semivertex angle and cruciform delta planform control surfaces. The investigation was conducted at a Mach number of 6.9 and a Reynolds number of 2.8×10^6 based on model length. The configuration variables included nose bluntness, control leading-edge bluntness, and control planform area.

For all configurations the longitudinal control effectiveness (ability of the controls to produce pitch) either remained constant or improved with angle of attack. The blunting of control leading edges resulted in a decrease in their effectiveness. An increase in body nose bluntness resulted in a decrease in control effectiveness at low angles of attack, but at angles of attack above 10° little variation with nose bluntness was noted. An increase in control planform area, leading-edge bluntness, or body nose bluntness resulted in an increase in trim drag and a decrease in trim-lift range and trim lift-drag ratio. The deflection of vertical surfaces for yaw control resulted in not only the desired yaw but also an excessive rolling moment at angle of attack. Differential deflection of either horizontal or vertical surfaces provided roll control; however, a considerable yawing moment accompanied the control deflections at angle of attack. The calculated values determined by shock expansion theory of pitch, yaw, and roll control characteristics at an angle of attack of 0° were slightly in excess of measured values.

INTRODUCTION

A generalized study of the effectiveness of aerodynamic controls at hypersonic speeds has been conducted in the Langley 11-inch hypersonic tunnel. For this investigation a right circular cone with a 5° semivertex angle was used as the basic body to support movable tail fins of delta planform and wedge cross section. The body nose bluntness was varied from 0 to 20 percent of the base diameter; both sharp and blunt controls were tested.

It was the purpose of the investigation to determine the effects of various geometric parameters on the overall control effectiveness at hypersonic Mach numbers. The investigation was conducted at a free-stream Mach number of 6.9 and at a Reynolds number (based upon model length) of 2.8×10^6. Six-component-force data measured over an angle-of-attack range from 0^o to 30^o are presented for each configuration. The effects of various control-surface deflections on the trim force characteristics and stability derivatives are summarized and discussed. Illustrations of the loss of effectiveness of the upper vertical tail because of body shielding are presented. The force and moment results due to control deflection are compared with shock expansion theory at an angle of attack of 0^o.

SYMBOLS

Longitudinal and lateral directional data are referred to the stability and body axes systems, respectively. The moment reference was at the 67.21-percent body station. Measurements for this investigation were taken in the U.S. Customary Units but are also given parenthetically in the International System of Units (SI).

A_f	planform area of both horizontal or vertical fins
A_r	base area of model, reference area, $\pi D^2/4$
C_A	axial-force coefficient, $(F_A - F_b)/q_\infty A_r$
ΔC_A	incremental axial-force coefficient due to control deflection
C_D	drag coefficient, $F_D'/q_\infty A_r$
C_L	lift coefficient, $F_L/q_\infty A_r$
$\frac{\partial C_L}{\partial \alpha}$	rate of change of lift coefficient with angle of attack
C_l	rolling-moment coefficient, $M_X/q_\infty A_r l$
ΔC_l	incremental rolling-moment coefficient due to control deflection
C_m	pitching-moment coefficient, $M_Y/q_\infty A_r l$

ΔC_m incremental pitching-moment coefficient due to control deflection

$\frac{\partial C_m}{\partial C_L}$ rate of change of pitching moment with lift coefficient

$\frac{\partial C_m}{\partial \delta_h}$ rate of change of pitching moment with deflection angle of horizontal controls

C_N normal-force coefficient, $F_N/q_\infty A_r$

ΔC_N incremental normal-force coefficient due to control deflection

C_n yawing-moment coefficient, $M_Z/q_\infty A_r l$

ΔC_n incremental yawing-moment coefficient due to control deflection

C_Y side-force coefficient, $F_Y/q_\infty A_r$

ΔC_Y incremental side-force coefficient due to control deflection

D model base diameter

d model nose diameter

F_A axial force along X-axis; positive direction, -X

F_b base-pressure correction, $(p_\infty - p_b) A_r$

$F_D' = F_N \sin \alpha + (F_A - F_b) \cos \alpha$

$F_L = F_N \cos \alpha + (F_b - F_A) \sin \alpha$

F_N normal force along Z-axis; positive direction, -Z

F_Y side force along Y-axis; positive direction, +Y

l length of sharp-cone model

L/D	lift-drag ratio, C_L/C_D
M	free-stream Mach number
M_X, M_Y, M_Z	moments about X-, Y-, and Z-axes (see fig. 3)
p_b	base pressure
p_∞	free-stream static pressure
q	dynamic pressure downstream of cone bow shock
q_∞	free-stream dynamic pressure
R	free-stream Reynolds number
X, Y, Z	reference axes
α	angle of attack, deg
δ	angle of control deflection, deg

Subscripts:

B	body axis system
h	horizontal controls
L	left or lower
R	right
S	stability axis system
tr	trim condition, $C_m = 0$

U upper

v vertical controls

MODELS AND TESTS

The conical model had a 5° semivertex angle and cruciform delta planform control surfaces; the model and the various fins and noses are shown in figure 1. Detail dimensions of all components are shown in the three-view drawing (fig. 2). Three sets of sharp leading-edge fins having area ratios A_f/A_r of 0.086, 0.182, and 0.343 and one set of blunt leading-edge fins having A_f/A_r of 0.359 and leading-edge-radius—body-length ratio of 0.0026 were tested. The fins were independently equipped with index pins to fix deflection angles of $\pm 10^{\circ}$, -20°, and -30°. Three variations of nose bluntness of diameter ratios d/D of 0, 0.10, and 0.20 were tested. The model and all components were machined from stainless steel.

The tests were conducted in the Mach number 6.86 test section of the Langley 11-inch hypersonic tunnel. The tunnel-wall boundary-layer thickness and hence the free-stream Mach number of this test section are dependent upon the stagnation pressure. For these tests, the average stagnation pressure was 25 atmospheres $\left(2.53 \times 10^6 \text{ N/m}^2\right)$ and the average stagnation temperature, 630° F (605° K) (to avoid liquefaction). These conditions resulted in an average free-stream Mach number of 6.88 and an average unit Reynolds number of 0.276×10^6 per inch (10.87×10^6 per meter). The absolute humidity was kept to less than 1.9×10^{-5} parts of water per part of dry air by weight for all tests.

All force and moment measurements were made by using a six-component water-cooled strain-gage internal balance. Readout was continuously recorded on pen-marked strip-chart self-balancing potentiometers.

Tests were conducted through an angle-of-attack range of 0° to 30°. Base pressures were measured on the base of the conical body and the axial-force component was adjusted to correspond to a base pressure equal to the free-stream static pressure.

PRECISION OF DATA

The maximum uncertainties in the measurement of the force and moment coefficients for the individual test points as a result of inaccuracies in the force balance readout system are presented as follows:

C_N	±0.009
C_A	±0.006
C_m	±0.001
C_l	±0.002
C_n	±0.001
C_Y	±0.003

The stagnation pressure was measured to an accuracy of ±1.5 inches of mercury (±5.1 kN/m^2) and the Mach number was known to ±0.01, the combination corresponding to an accuracy of free-stream dynamic pressure of ±0.02 pound per square inch (±0.138 kN/m^2). The angles of attack were set to ±0.20^o and the control deflections, to to ±0.10^o.

RESULTS AND DISCUSSION

The results of the tests are presented in coefficient form with the longitudinal data referred to the stability axis system and the directional and lateral data to the body axis system (fig. 3). The selection of the moment reference was based on reference 1, in which it was shown experimentally and theoretically that the center of pressure of the simple right circular cone was essentially fixed for a given cone angle and was independent of angle-of-attack change through a 60^o angle-of-attack range. The moment reference was therefore placed at the 67.21-percent body station, the location of the center of pressure, to make possible an assessment of the trim penalties for various control alterations and deflections with minimal effects contributed by the basic conical body.

Longitudinal Stability and Control

The basic longitudinal pitch data for the body alone with varying degrees of nose bluntness are presented in figure 4. The effects of increasing nose bluntness on the basic conical body are as might be expected from primary geometric considerations. With increasing nose bluntness there was an increase in drag and longitudinal stability and a decrease in lift and lift-drag ratio throughout the angle-of-attack range. The loss of lift was due to the decrease in lifting surface and the increase in stability was attributable to the forward location of this lost lifting surface.

The basic longitudinal control data and schlieren photographs of various configurations are presented in figures 5 to 13 and are summarized in figures 14 to 16 in the form of incremental pitching moments due to control deflection. The term "incremental pitching moment" as used is the difference between the pitching moment measured with

control deflection and that measured with zero control deflection at a given angle of attack on the complete cruciform configuration. A study of these figures shows that the ability of the controls to produce pitch (hereafter called control effectiveness) either remains constant or improves with angle of attack for all controls irrespective of size, leading-edge bluntness, or body nose bluntness. Generally the effectiveness of the sharp leading-edge controls appears to increase proportionally with control area. The blunt leading-edge controls are not as effective in the production of pitch (particularly at the higher deflections) as the large sharp controls, although the area of the blunt controls is about 4.7 percent greater than the area of the large sharp controls.

Increasing the body nose bluntness decreases the control effectiveness at low angles of attack partly because of the losses in dynamic pressure behind the strong detached nose shock wave; but there was little change in effectiveness at angles of attack above 10°.

The longitudinal characteristics at trim for all variations of controls and nose geometry are presented in figures 17 to 19. An increase in size of the controls from 8.6 to 34.3 percent of the base area resulted in an increase in trim drag and a 24.3-percent decrease in maximum trim L/D (fig. 17). An increase in nose bluntness and/or control leading-edge bluntness is accompanied by an increase in trim drag and a decrease in trim lift and thus by a substantial reduction of trim L/D and maximum trim lift coefficient. (See figs. 18 and 19.) A comparison between the sharp-nosed body with the large sharp leading-edge controls and the 0.20-blunt body with the blunt leading-edge controls shows that there was about a 50-percent loss in trim maximum lift-drag ratio, maximum trim lift coefficient, and trim angle of attack because of the bluntness. (See figs. 18 and 19.) This loss provides an insight into what might happen to the control of a configuration that has a fixed center-of-gravity location and a variation of nose and control leading-edge bluntness because of ablation of surfaces in stagnation regions. The range of trim angle of attack and thus lift coefficient could possibly be extended by varying the location of the center of gravity during flight, but the trim lift-drag ratio would suffer from the increasing drag and reduced lift due to the effects of bluntness, regardless of the location of the center of gravity.

The longitudinal stability parameters at trim are presented in figures 20 to 22 and although primarily for use during simulator studies the variations of the control power and the level of the static stability are of particular interest. The lift-curve slope was positive at trim and was constant within plus or minus two times the experimental error in lift coefficient for any given configuration throughout the trim-lift range. These are most desirable vehicle characteristics and are important to the equilibrium flight condition of the vehicle and its dynamic longitudinal stability. All configurations show positive static stability at the higher trim lift coefficients and were extremely stable near zero lift. The power of the controls to produce pitch may be seen to increase with control

size and remain relatively constant with increasing trim lift. (See fig. 20.) Figure 21 shows that the control power of the large sharp leading-edge controls was essentially constant for variations of nose bluntness and maintained this level throughout the trim-lift range. A comparison of figures 21 and 22 shows that the control power is markedly decreased with leading-edge bluntness and thus results in a serious loss in the trim-lift range. A rearward shift of the center of gravity would help to recover a portion of this lost trim-lift range.

Comparison of experimental results with theory has been limited to an angle of attack of 0° where the inviscid flow field about the cone is known. (See ref. 2.) Control characteristics were calculated by using shock expansion theory, assuming local flow conditions equal to those on the cone surface, and correcting the resulting coefficients to free-stream conditions by multiplying by the ratio of the local-surface dynamic pressure to the free-stream dynamic pressure. For a free-stream Mach number of 6.9 this dynamic-pressure ratio amounts to about 1.43. The controls were well within the bow shock wave at $\alpha = 0^{\circ}$. (See fig. 13.) No effects of leading-edge shock detachment or pressure leakage along the control-body juncture were included. Laminar skin friction was assumed and found to amount to approximately 1 percent of the calculated incremental normal-force coefficient. Figure 23 shows a comparison of theoretical and experimental incremental longitudinal characteristics with control deflection for the medium sharp leading-edge controls. Reasonably good agreement may be seen to exist between experiment and theory. Theoretical curves for which no dynamic-pressure correction was taken into account underestimate the experimental data as expected, whereas use of this increase results in an overestimation at the higher control deflections. This overestimation may be accounted for by losses in pressure due to the increase in the control-body juncture with deflection angle, the variation in dynamic pressure and flow angle that takes place between the cone surface and bow wave, and the blanketing of the control surface by the boundary-layer buildup along the body surface.

Directional Control

The basic longitudinal, lateral, and directional characteristics due to yaw control for all variations of control size, leading edge, and body nose bluntness are presented in figures 24 to 26. For these tests, the horizontal controls were set at $\delta_h = 0^{\circ}$. An increase in vehicle longitudinal stability, lift force, and drag force, and a loss in lift-drag ratio may be seen to occur with increasing control area for a given yaw control deflection. Side force and yawing moment increased with control area and also with angle of attack. The rolling moment due to yaw control was zero at zero angle of attack but increased with angle of attack as the effectiveness of the upper vertical control was lost because of body shielding. The magnitude of this rolling moment may be undesirable but could conceivably be nullified by use of a differential deflection of the vertical or

horizontal controls. For a given yaw control area and deflection the longitudinal stability and drag increased with increasing body nose bluntness whereas the lift and lift-drag ratio decreased. (See fig. 25.) Except at low angles of attack where the side force and yawing moment decreased with increasing nose bluntness, very little change in these parameters was noted at angles of attack. These losses at low angles of attack with nose bluntness are due to the dynamic-pressure loss through the strong detached bow shock waves shown in the schlieren photographs, figure 13. At the higher angles of attack the region of low energy flow behind the bow wave has washed downstream with the crossflow and that flow in the region of the controls has traveled through a weaker shock wave well away from the bow region and thus has a gain rather than a loss of dynamic pressure. The blunt leading-edge controls gave increases in longitudinal stability and decreases in lift-drag ratio when compared with controls having sharp leading edges; however, no significant changes resulted in the side-force, rolling-moment, or yawing-moment parameters. (See figs. 25 and 26.) Figures 27 to 29 show the variation of the incremental lateral-directional characteristics due to yaw control. The values shown in these figures are only slightly different from those presented in the basic data plots inasmuch as the values read with zero control deflection were small.

Figure 30 presents a comparison of theoretical and experimental directional characteristics due to yaw control. These calculations, which are analogous to those made for longitudinal control, were made at zero angle of attack by using the method and assumptions described in the section entitled "Longitudinal Stability and Control." As with the longitudinal characteristics the 43-percent gain in q through the bow shock is reflected directly in the experimental coefficient which falls between those calculated with and without the dynamic-pressure correction.

Roll Control

The basic longitudinal, lateral, and directional characteristics of the sharp conical body with differential deflection of both horizontal and vertical controls are presented in figure 31. A comparison of the sharp and blunt controls shows only a slight increase in longitudinal stability and decrease in lift-drag ratio for the blunt controls due to the increased drag and reduced lift associated with the added bluntness. Figure 31(c) shows that within the accuracy of the data there was little loss in roll control due to leading-edge bluntness. Figure 32 presents the incremental lateral-directional characteristics due to roll control and shows that the differential deflection of either the horizontal or vertical controls results not only in a roll contribution throughout the angle-of-attack range but also a sizable contribution of yawing moment. Any sizable yawing moment due to roll control is undesirable and, although a small positive yaw accompanying a positive roll is desirable in the negotiation of turns, the yawing moments exhibited herein may require cross control and thus be unfavorable. For the roll due to differential horizontal

control deflection the yaw contribution is not as large as that due to vertical control deflection but it is of the wrong sign to be helpful. These yawing moments are due to the increasing drag of the positively deflected left horizontal control and the decreasing drag of the negatively deflected right horizontal control with increasing angle of attack. It might be possible to reduce the magnitude of these yawing moments somewhat by differentially varying the degree of control deflection between the left and right control surfaces. This type of control would have to vary with angle of attack if it were to be expected to produce roll with no cross coupling. The yaw due to differential vertical control deflection is favorable in sign but extremely large in magnitude. These yawing moments were caused by the lower vertical control in conjunction with the loss in effectiveness of the upper vertical control as it became shielded by the body with angle of attack. Without shielding the upper vertical control would contribute a yawing moment of opposite sign to help decrease if not counteract the large measured moment.

Figure 33 presents a comparison of experimental incremental roll control characteristics at an angle of attack of zero with calculations made by using the methods and assumptions given in the section entitled "Longitudinal Stability and Control."

CONCLUSIONS

An analysis of experimental data on a finned conical body having a semivertex angle of 5° and variations of control geometry and nose bluntness at a Mach number of 6.9 and a Reynolds number of 2.8×10^6 based on model length leads to the following conclusions:

1. The basic conical body exhibits an increase in drag and static longitudinal stability with increasing nose bluntness and a decrease in lift and lift-drag ratio throughout the 30° angle-of-attack range.

2. Longitudinal control effectiveness (ability of the controls to produce pitch) either remains constant or improves with angle of attack irrespective of control size, leading-edge bluntness, or body nose bluntness.

3. Generally, the control effectiveness of the sharp leading-edge controls is proportional to control planform area.

4. The blunting of control leading edges results in a decrease in their effectiveness.

5. An increase in body nose bluntness results in a decrease in control effectiveness at low angles of attack, but at angles of attack above 10° little variation with nose bluntness is noted.

6. An increase in control planform area, leading-edge bluntness, or body nose bluntness results in an increase in trim drag and a decrease in trim-lift range and trim lift-drag ratio.

7. The deflection of vertical controls for yaw control results in not only the desired yaw but also considerable roll with increasing angle of attack because of shielding of the upper vertical control. The longitudinal stability increases with increasing body nose bluntness and control area for a given yaw control, and the lift-drag ratio decreases.

8. Differential deflection of either horizontal or vertical controls provides roll control; however, a considerable yawing moment accompanies the control deflections at angle of attack because of the high drag of the positively deflected horizontal tail or shielding of the upper vertical tail.

9. The effects of control size on both yaw and roll control are similar to those shown on pitch control; however, the effect of control leading-edge blunting is negligible.

10. The calculated values of pitch, yaw, and roll control characteristics at an angle of attack of 0° are slightly in excess of measured values partly because of losses at the control-body juncture, the variation in dynamic pressure between the body surface and the bow shock, and the boundary-layer buildup along the body.

Langley Research Center,
National Aeronautics and Space Administration,
Langley Station, Hampton, Va., February 24, 1966.

REFERENCES

1. Penland, Jim A.: A Study of the Stability and Location of the Center of Pressure on Sharp, Right Circular Cones at Hypersonic Speeds. NASA TN D-2283, 1964.

2. Sims, Joseph L.: Tables for Supersonic Flow Around Right Circular Cones at Zero Angle of Attack. NASA SP-3004, 1964.

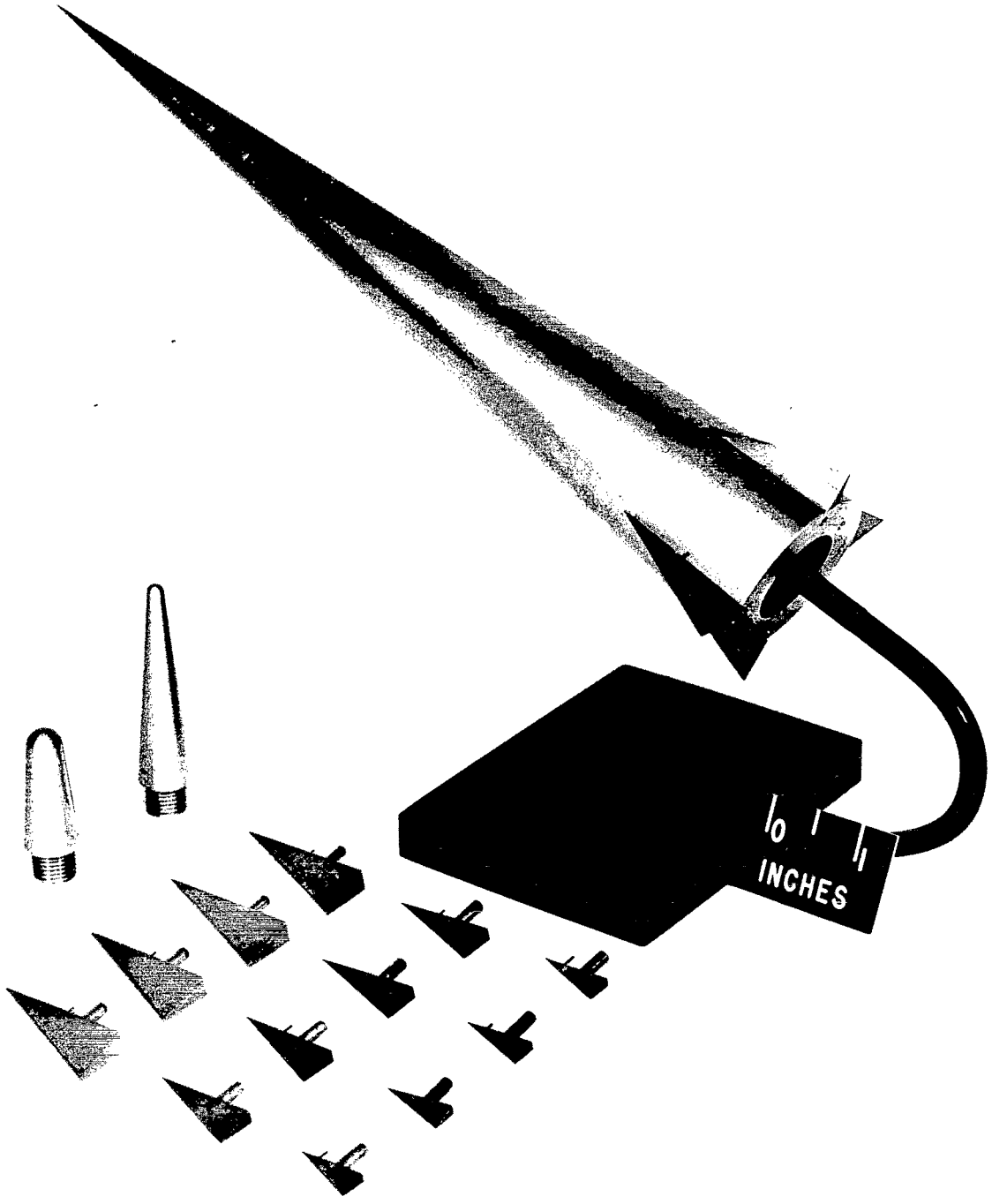

Figure 1.- Photograph of model, noses, and controls. L-65-8022

INCHES	CENTIMETERS
0.027	0.069
0.092	0.234
0.184	0.467
0.295	0.749
0.430	1.092
0.534	1.356
0.569	1.445
0.585	1.486
0.595	1.511
0.707	1.796
1.130	2.870
1.329	3.376
1.556	3.952
1.602	4.069
1.838	4.669
2.292	5.822
3.250	8.255
7.057	17.925
10.500	26.670

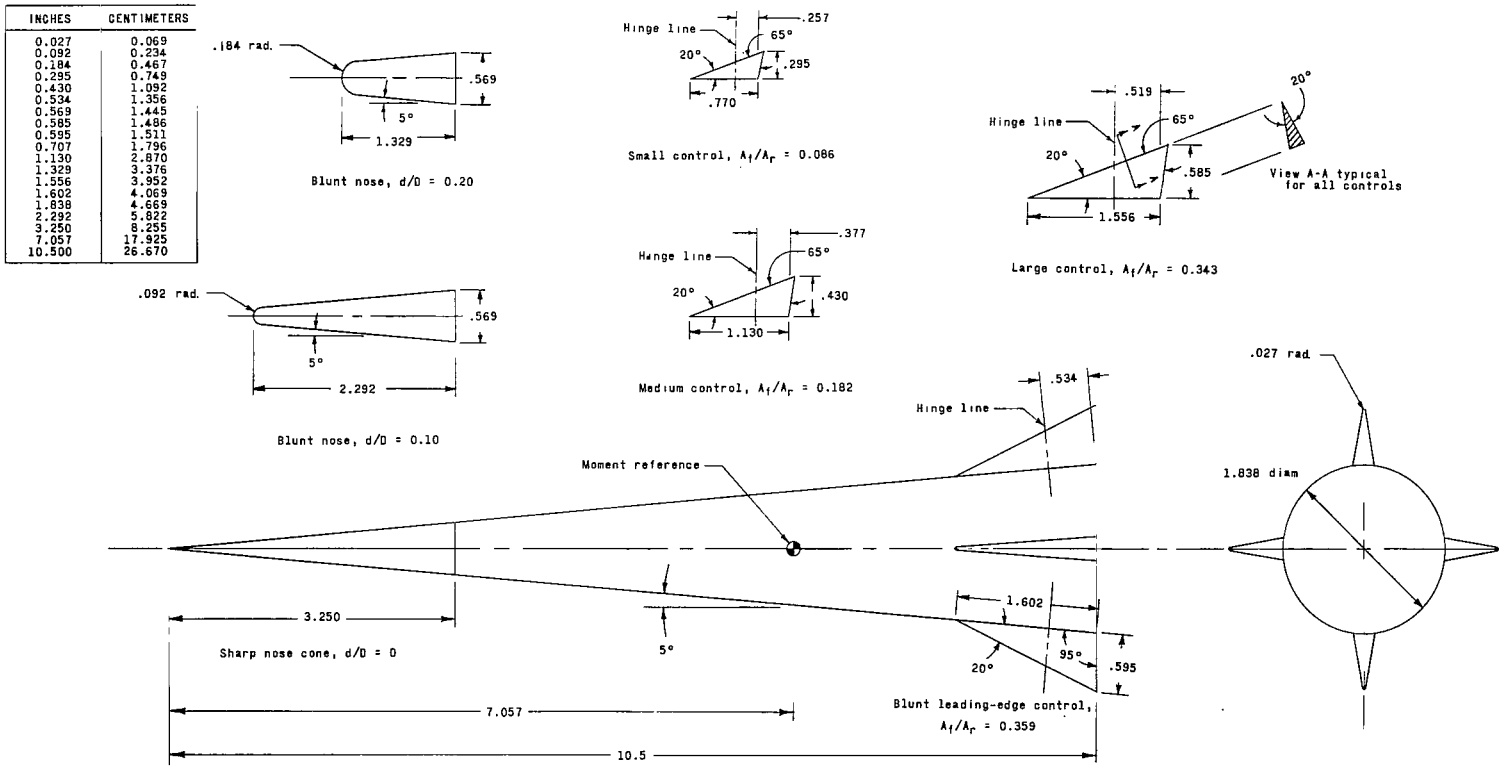

Figure 2.- Model details. Dimensions on drawing in inches, dimensions in table in centimeters.

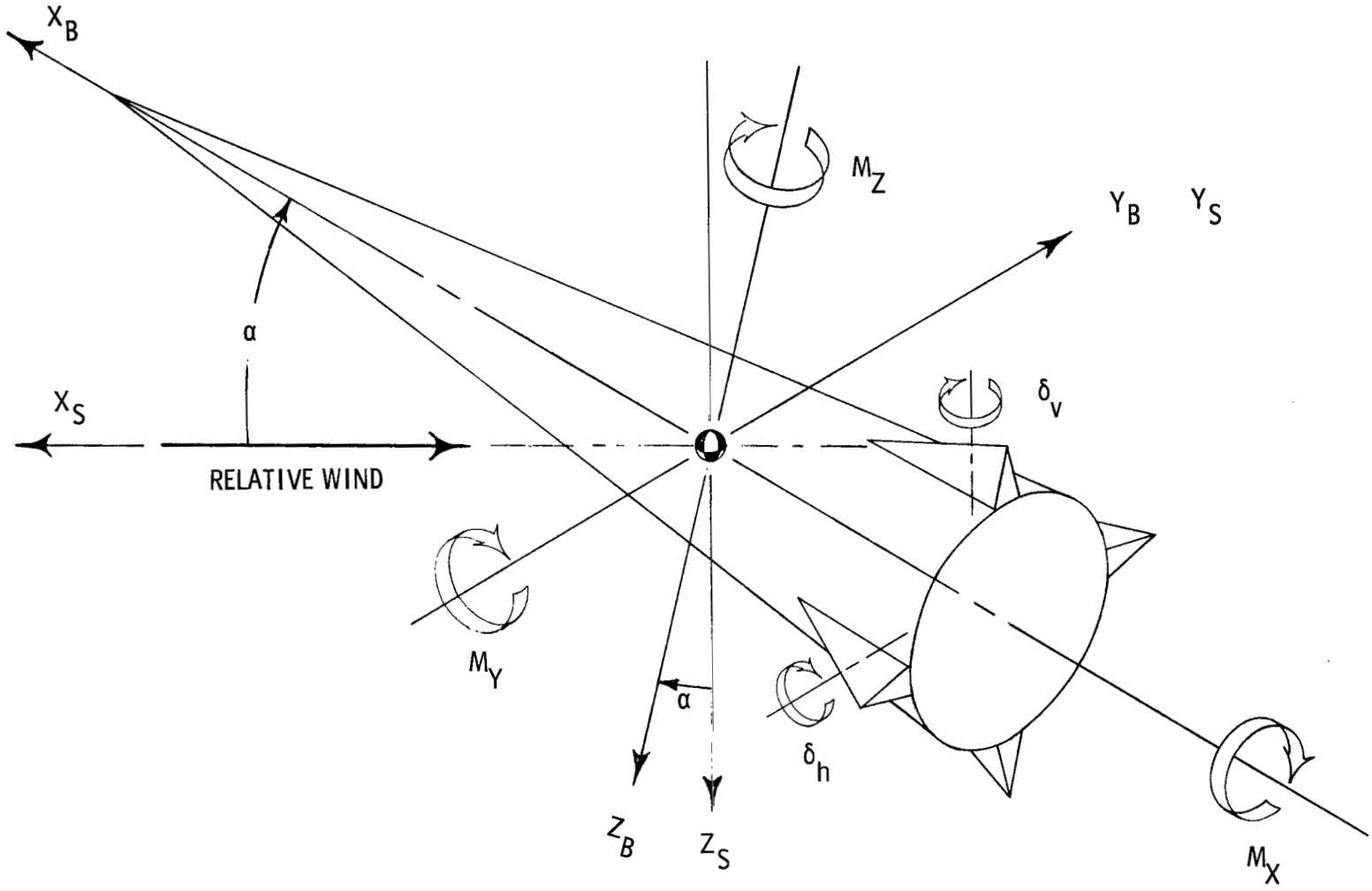

Figure 3.- Axis system. Arrows indicate positive directions.

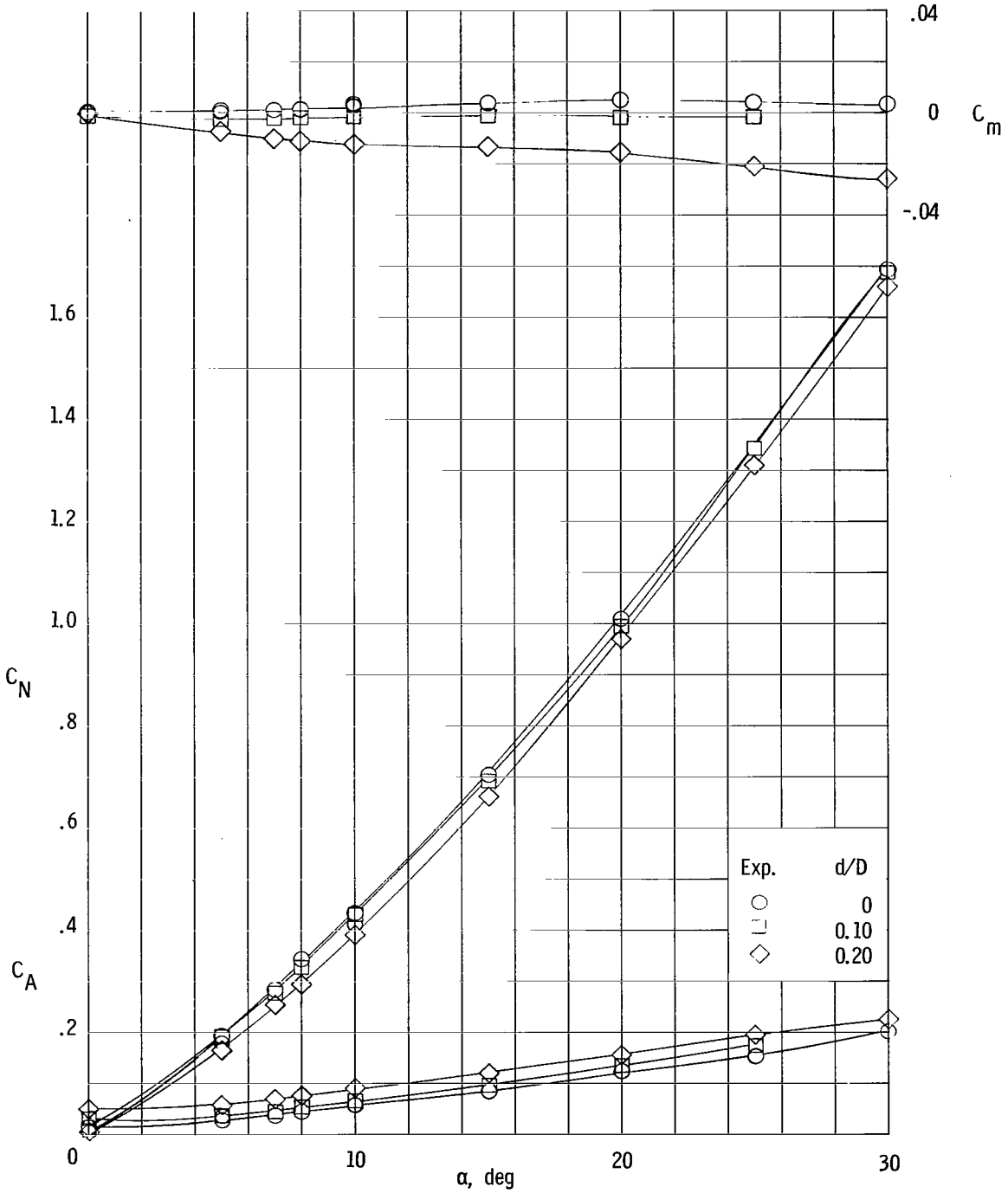

(a) Pitching-moment, normal-force, and axial-force coefficients.

Figure 4.- Longitudinal characteristics in pitch of 5^0 cone having various nose bluntness ratios.

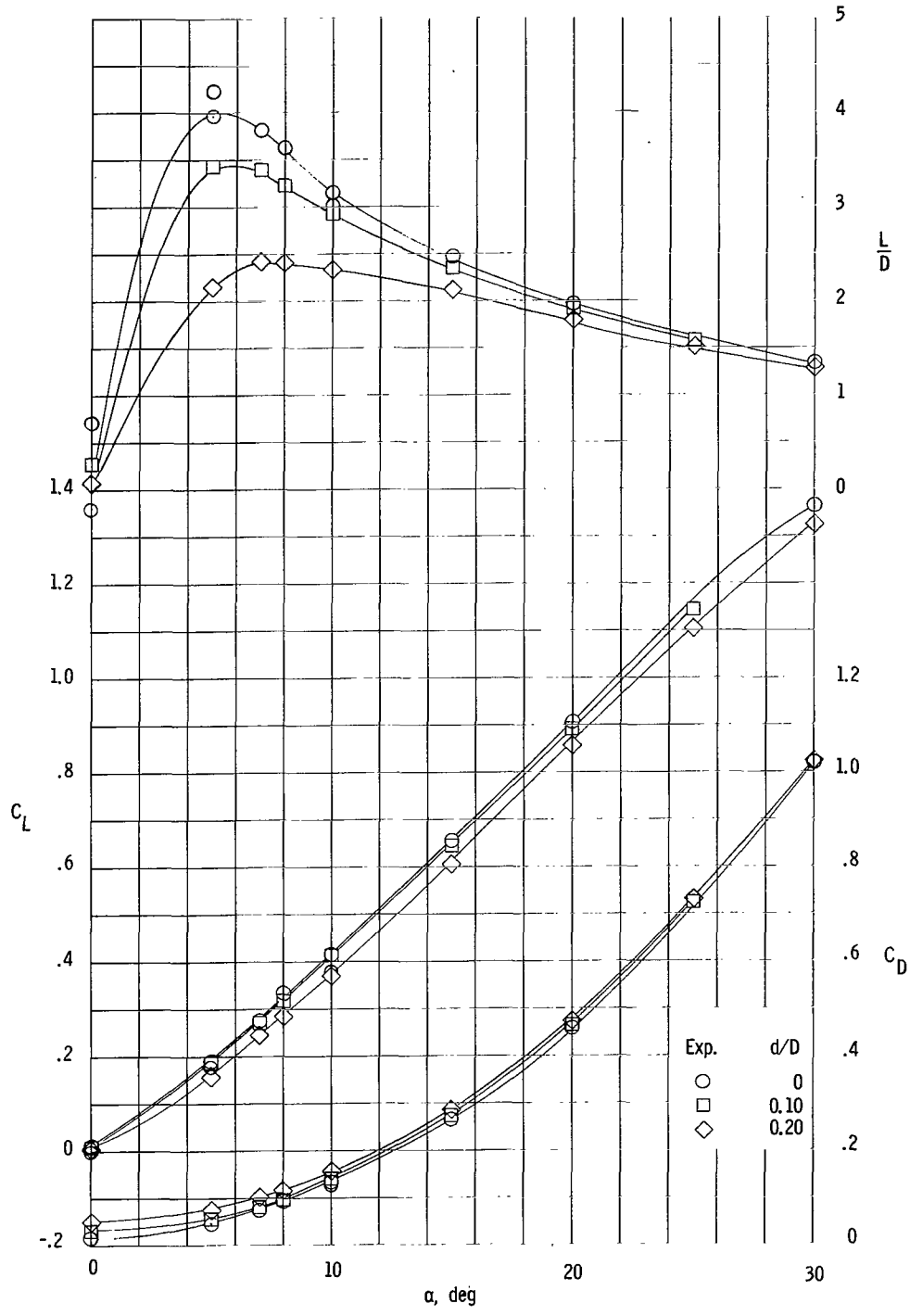

(b) Lift and drag coefficients and lift-drag ratio.

Figure 4.- Concluded.

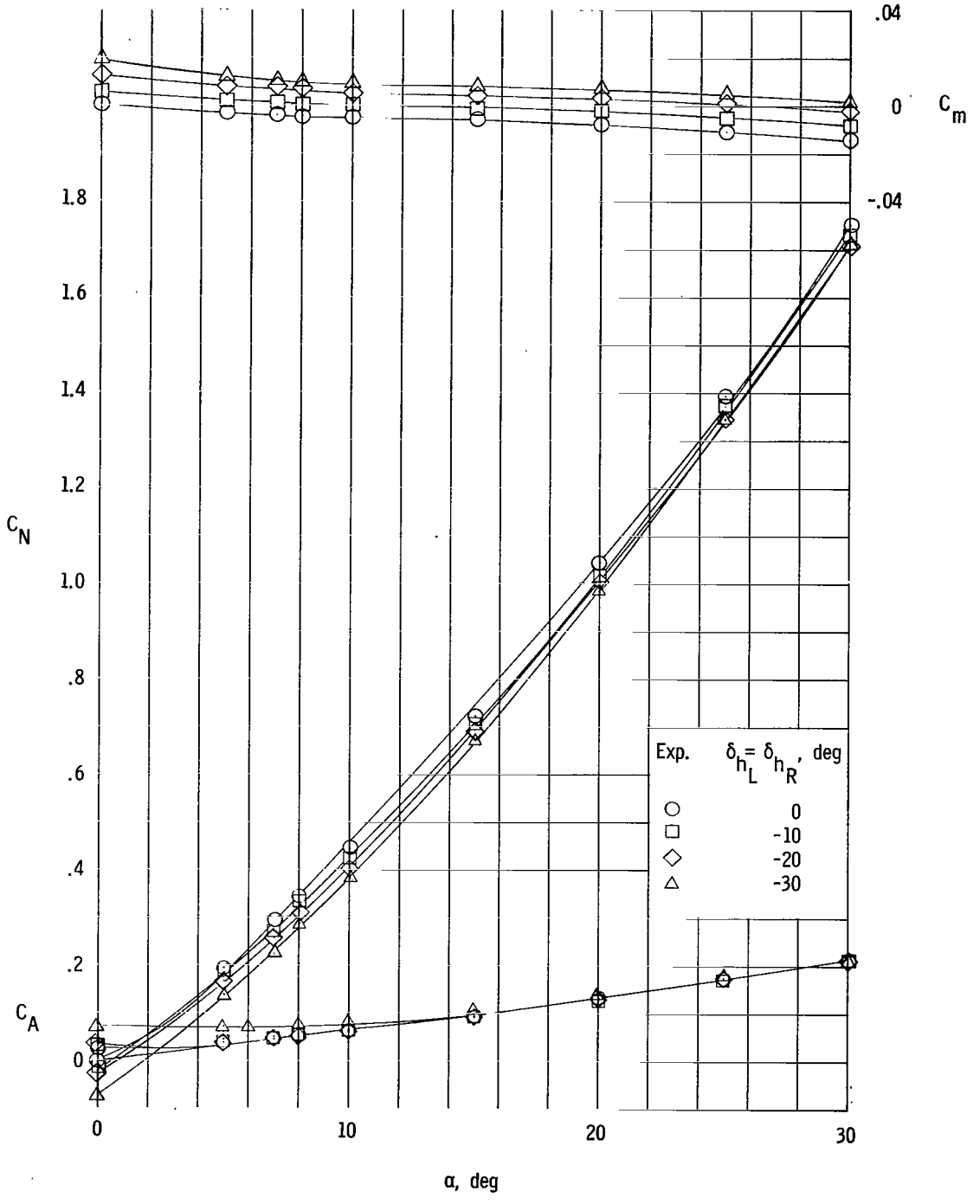

(a) Pitching-moment, normal-force, and axial-force coefficients.

Figure 5.- Longitudinal aerodynamic characteristics in pitch of sharp 5° cone having sharp L.E. controls. $A_f/A_r = 0.086$.

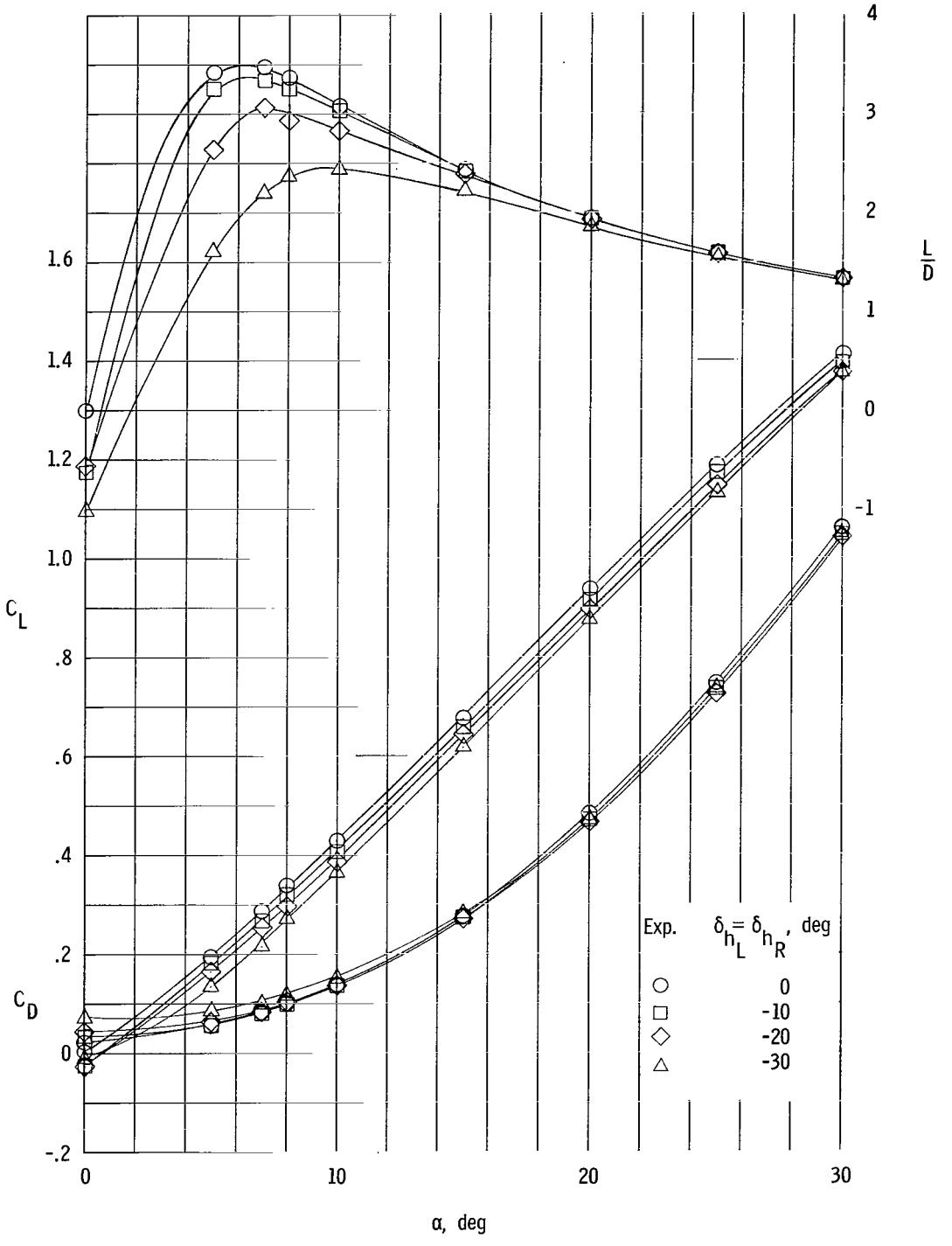

(b) Lift and drag coefficients and lift-drag ratio.

Figure 5.- Concluded.

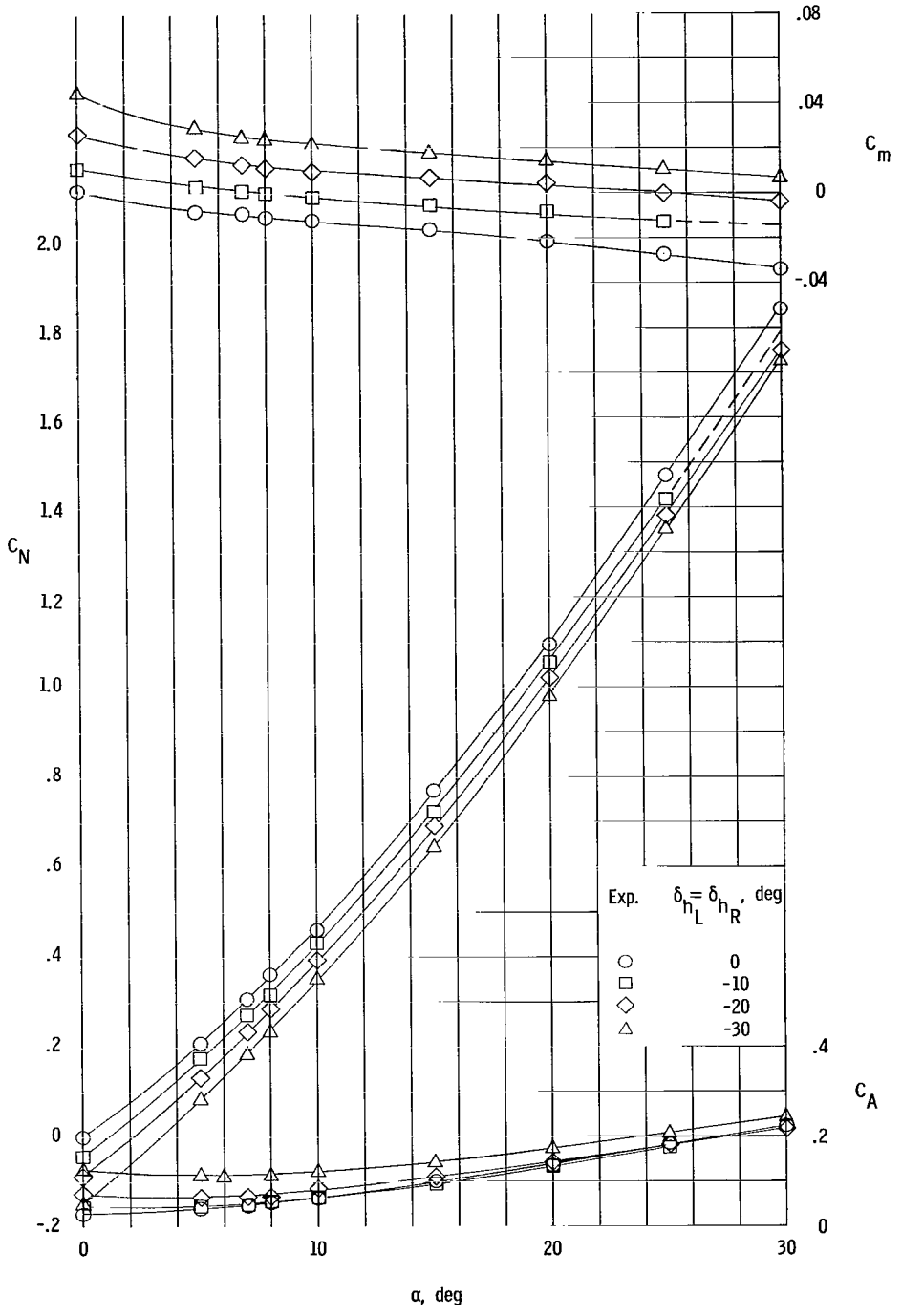

(a) Pitching-moment, normal-force, and axial-force coefficients.

Figure 6.- Longitudinal aerodynamic characteristics in pitch of sharp 5° cone having sharp L.E. controls. $A_f/A_r = 0.182$.

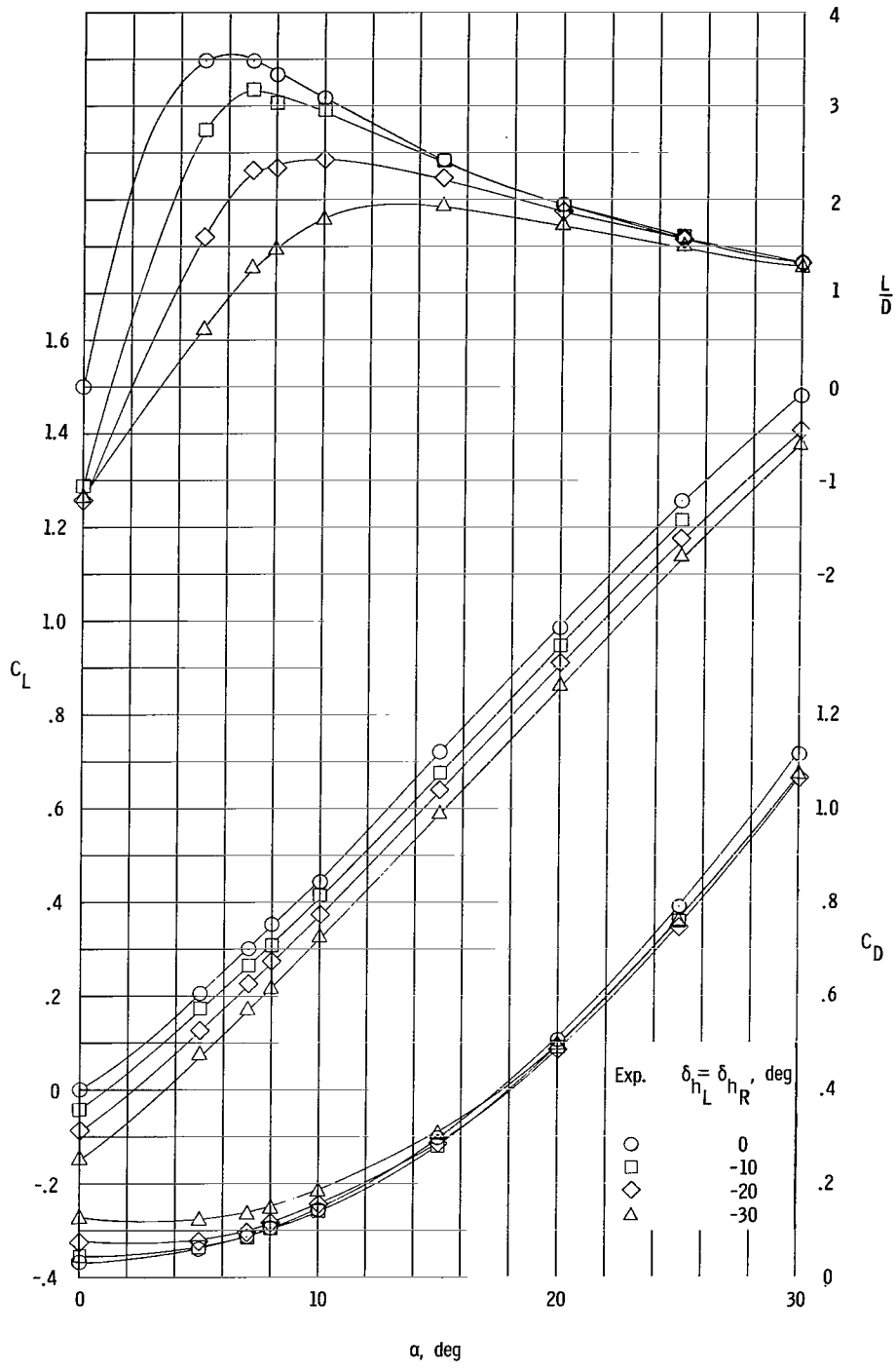

(b) Lift and drag coefficients and lift-drag ratio.

Figure 6.- Concluded.

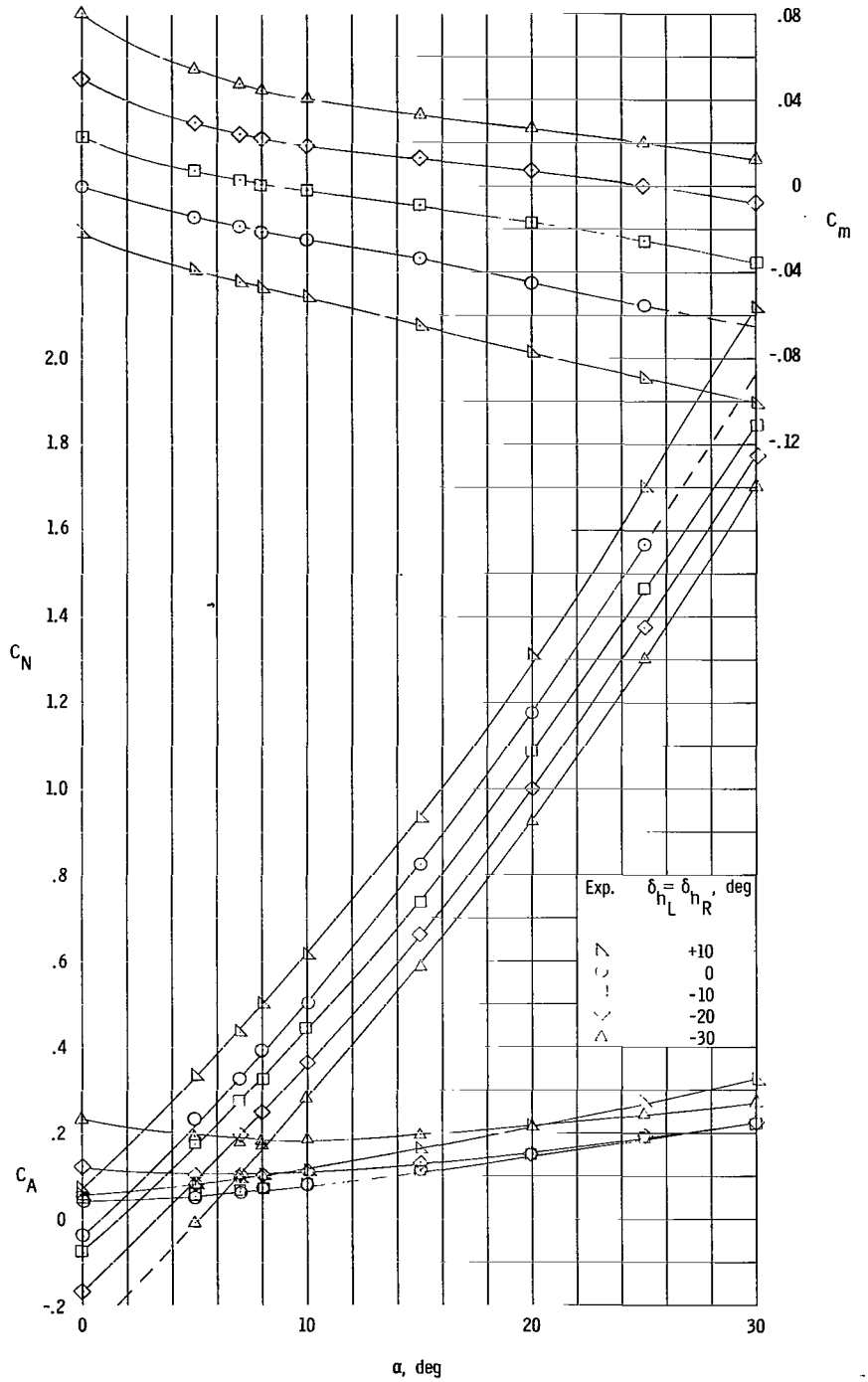

(a) Pitching-moment, normal-force, and axial-force coefficients.

Figure 7.- Longitudinal aerodynamic characteristics in pitch of sharp 5^0 cone having sharp L.E. controls. $A_f/A_r = 0.343$.

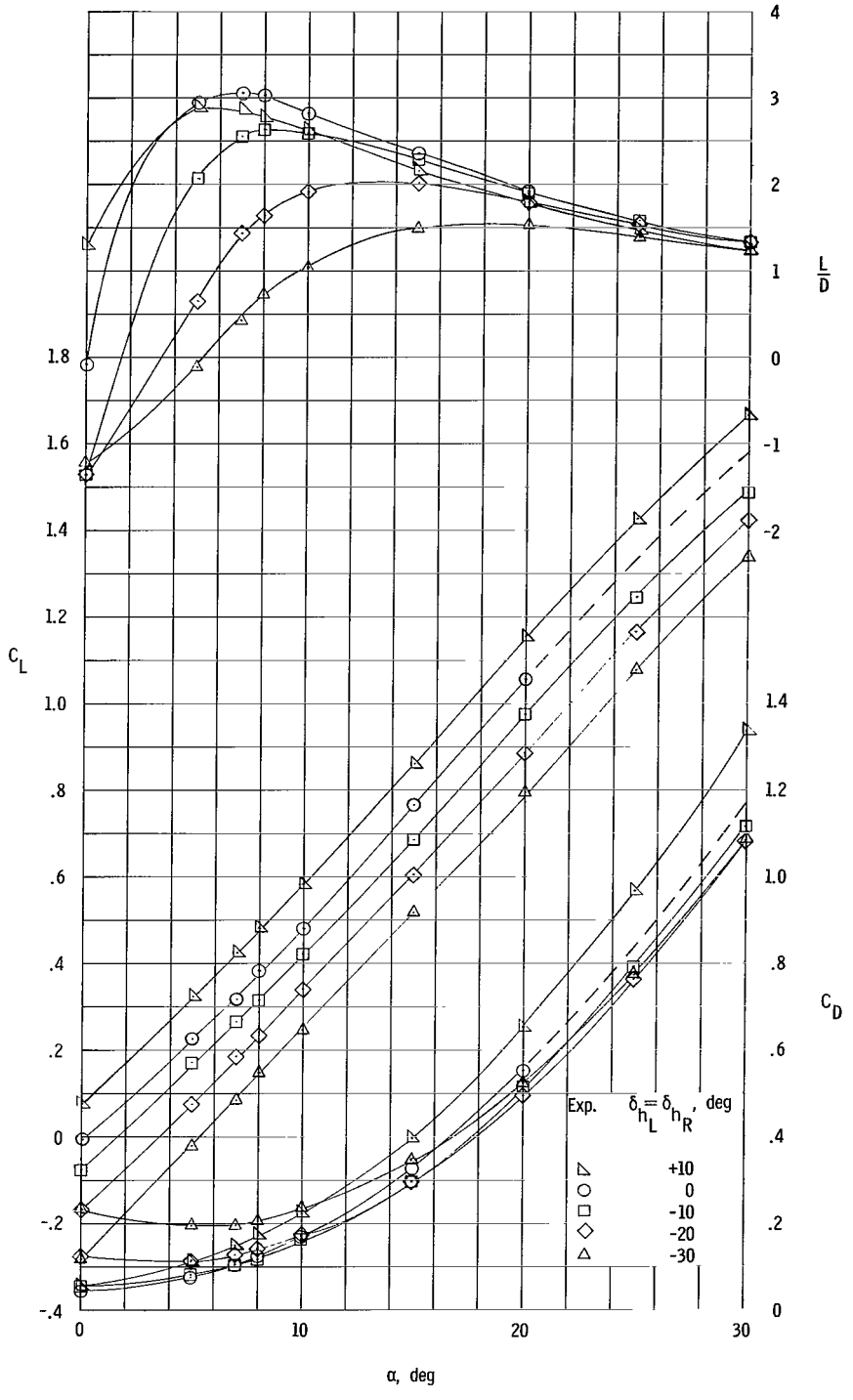

(b) Lift and drag coefficients and lift-drag ratio.

Figure 7.- Concluded.

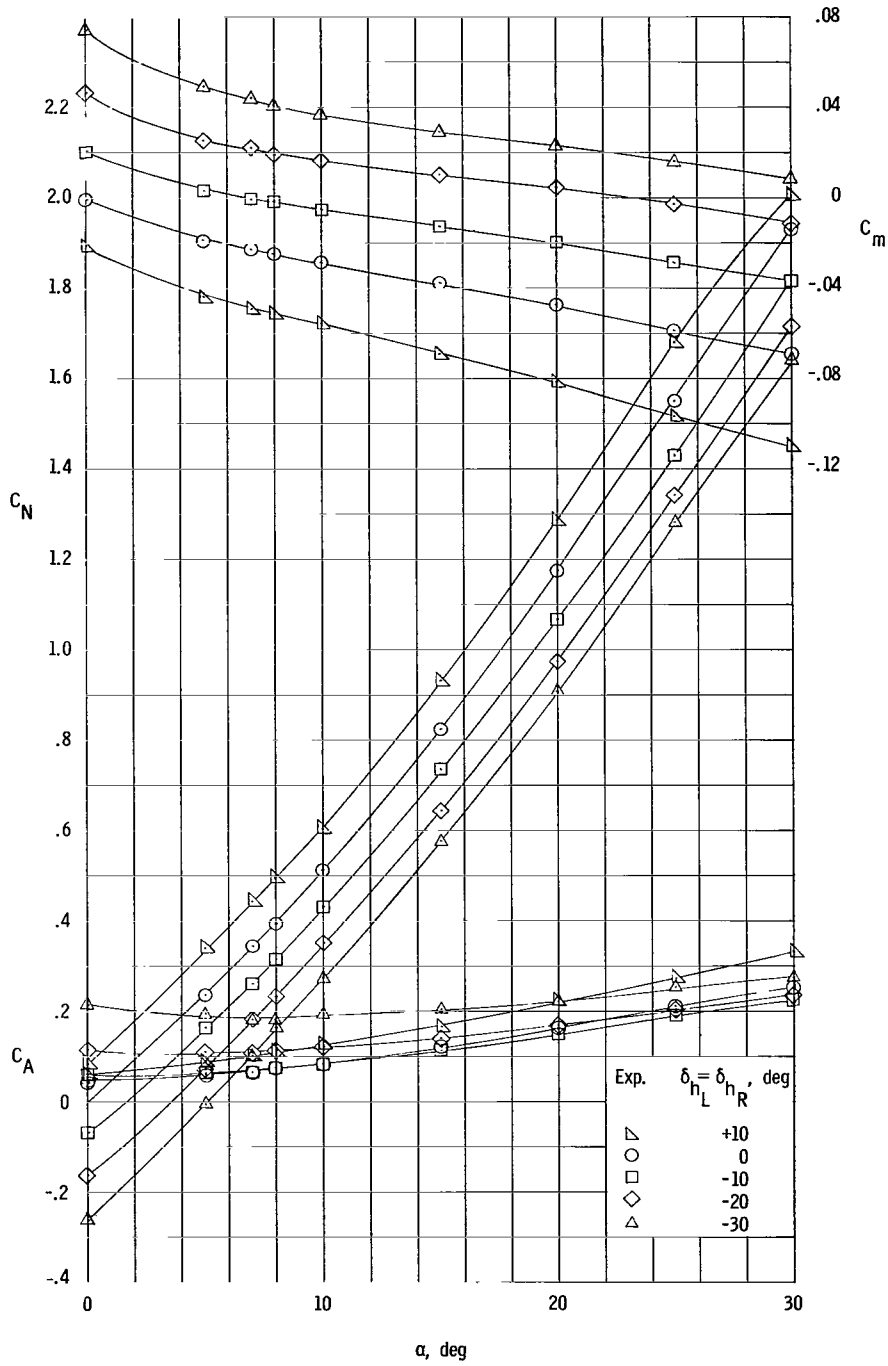

(a) Pitching-moment, normal-force, and axial-force coefficients.

Figure 8.- Longitudinal aerodynamic characteristics in pitch of blunt 5° cone having d/D = 0.10 and sharp L.E. controls. A_f/A_r = 0.343.

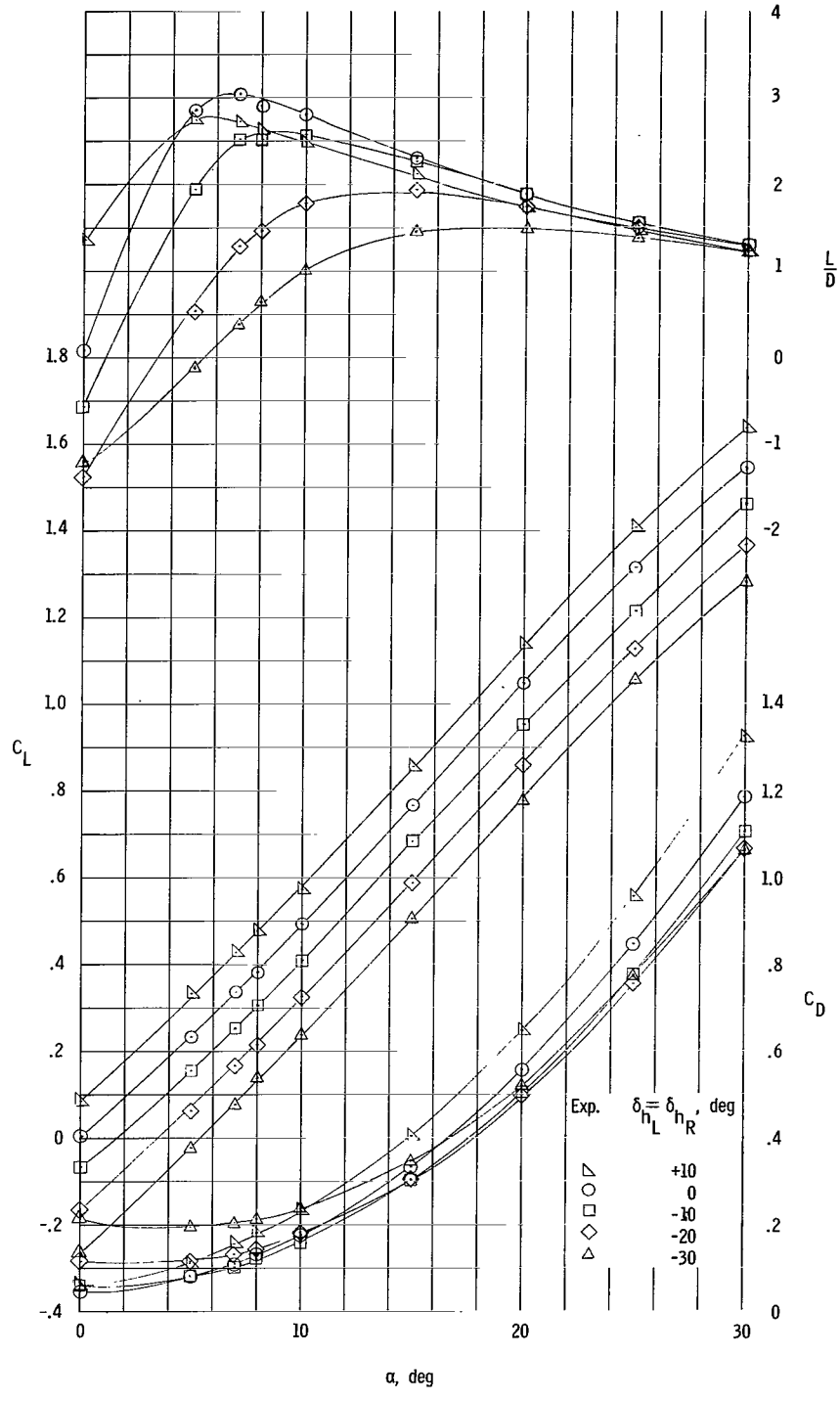

(b) Lift and drag coefficients and lift-drag ratio.

Figure 8.- Concluded.

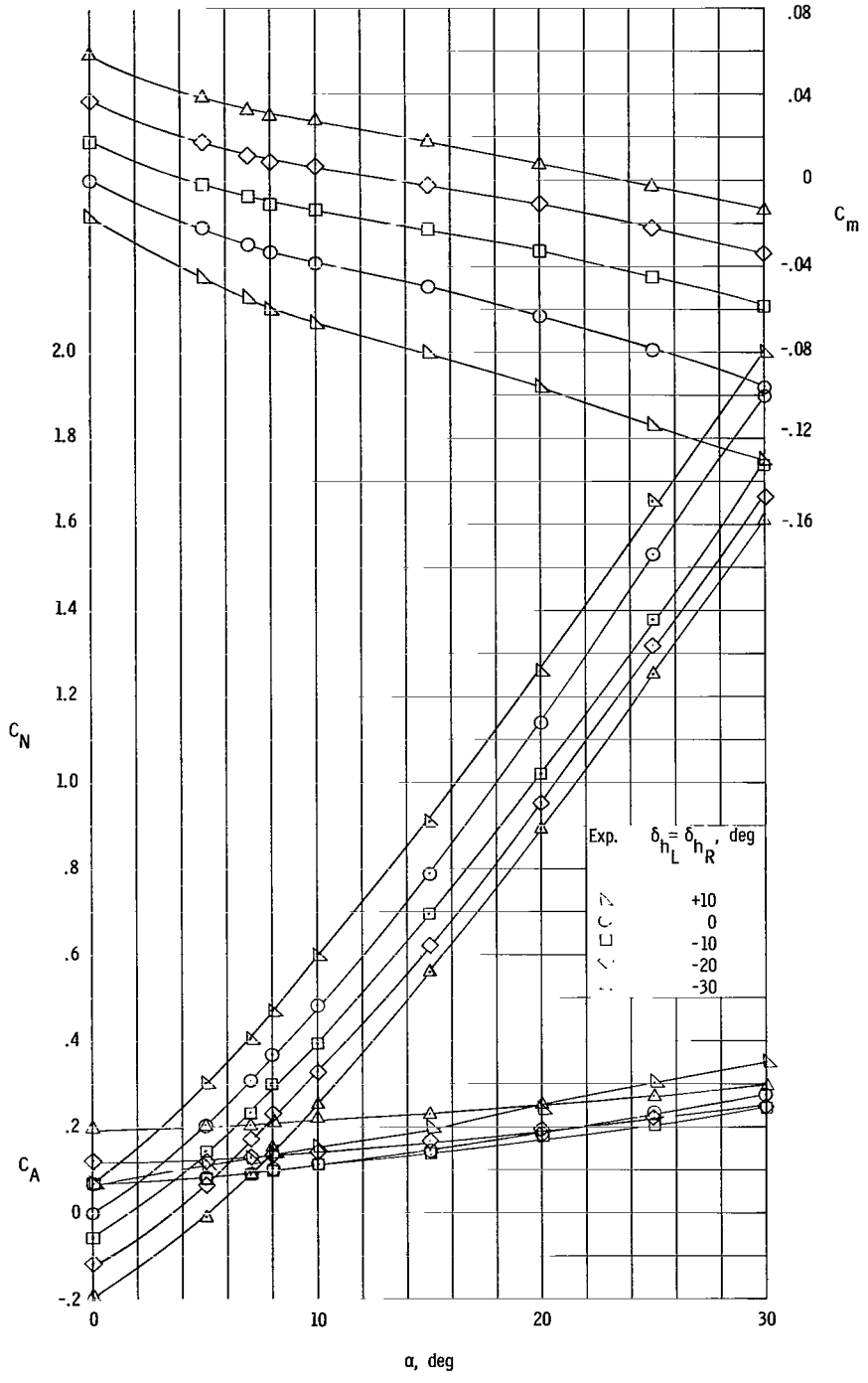

(a) Pitching-moment, normal-force, and axial-force coefficients.

Figure 9.- Longitudinal aerodynamic characteristics in pitch of blunt 5° cone having d/D = 0.20 and sharp L.E. controls. A_f/A_r = 0.343.

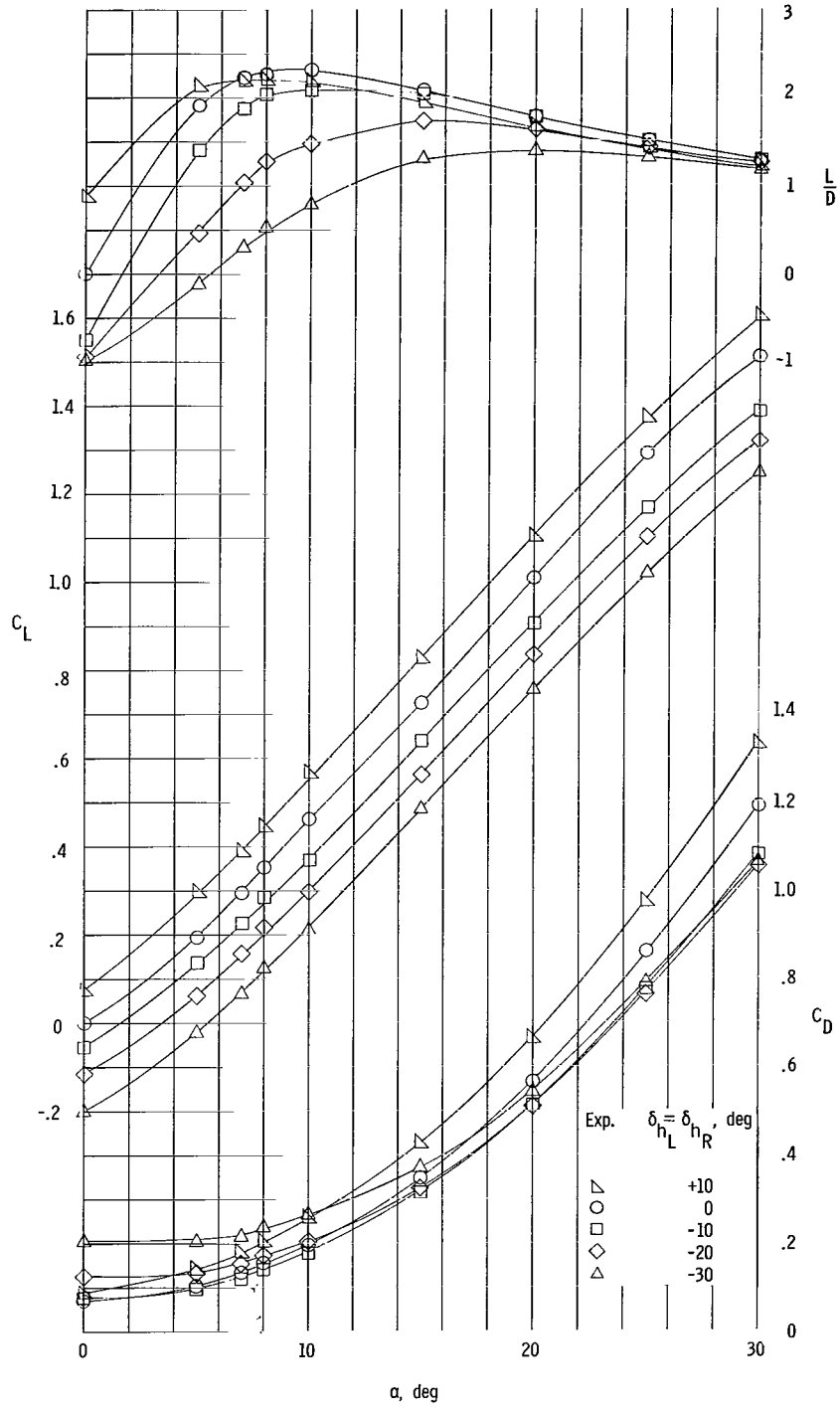

(b) Lift and drag coefficients and lift-drag ratio.

Figure 9.- Concluded.

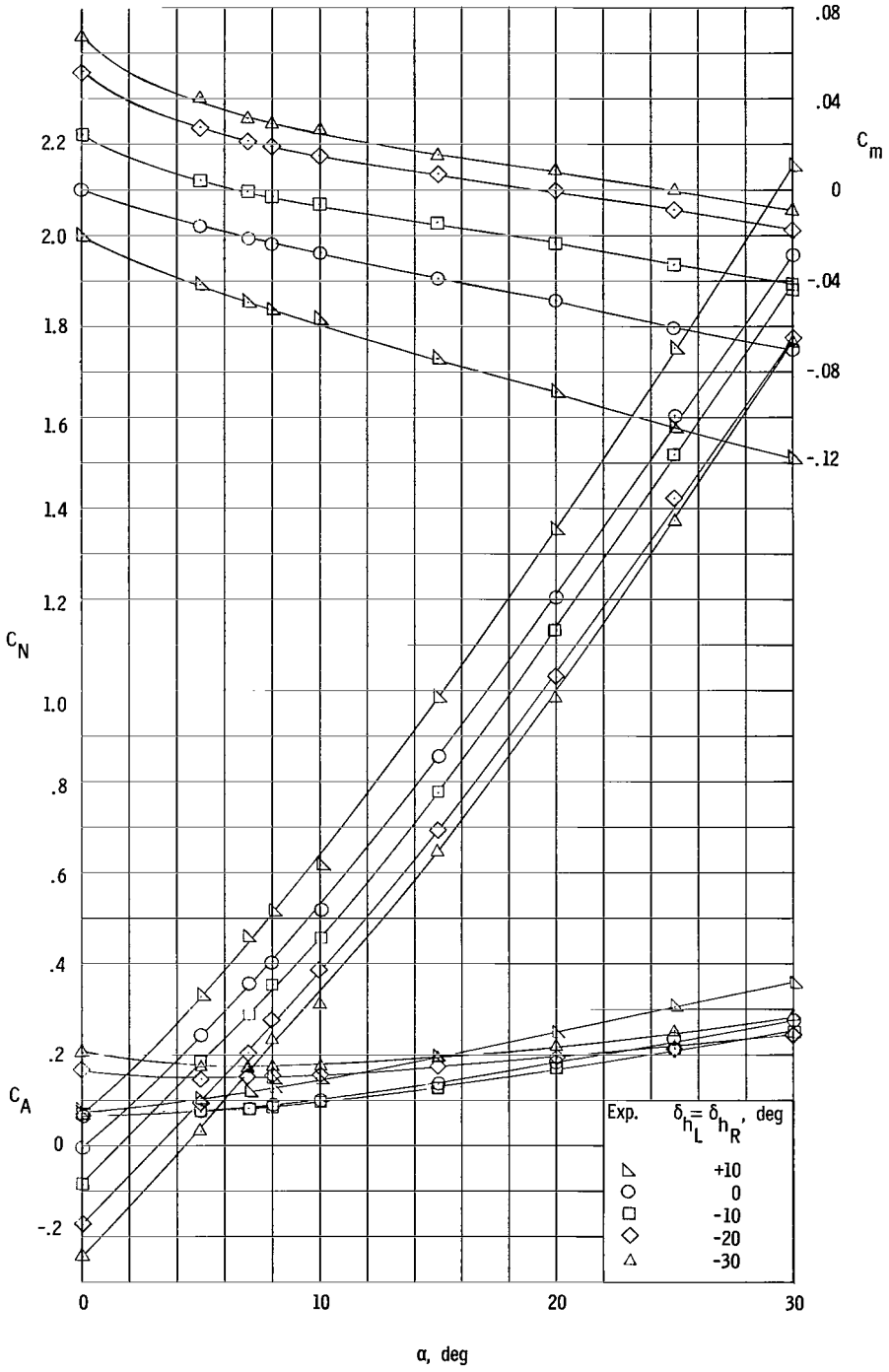

(a) Pitching-moment, normal-force, and axial-force coefficients.

Figure 10.- Longitudinal aerodynamic characteristics in pitch of sharp 5° cone having blunt L.E. controls. $A_f/A_r = 0.359$.

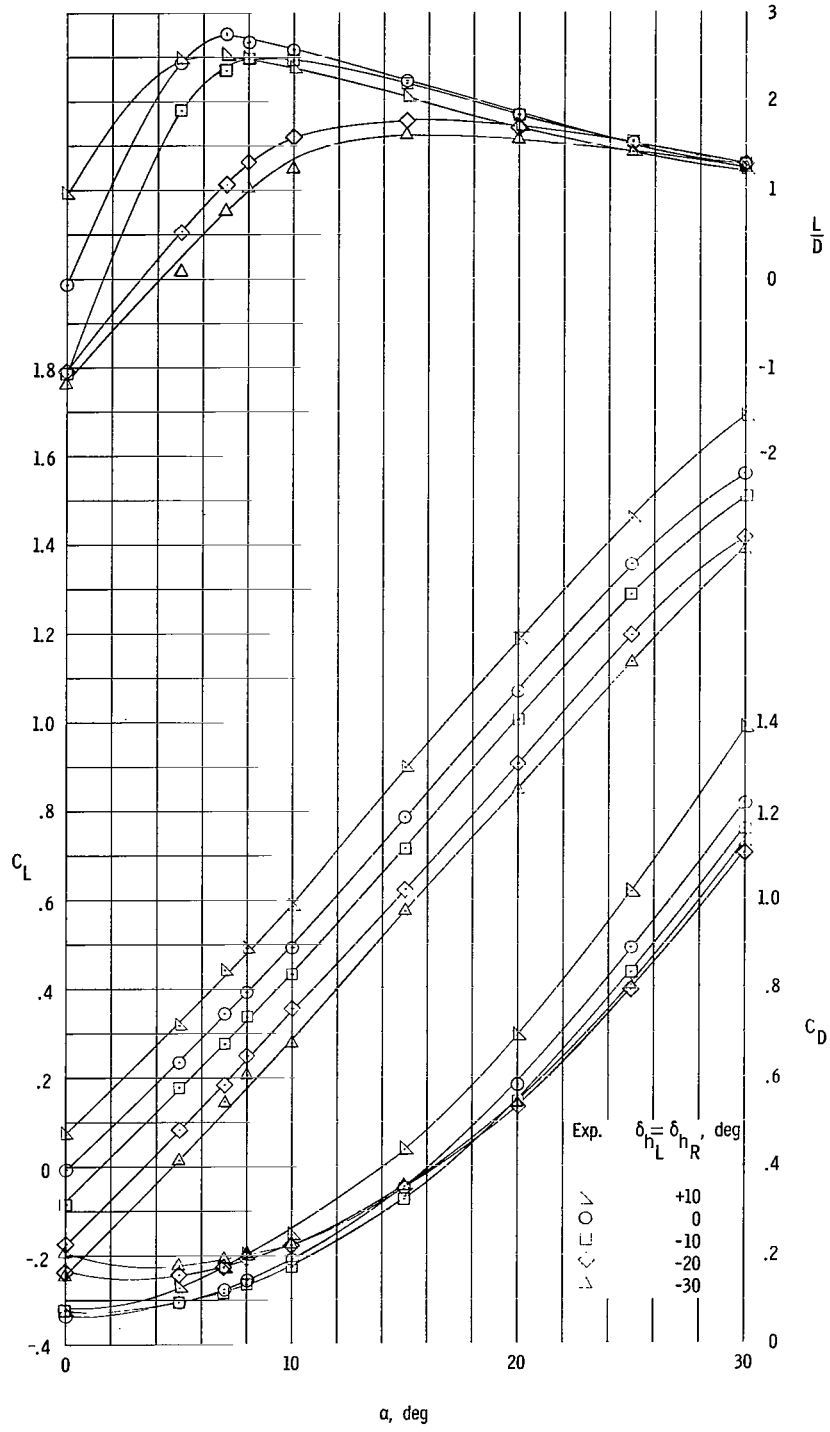

(b) Lift and drag coefficients and lift-drag ratio.

Figure 10.- Concluded.

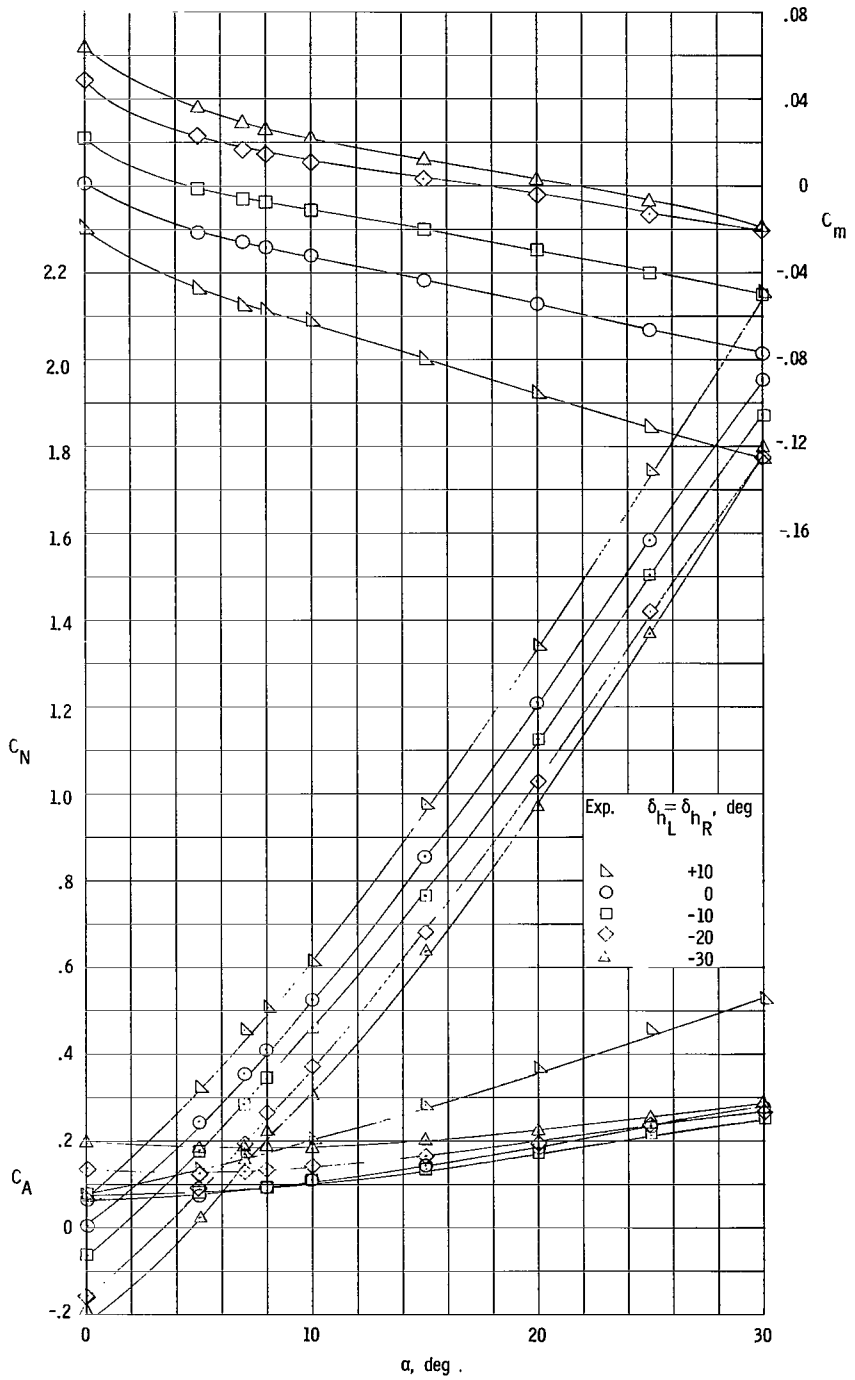

(a) Pitching-moment, normal-force, and axial-force coefficients.

Figure 11.- Longitudinal aerodynamic characteristics in pitch of blunt 5° cone having d/D = 0.10 and blunt L.E. controls. A_f/A_r = 0.359.

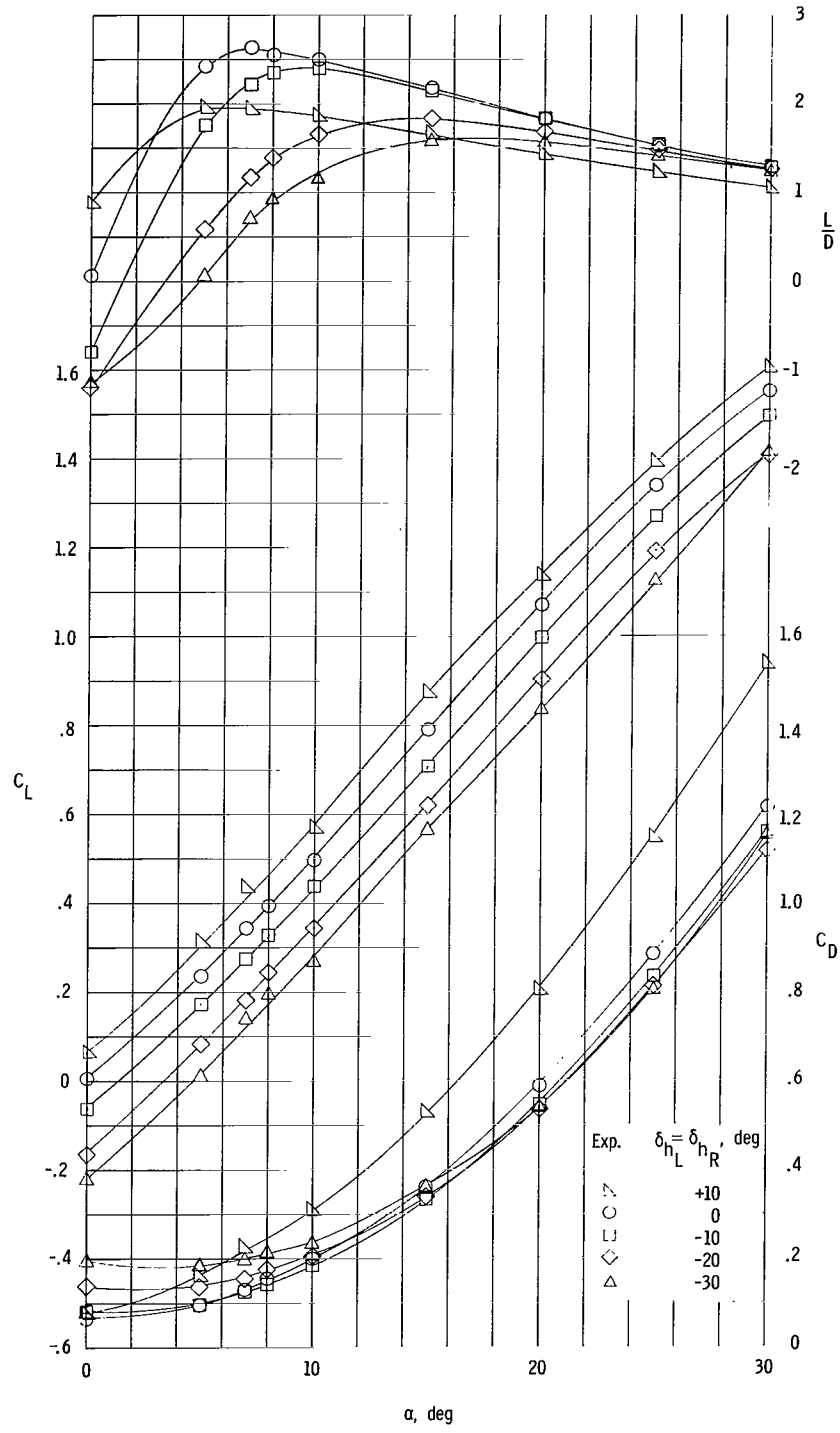

(b) Lift and drag coefficients and lift-drag ratio.

Figure 11.- Concluded.

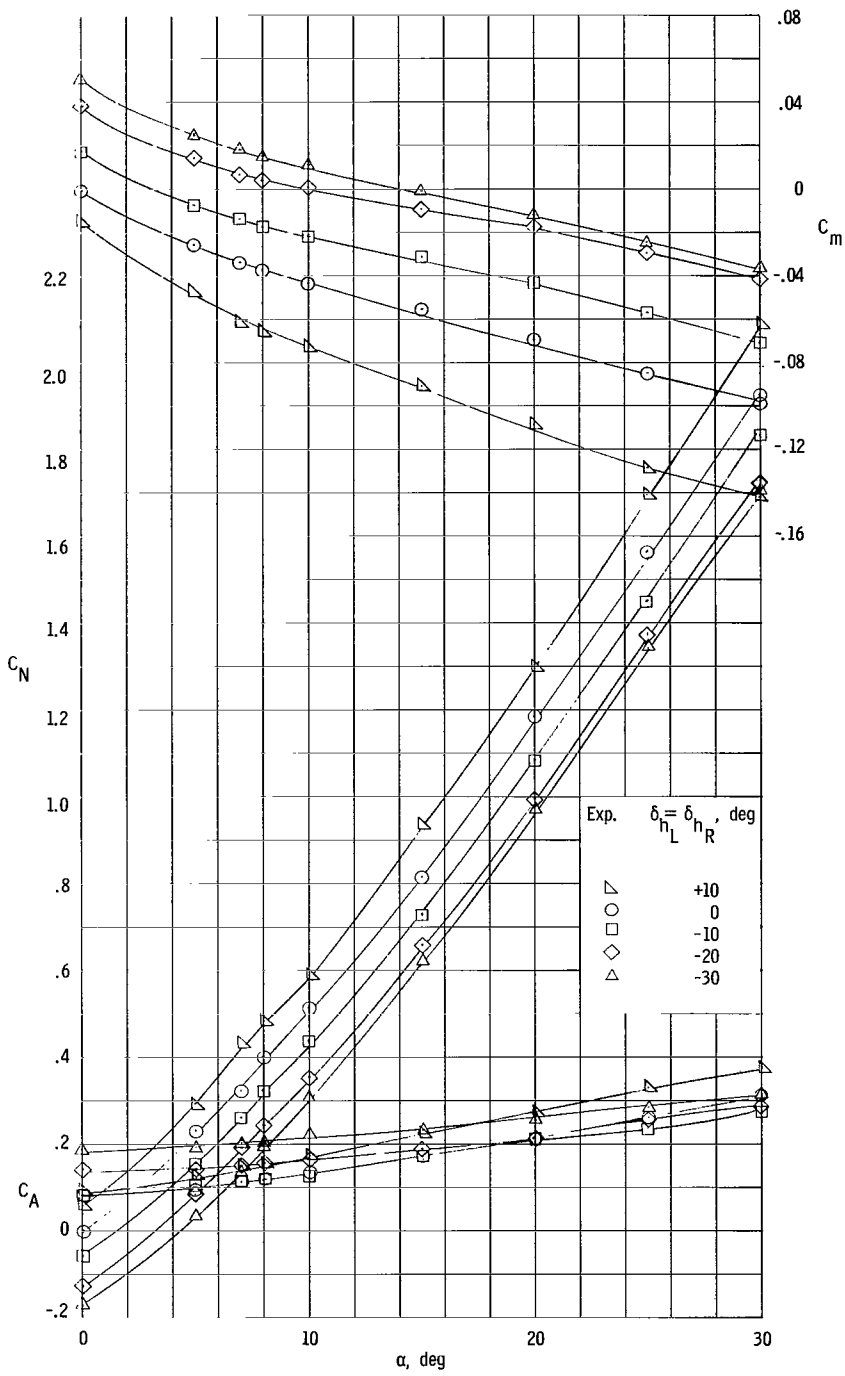

(a) Pitching-moment, normal-force, and axial-force coefficients.

Figure 12.- Longitudinal aerodynamic characteristics in pitch of blunt 5^0 cone having d/D = 0.20 and blunt L.E. controls. A_f/A_r = 0.359.

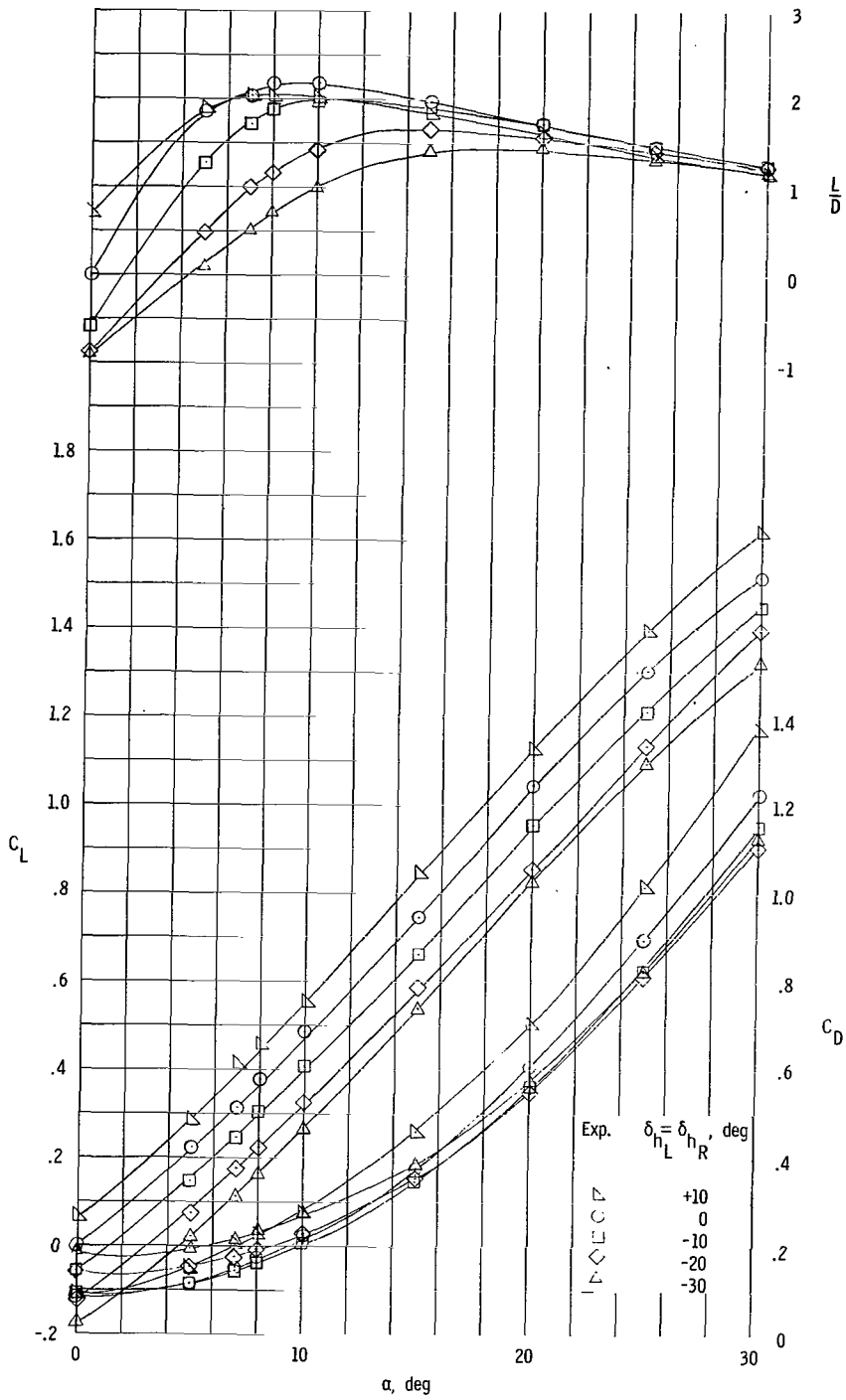

(b) Lift and drag coefficients and lift-drag ratio.

Figure 12.- Concluded.

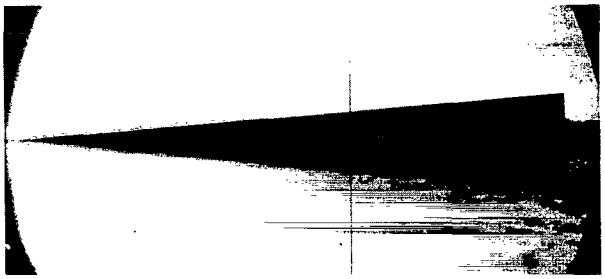

$\alpha = 0^0$

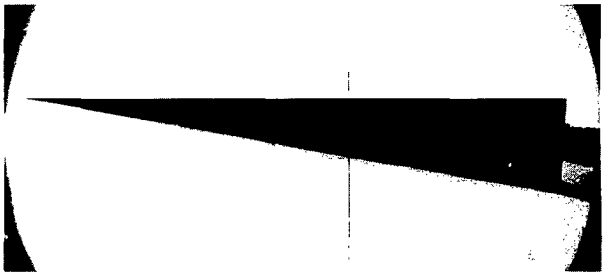

$\alpha = 5^0$

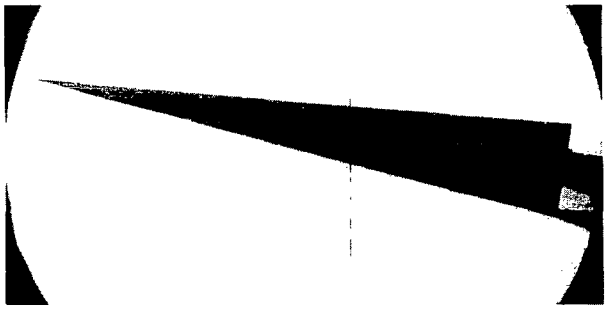

$\alpha = 10^0$

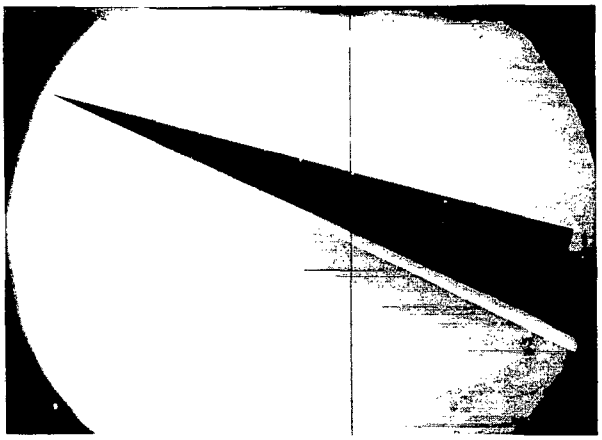

$\alpha = 20^0$

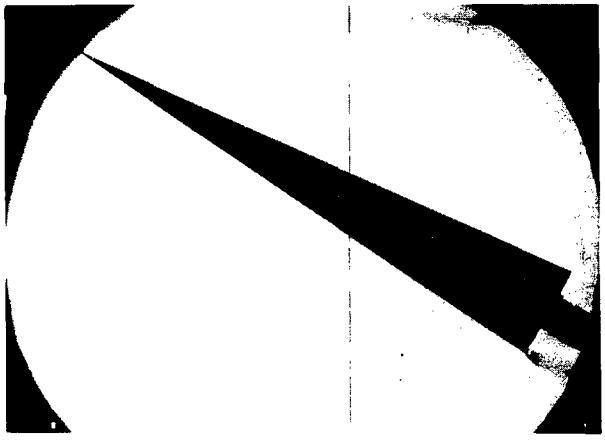

$\alpha = 30^0$

(a) Sharp nose cone. d/D = 0.

L-66-1107

Figure 13.- Schlieren photographs of various models.

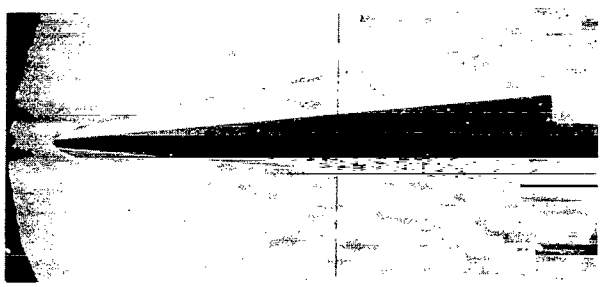

$\alpha = 0^0$

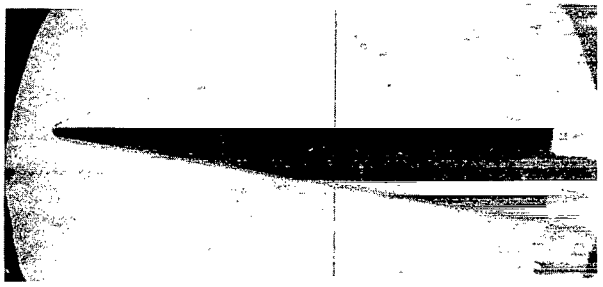

$\alpha = 5^0$

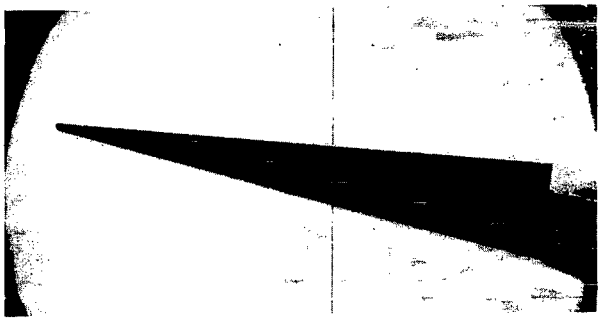

$\alpha = 10^0$

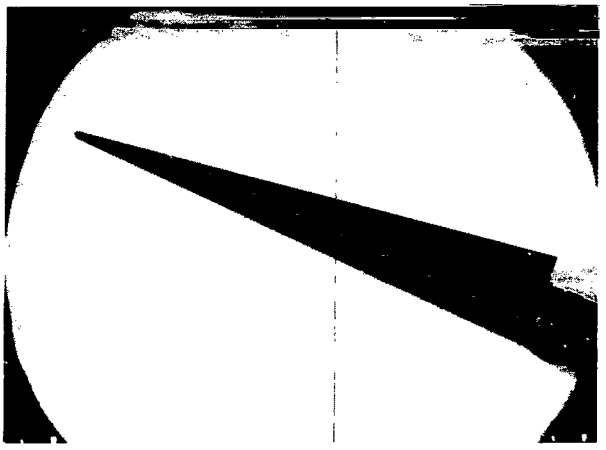

$\alpha = 20^0$

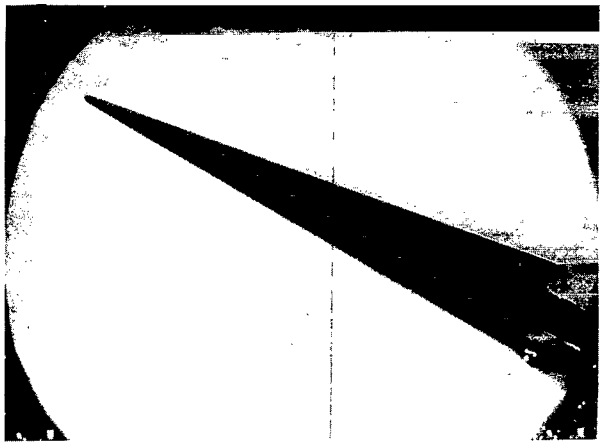

$\alpha = 25^0$

(b) Blunt nose cone. d/D = 0.10.

L-66-1108

Figure 13.- Continued.

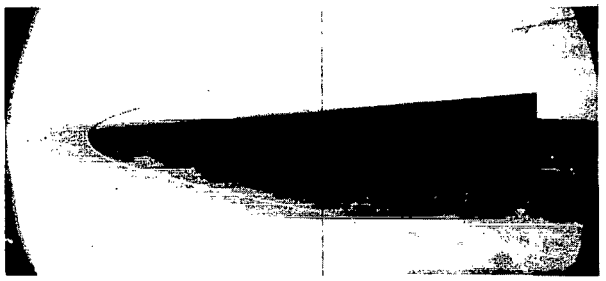

$\alpha = 0^0$

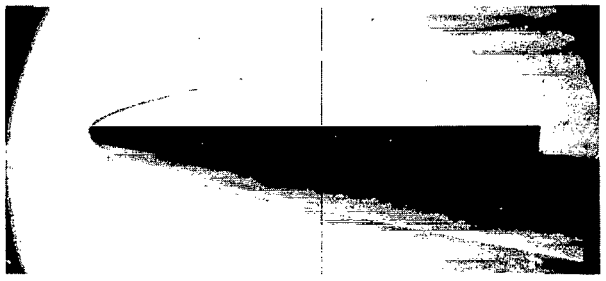

$\alpha = 5^0$

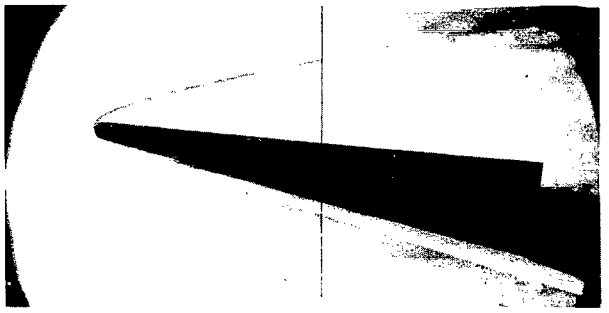

$\alpha = 10^0$

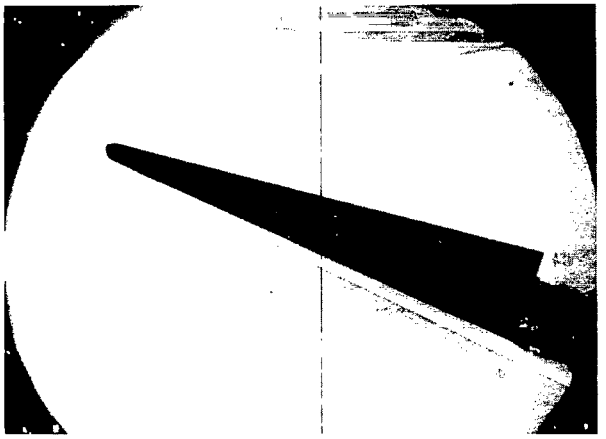

$\alpha = 20^0$

$\alpha = 30^0$

(c) Blunt nose cone. d/D = 0.20. L-66-1109

Figure 13.- Continued.

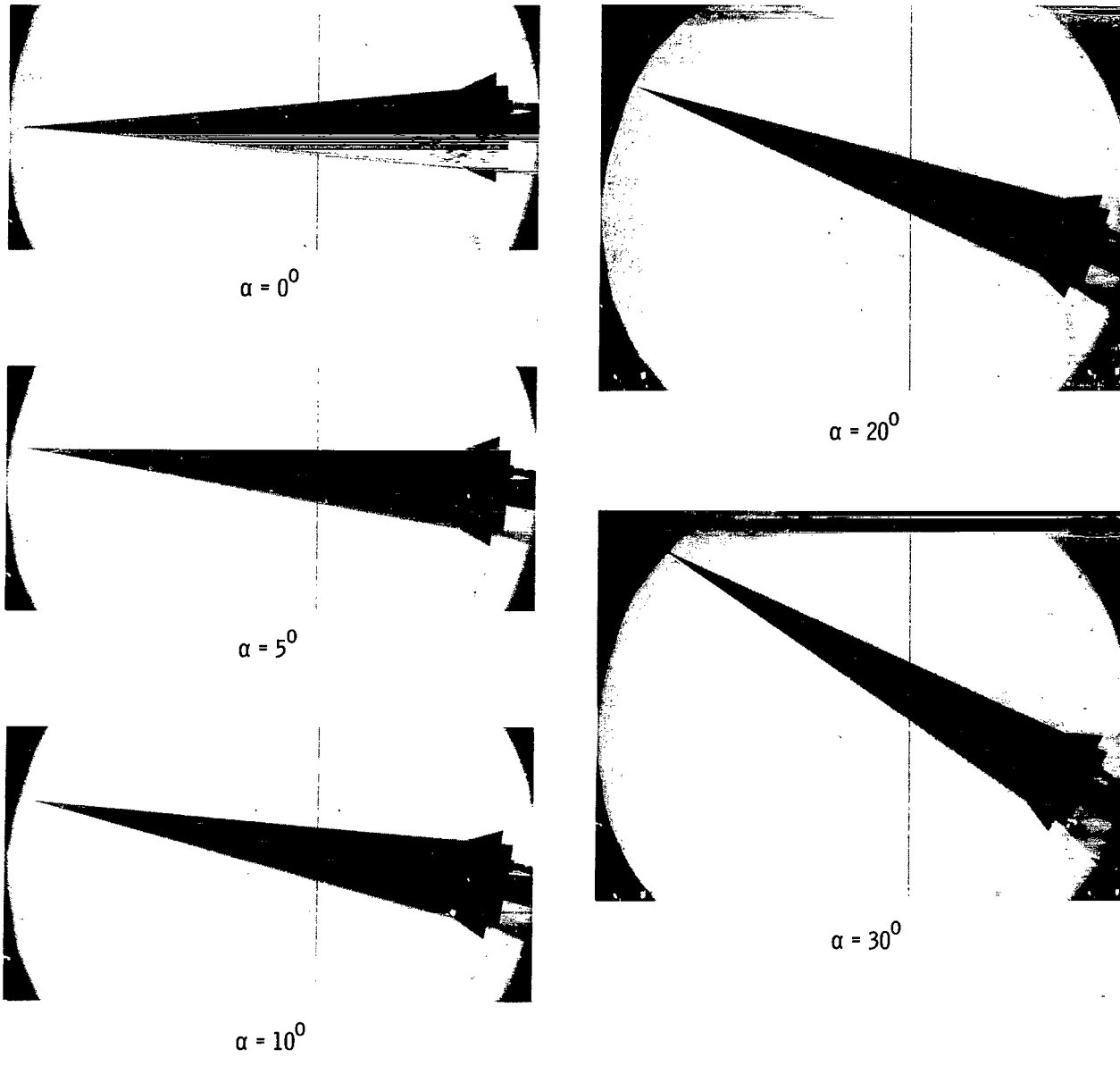

(d) Sharp nose cone; sharp L.E. controls. $A_f/A_r = 0.086$; $\delta_h = \delta_v = 0^0$. L-66-1110

Figure 13.- Continued.

$\alpha = 0^0$

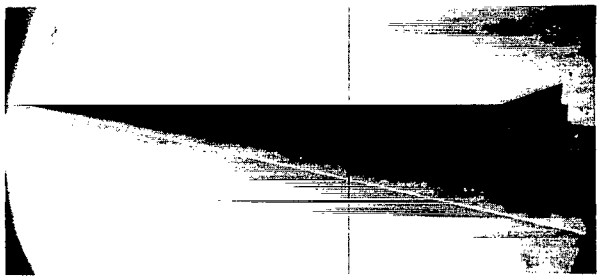

$\alpha = 5^0$

$\alpha = 10^0$

$\alpha = 20^0$

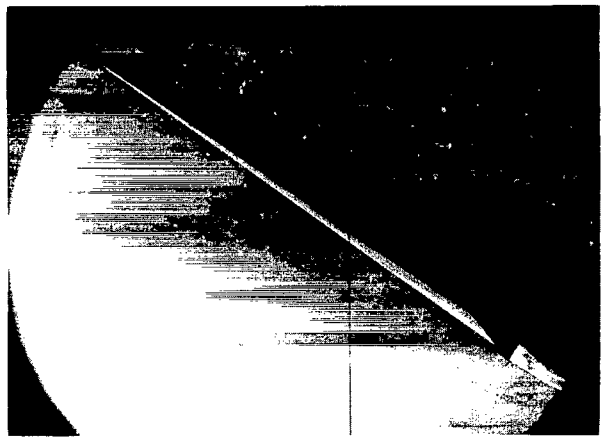

$\alpha = 30^0$

(e) Sharp nose cone; sharp L.E. controls. $A_f/A_r = 0.182$; $\delta_h = \delta_v = 0^0$. L-66-1111

Figure 13.- Continued.

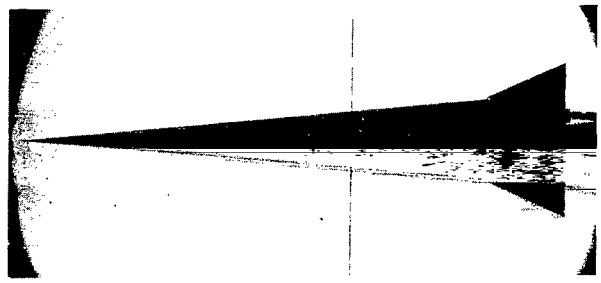

$\alpha = 0^0$

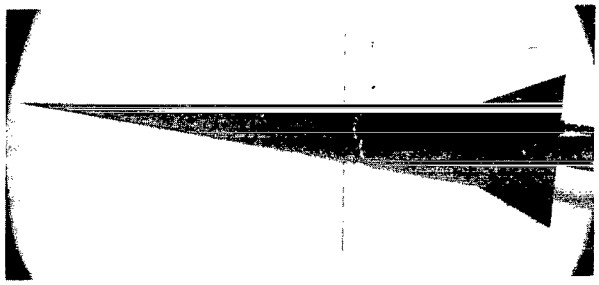

$\alpha = 5^0$

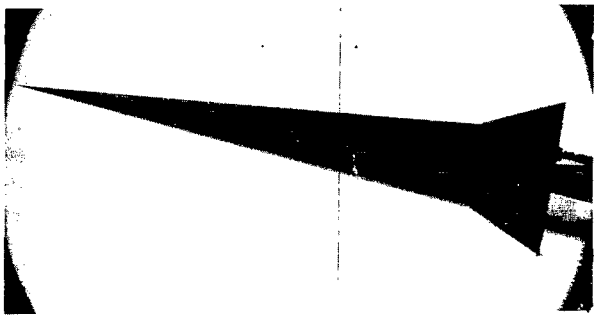

$\alpha = 10^0$

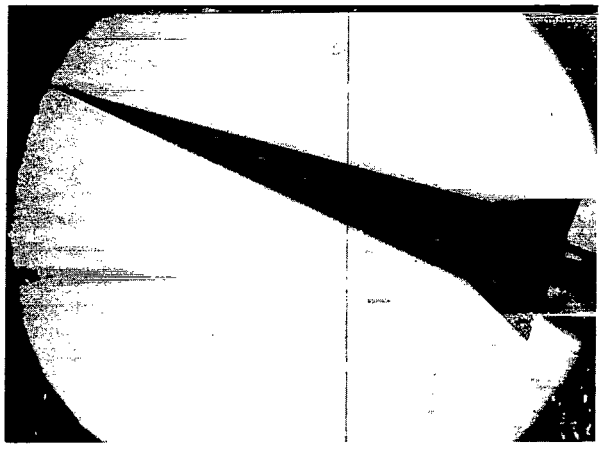

$\alpha = 20^0$

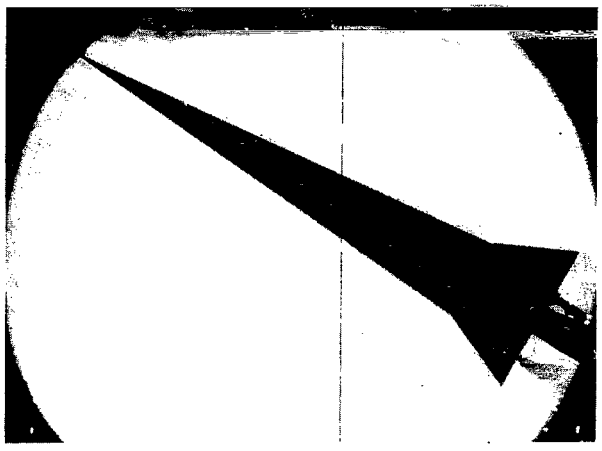

$\alpha = 30^0$

(f) Sharp nose cone; sharp L.E. controls. $A_f/A_r = 0.343$; $\delta_h = \delta_v = 0^0$. L-66-1112

Figure 13.- Concluded.

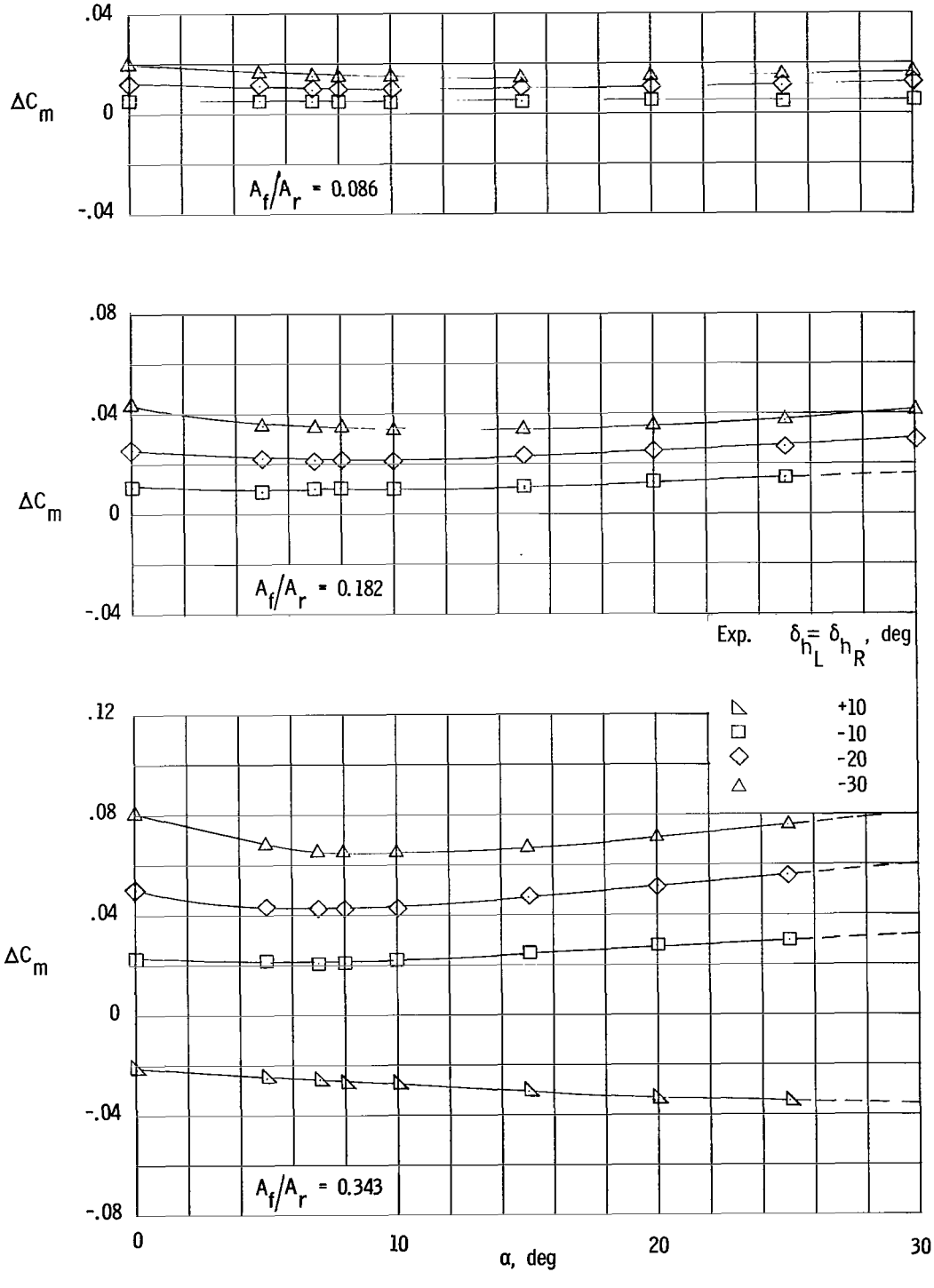

Figure 14.- Incremental pitching moment due to control deflection for various sharp L.E. controls on sharp 5^0 cone.

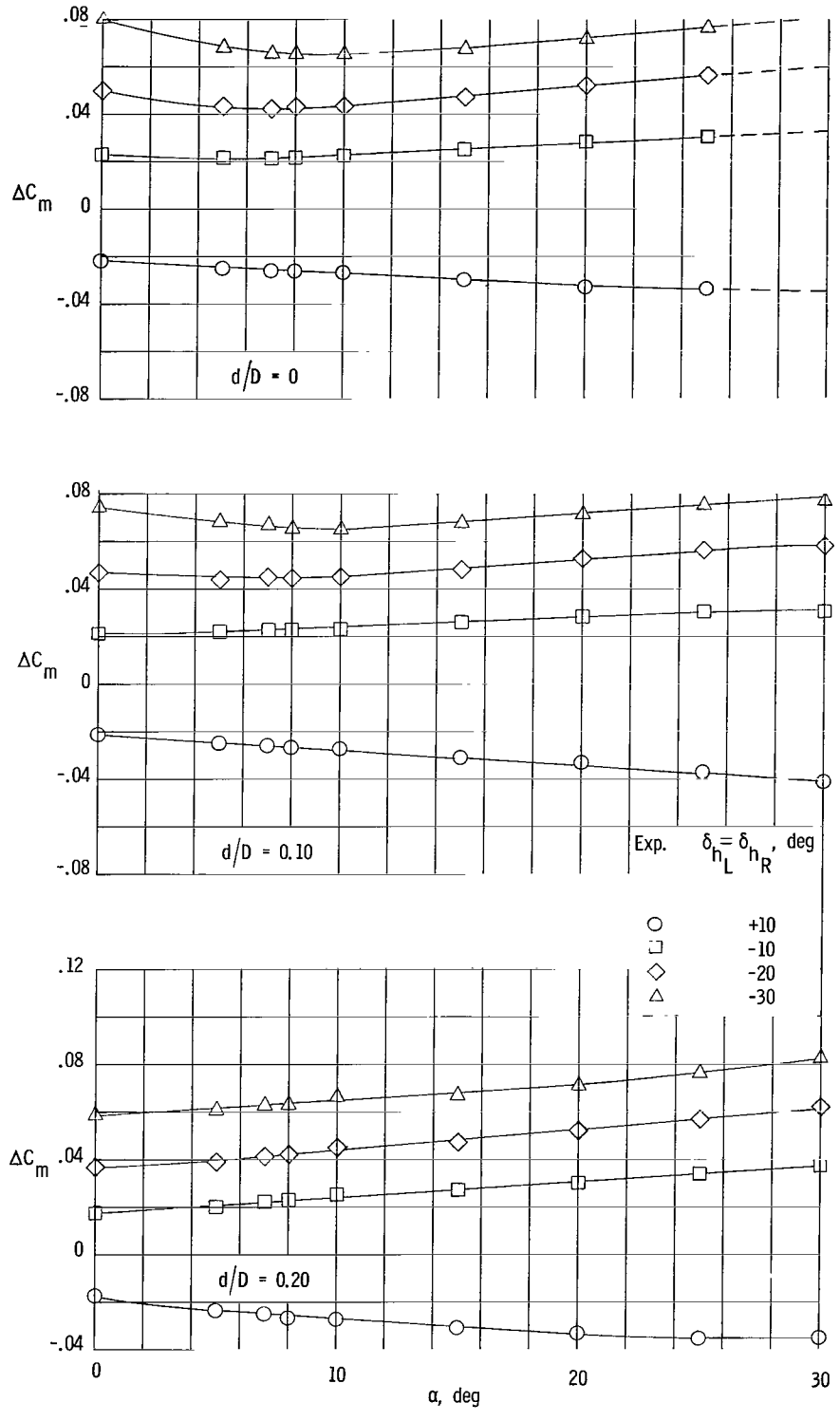

Figure 15.- Incremental pitching moment due to control deflection for various blunt 5° cones. A_f/A_r = 0.343.

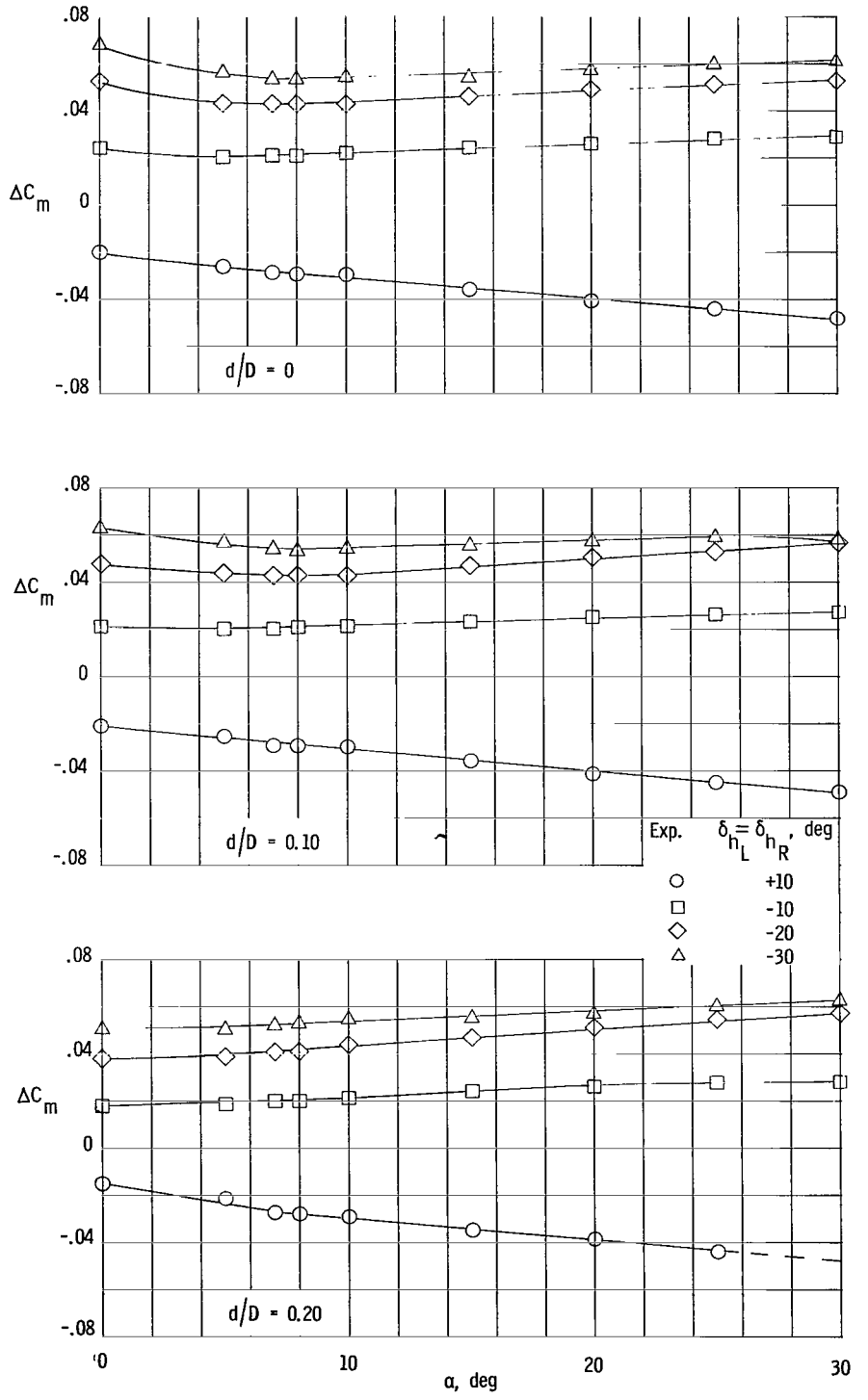

Figure 16.- Incremental pitching moment due to control deflection of blunt L.E. controls for various blunt 5° cones. $A_f/A_r = 0.359$.

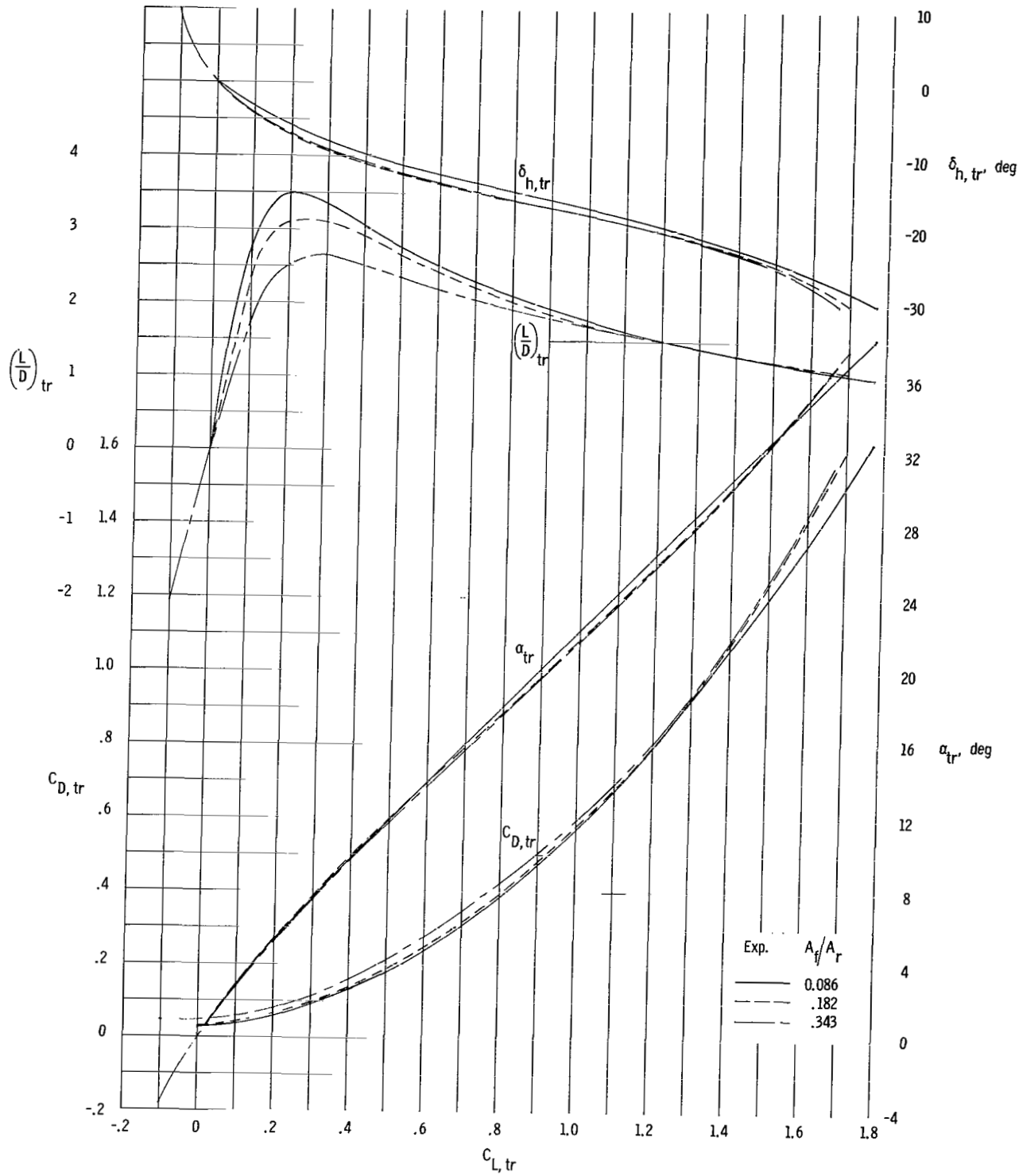

Figure 17.- Longitudinal characteristics at trim of sharp 5° cone with various sharp L.E. controls.

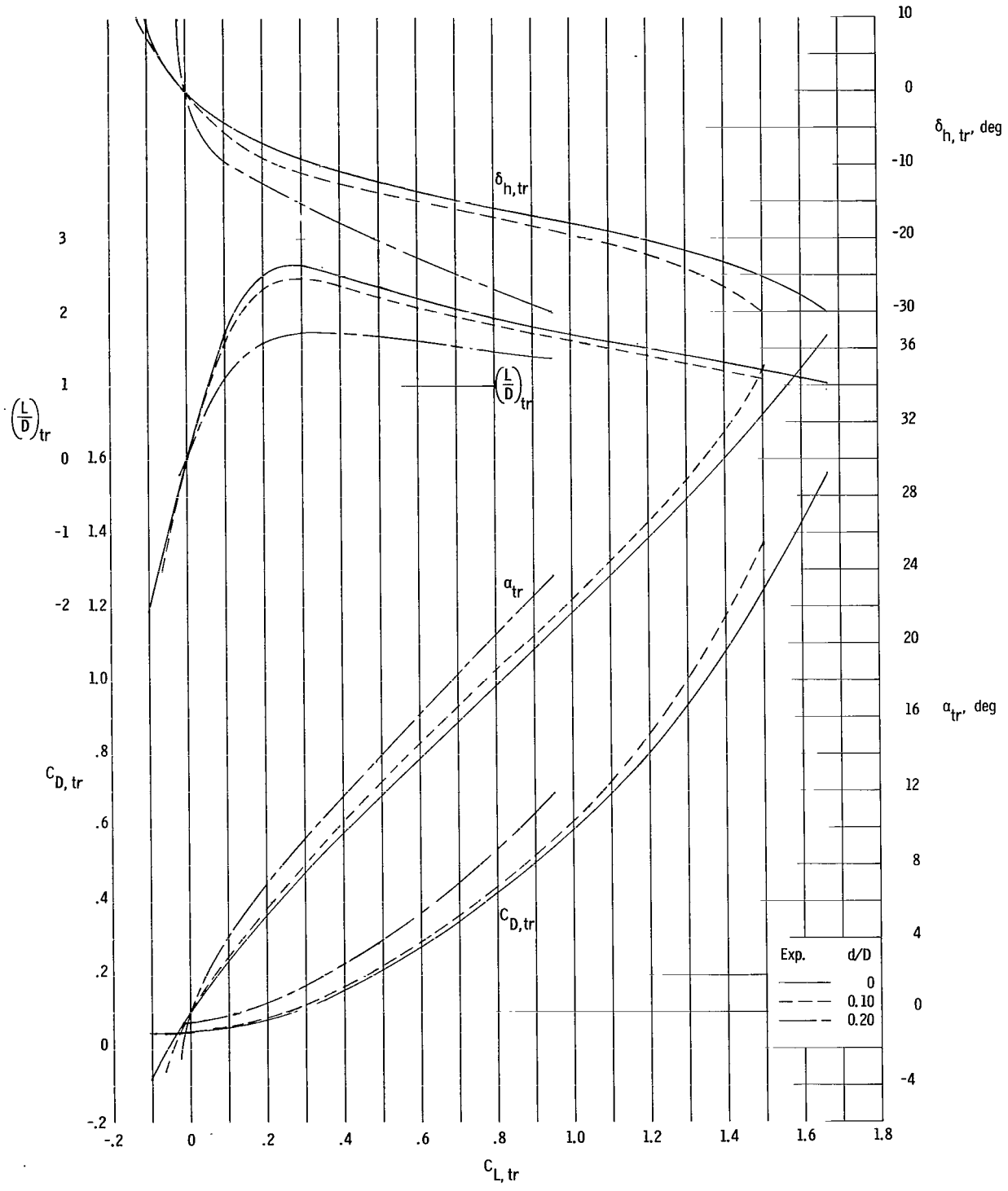

Figure 18.- Longitudinal aerodynamic characteristics at trim of 5° cone having sharp L.E. controls and various nose bluntness ratios. $A_f/A_r = 0.343$.

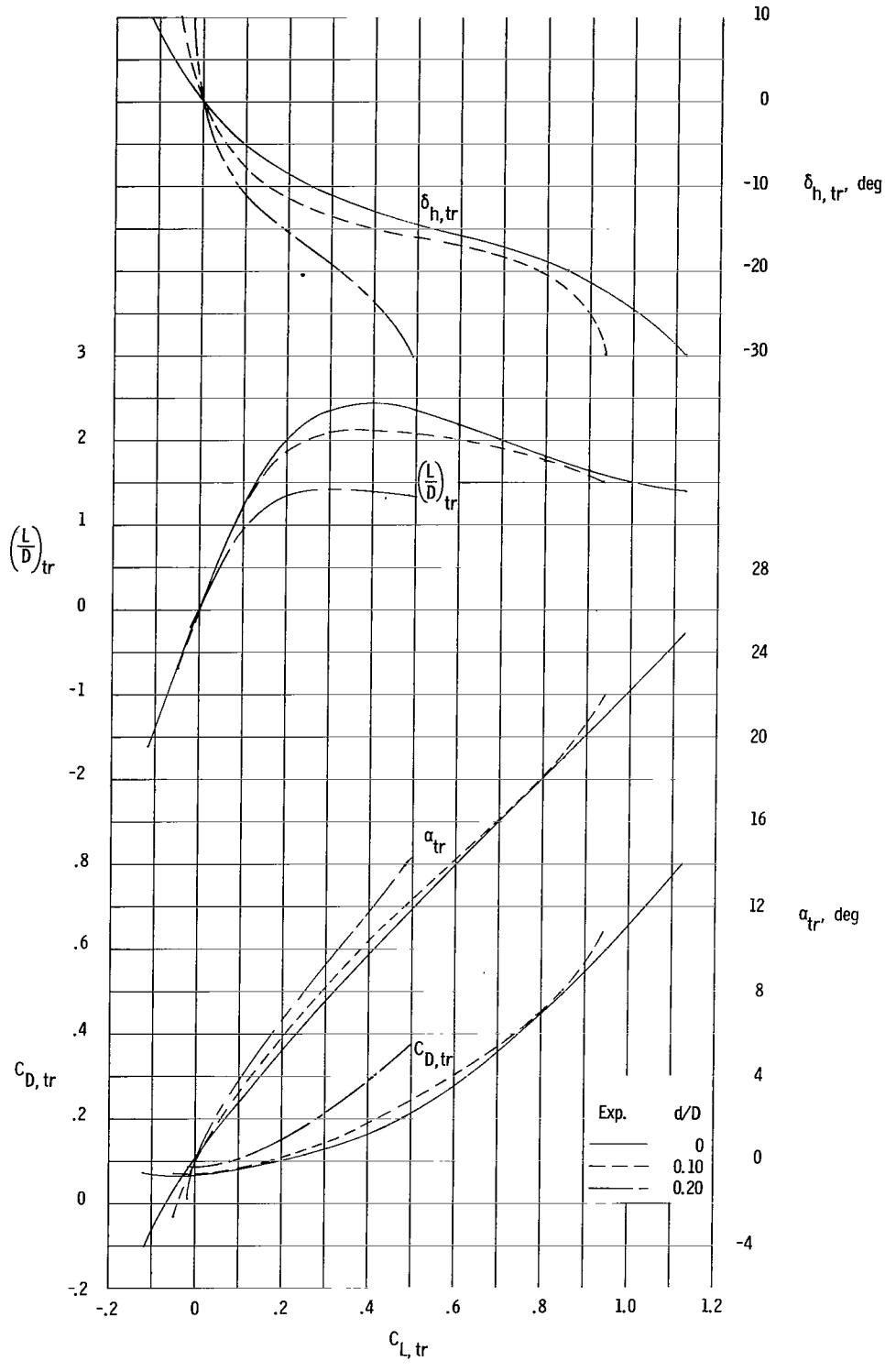

Figure 19.- Longitudinal aerodynamic characteristics at trim of 5° cone having blunt L.E. controls and various nose bluntness ratios. $A_f/A_r = 0.359$.

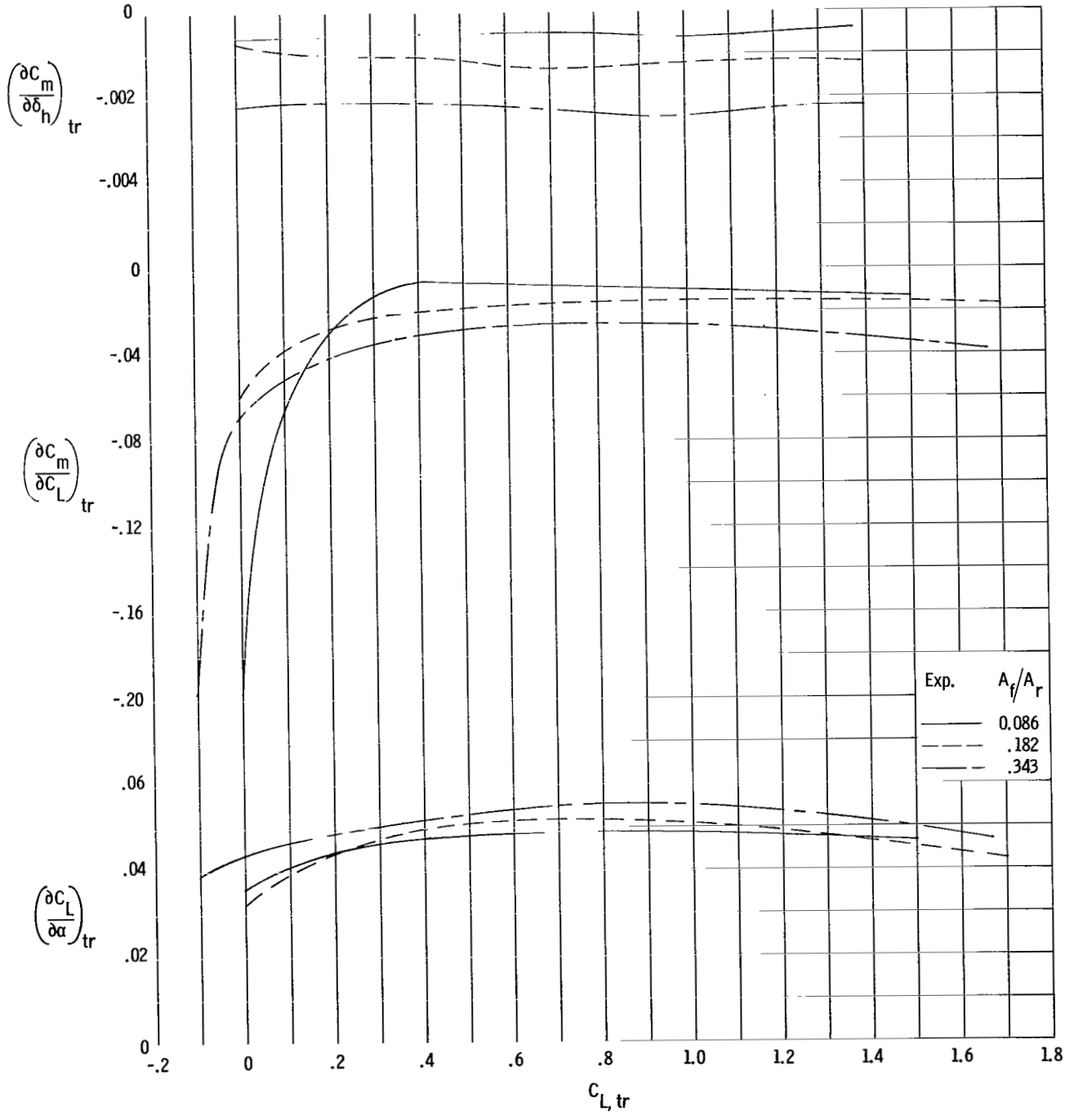

Figure 20.- Longitudinal stability parameters at trim of sharp 5° cone having various sharp L.E. controls.

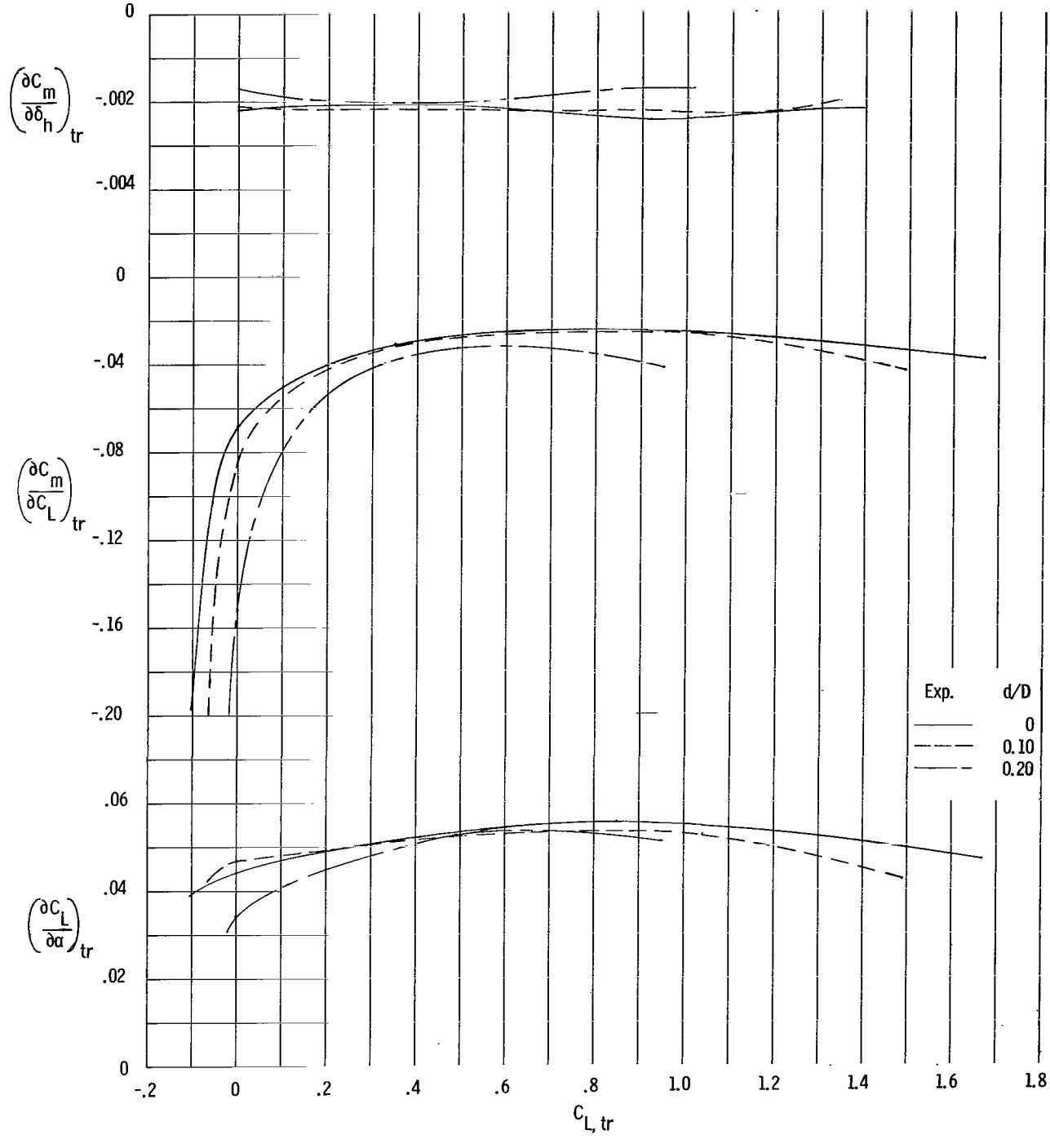

Figure 21.- Longitudinal stability parameters at trim of 5^0 cone having sharp L.E. controls and various nose bluntness ratios. $A_f/A_r = 0.343$.

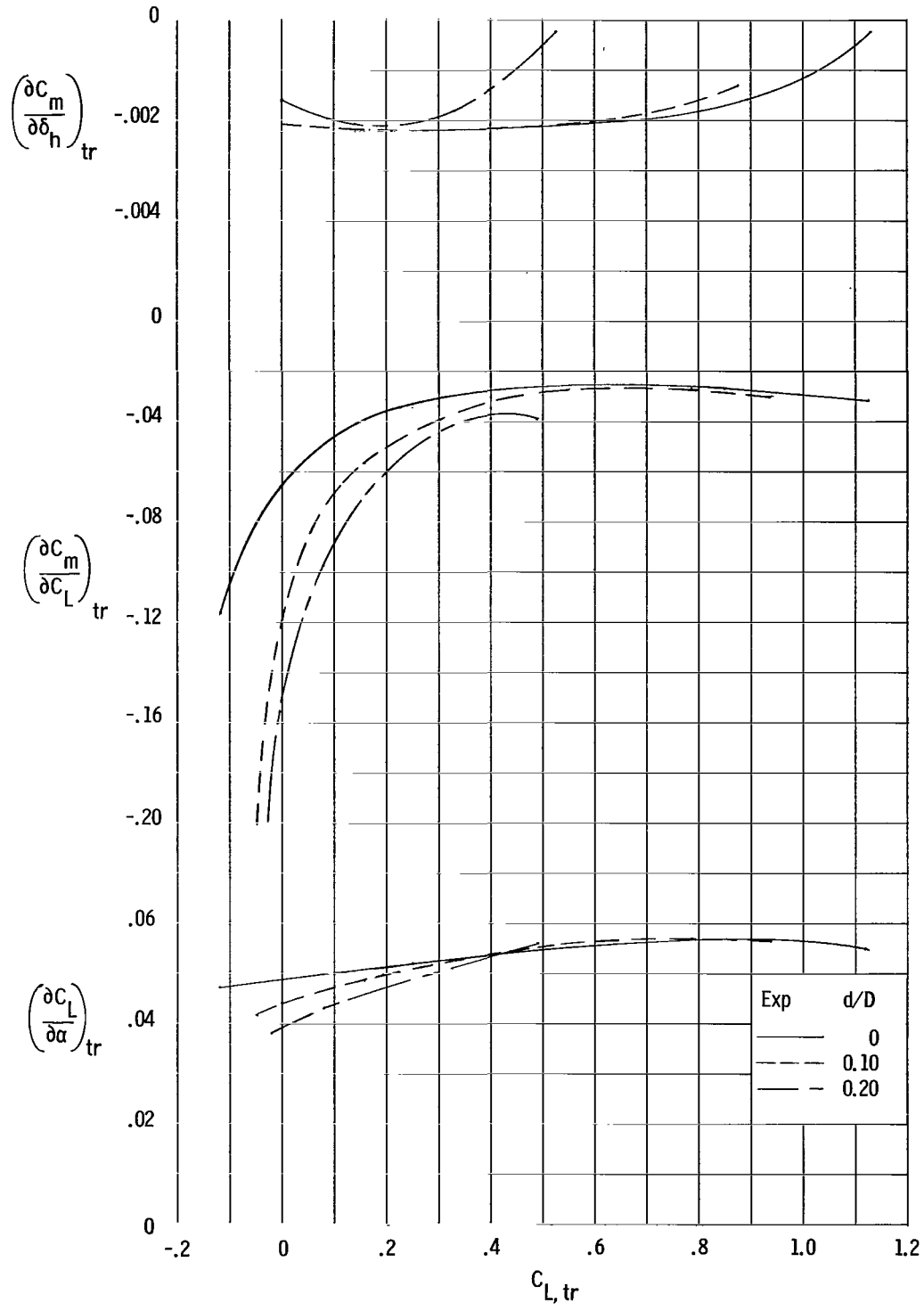

Figure 22.- Longitudinal stability parameters at trim of 5° cone having blunt L.E. controls and various nose bluntness ratios. $A_f/A_r = 0.359$.

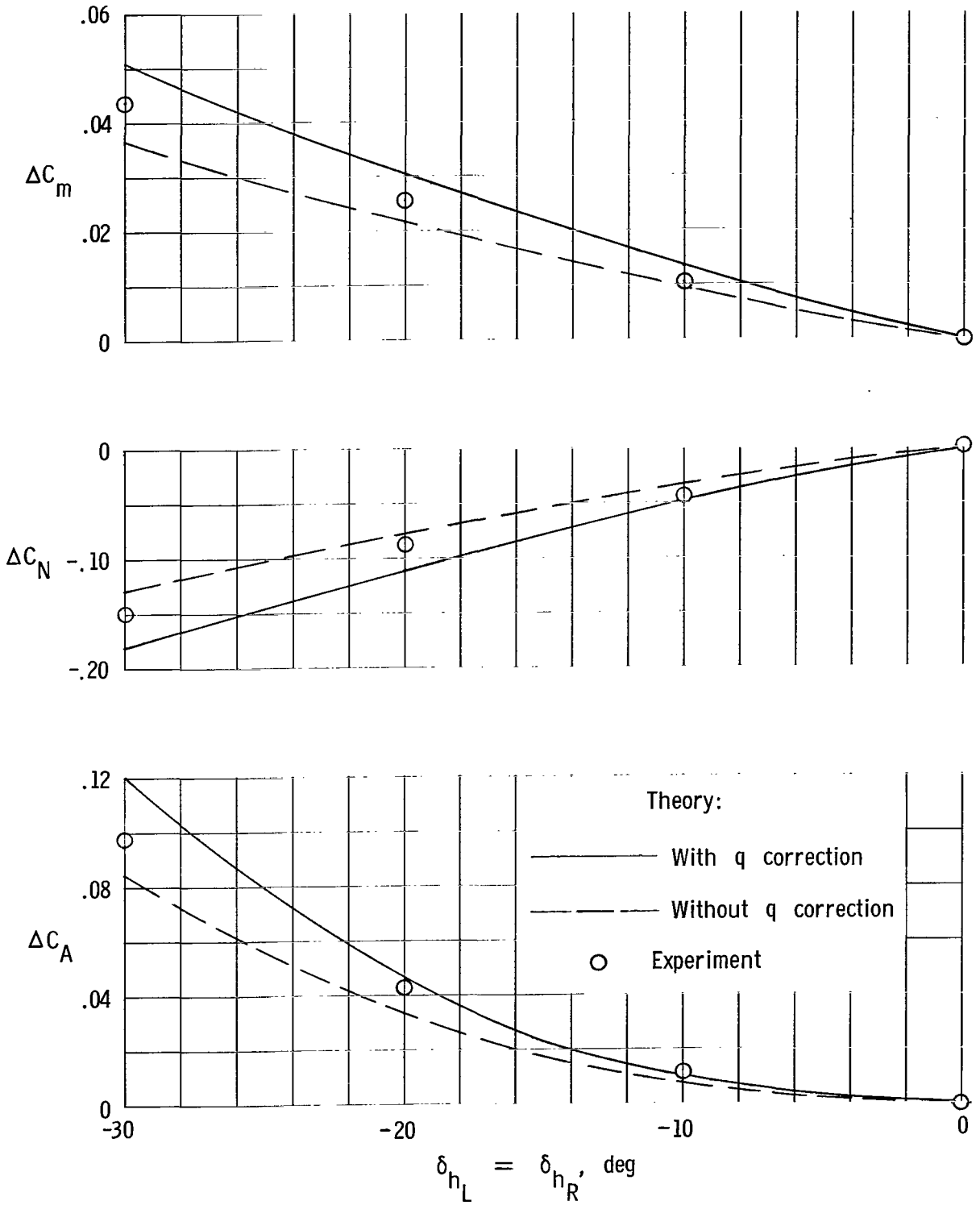

Figure 23.- Comparison of experimental and theoretical incremental longitudinal control characteristics. $\alpha = 0^0$; $A_f/A_r = 0.182$; $d/D = 0$.

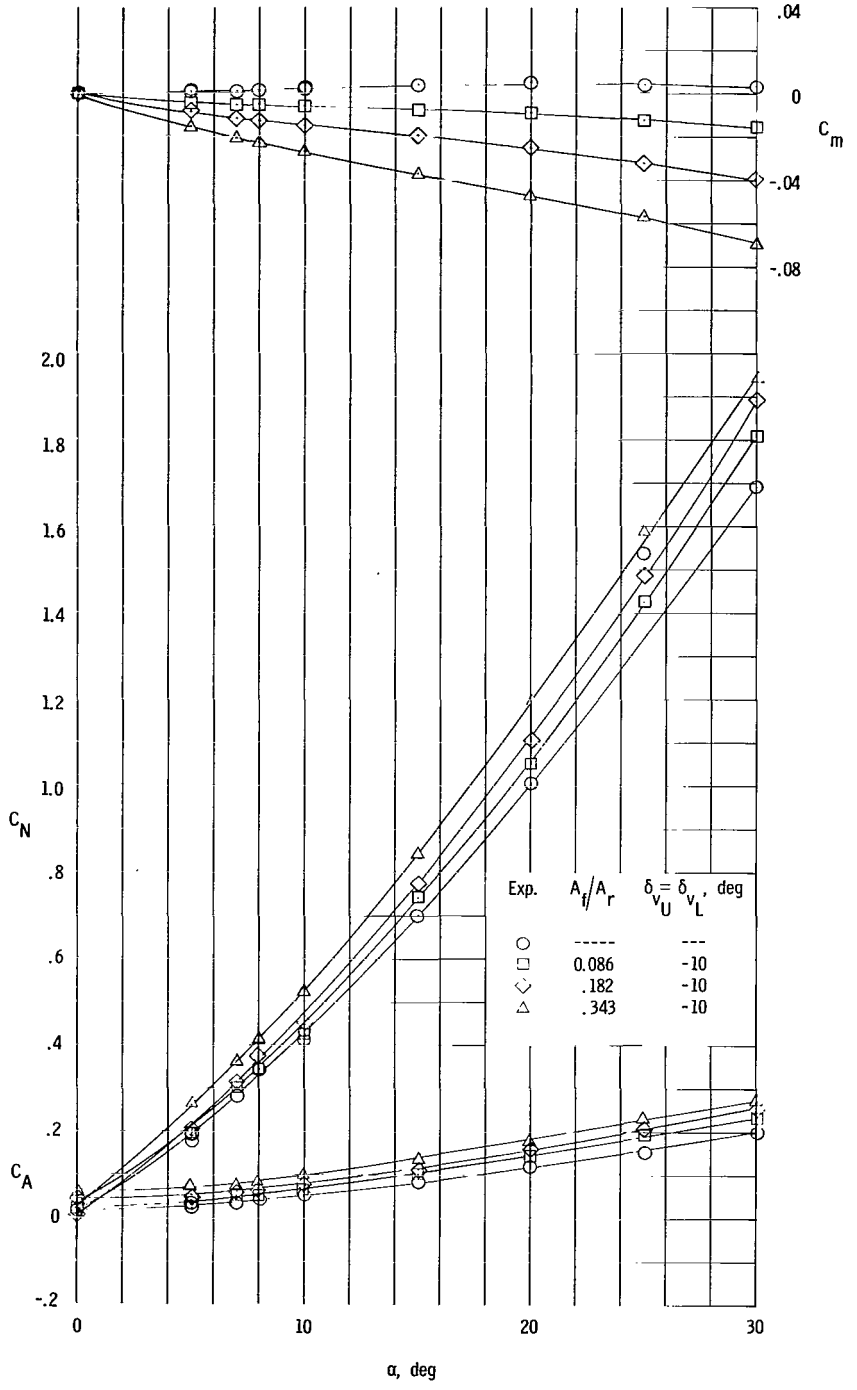

(a) Pitching-moment, normal-force, and axial-force coefficients.

Figure 24.- Longitudinal, lateral, and directional characteristics of sharp 5° cone having yaw control and various sharp L.E. controls. $\delta_h = 0°$.

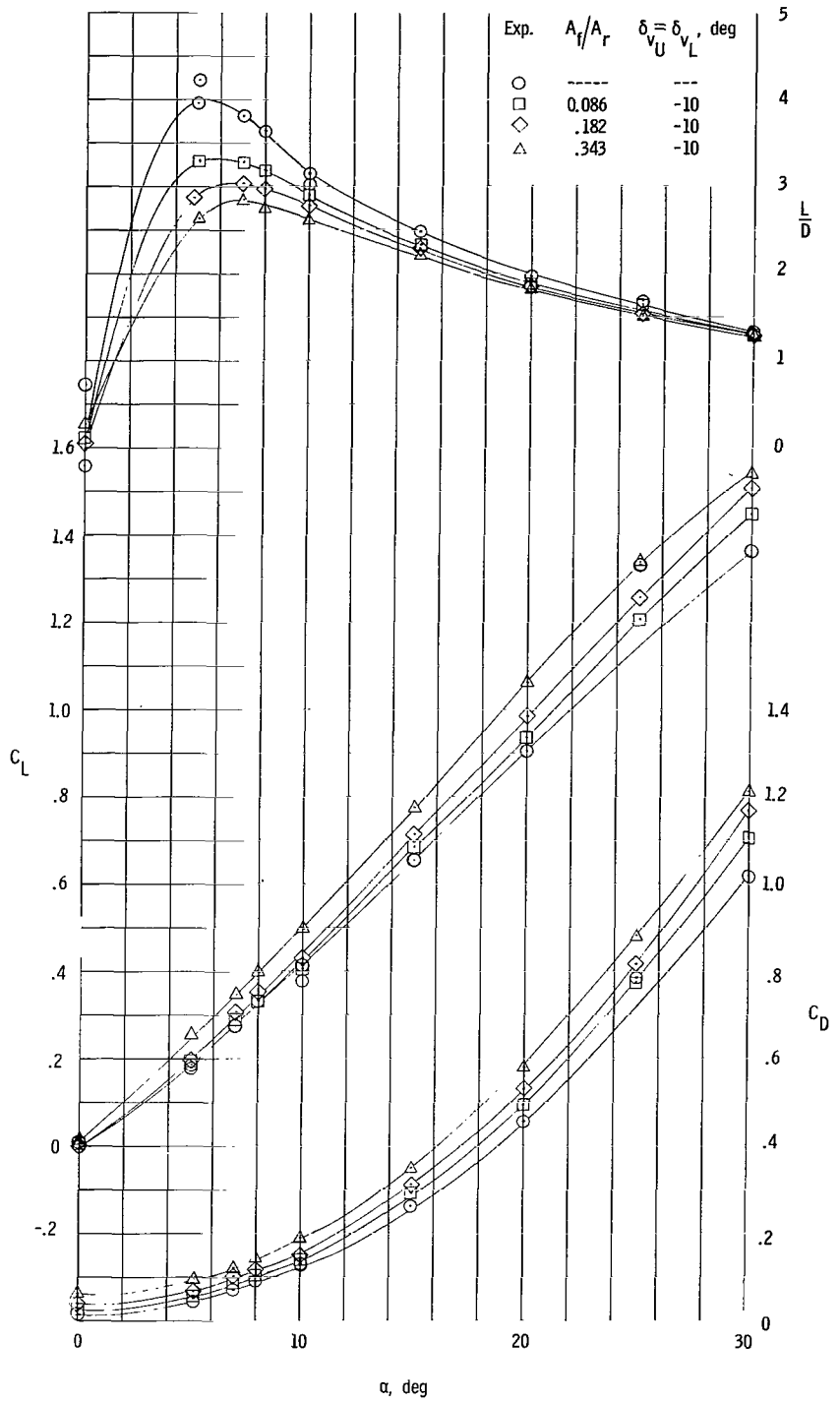

(b) Lift and drag coefficients and lift-drag ratio.

Figure 24.- Continued.

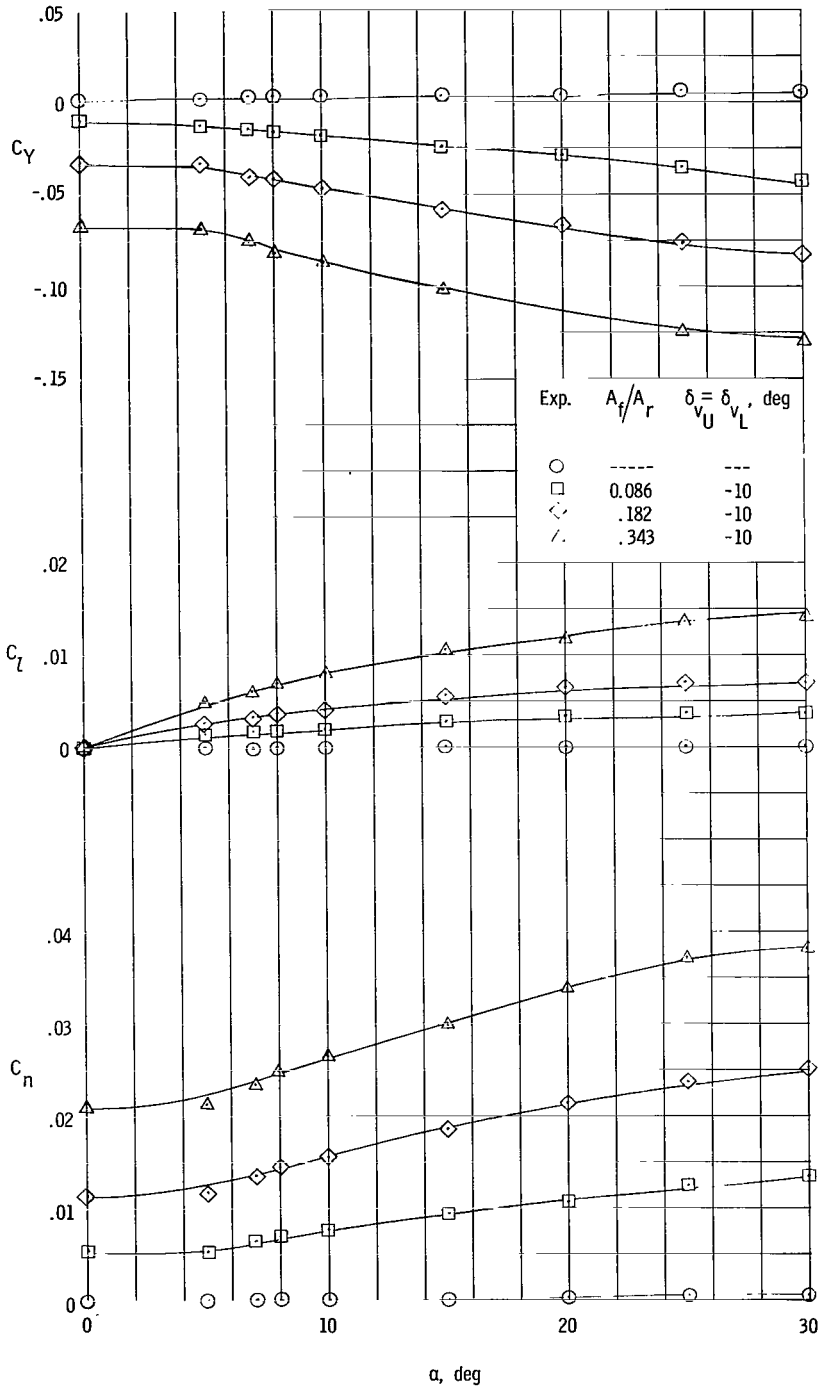

(c) Side-force, rolling-moment, and yawing-moment coefficients.

Figure 24.- Concluded.

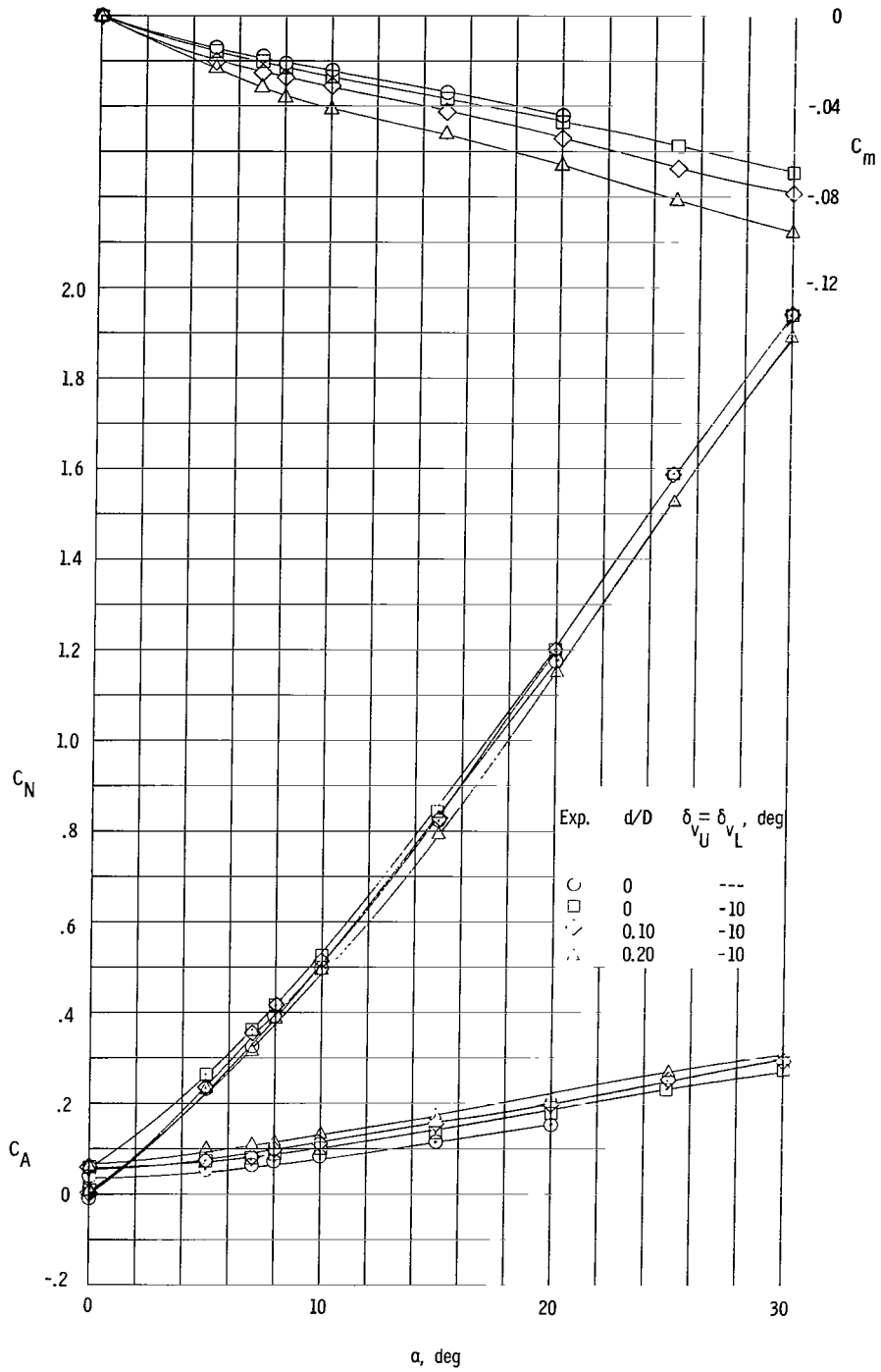

(a) Pitching-moment, normal-force, and axial-force coefficients.

Figure 25.- Longitudinal, lateral, and directional characteristics of 5^0 cone having yaw control, various nose bluntness ratios, and sharp L.E. controls. $A_f/A_r = 0.343$; $\delta_h = 0^0$.

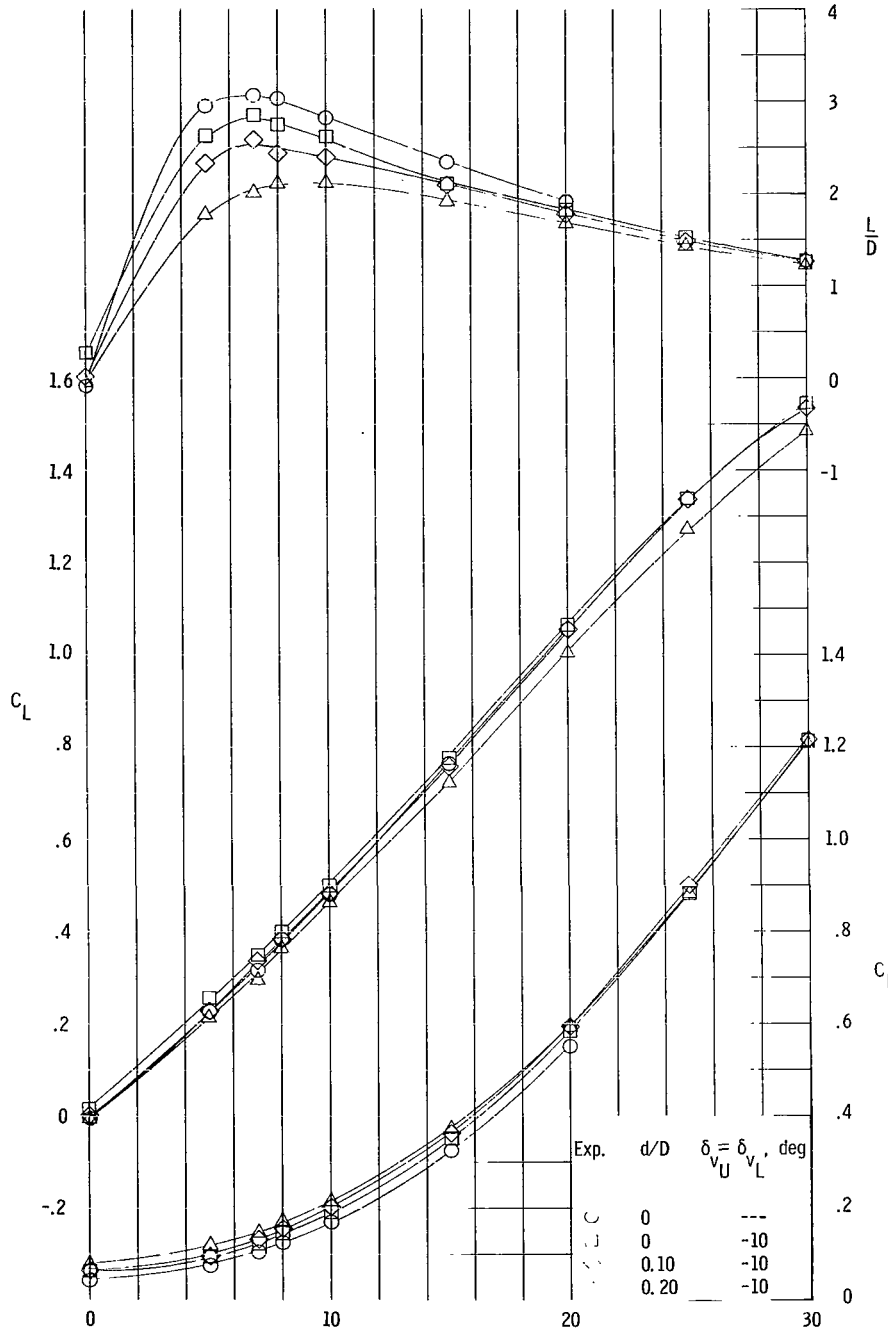

(b) Lift and drag coefficients and lift-drag ratio.

Figure 25.- Continued.

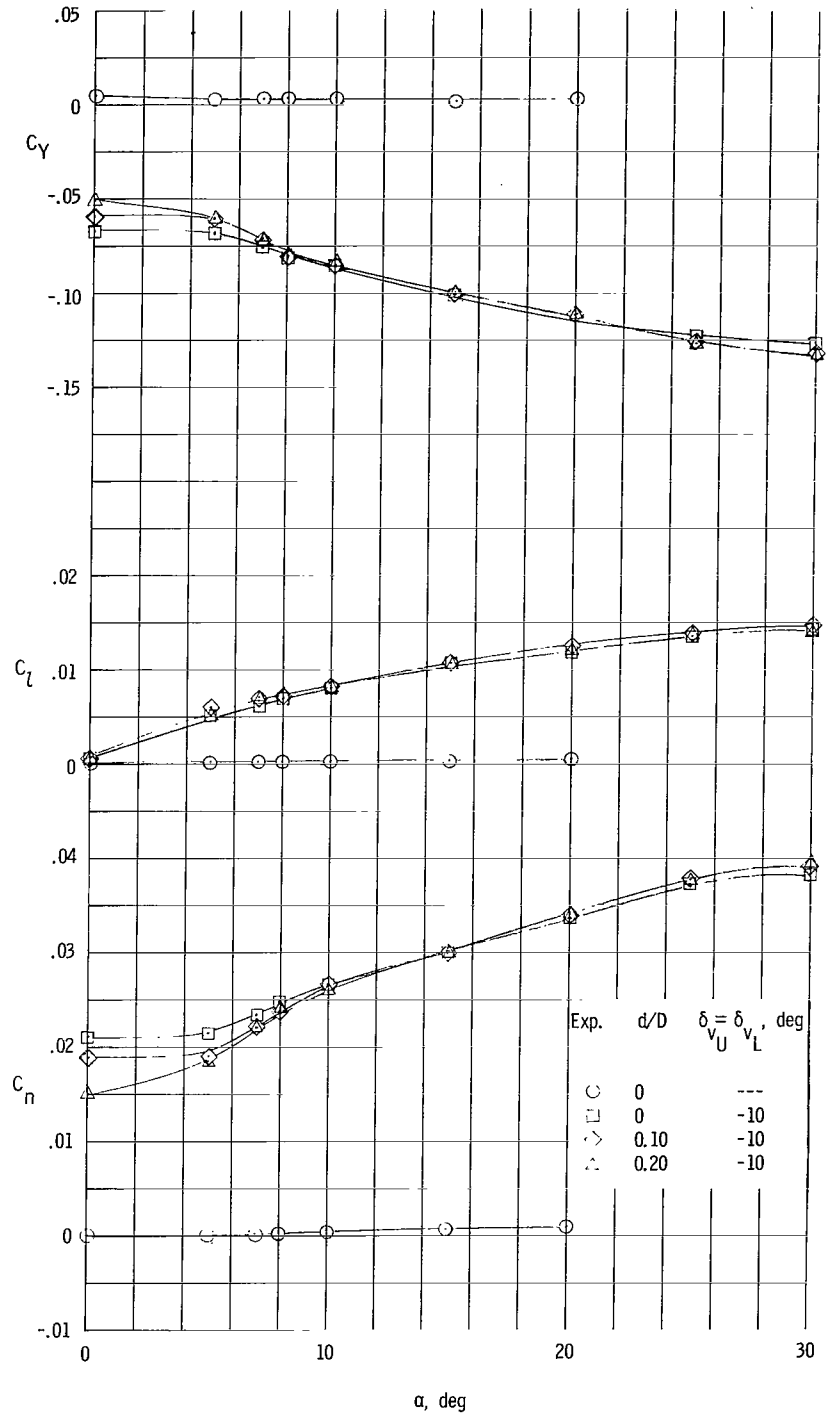

(c) Side-force, rolling-moment, and yawing-moment coefficients.

Figure 25.- Concluded.

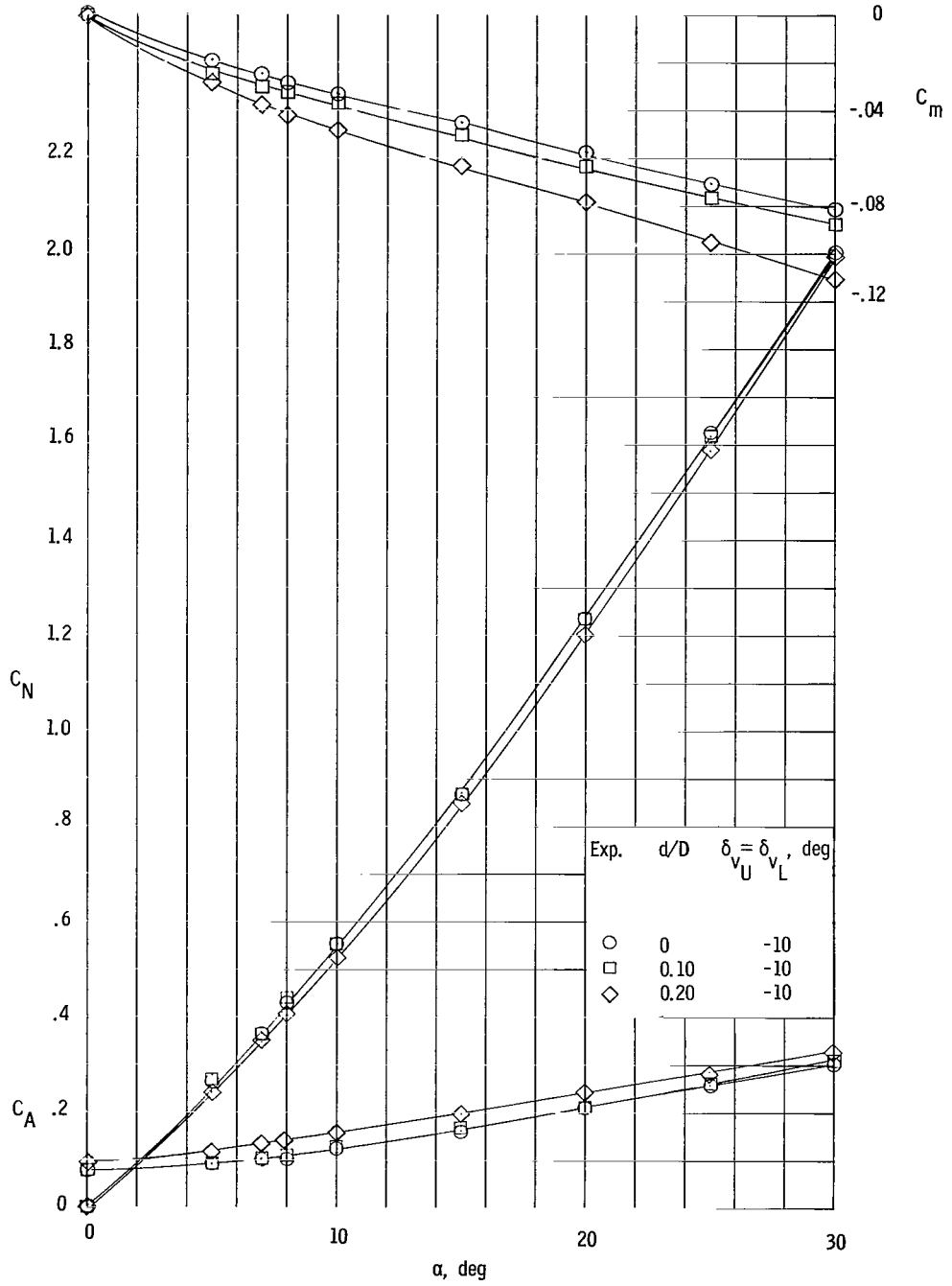

(a) Pitching-moment, normal-force, and axial-force coefficients.

Figure 26.- Longitudinal, lateral, and directional characteristics of 5^0 cone having yaw control, various nose bluntness ratios, and blunt L.E. controls. $A_f/A_r = 0.359$; $\delta_h = 0^0$.

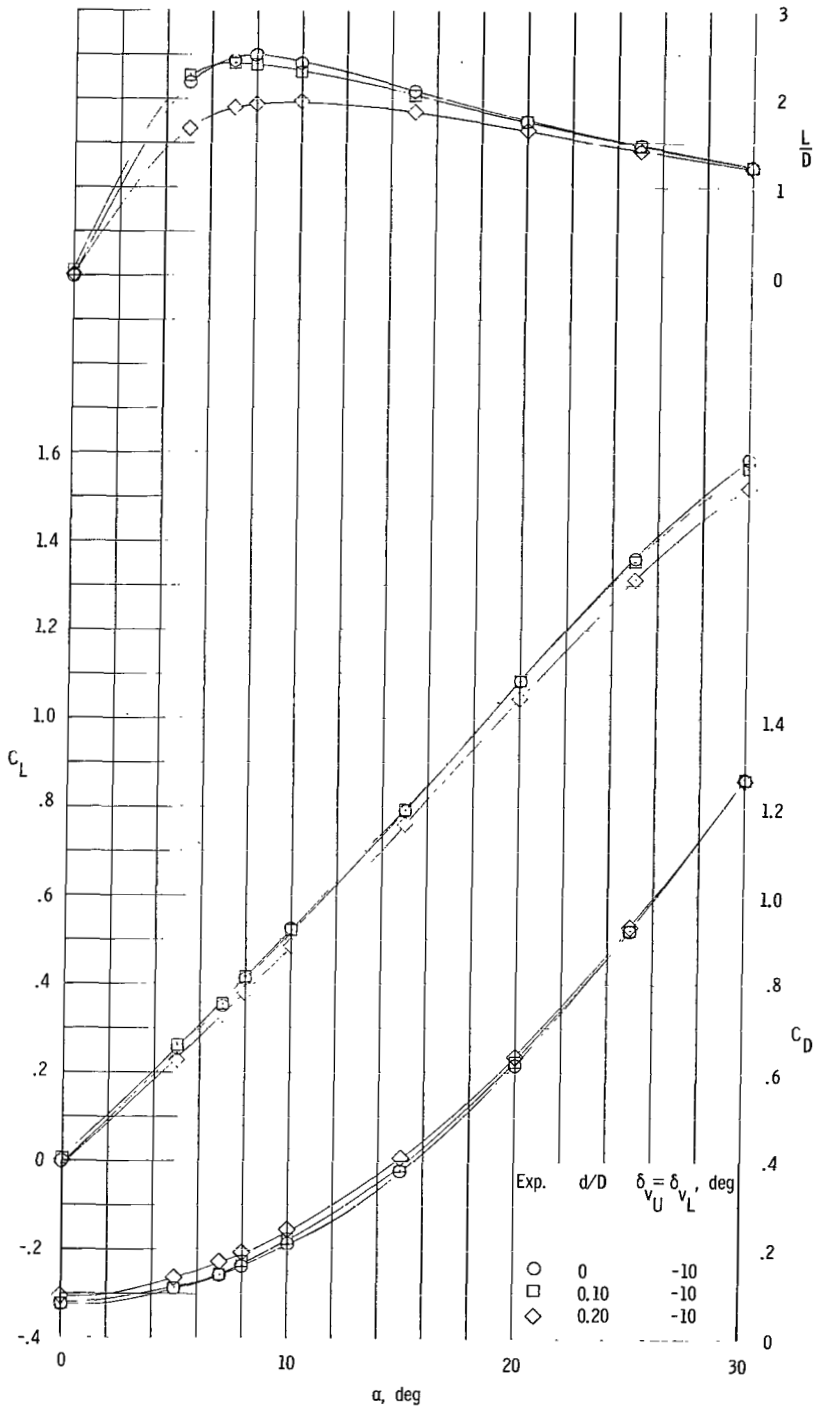

(b) Lift and drag coefficients and lift-drag ratio.

Figure 26.- Continued.

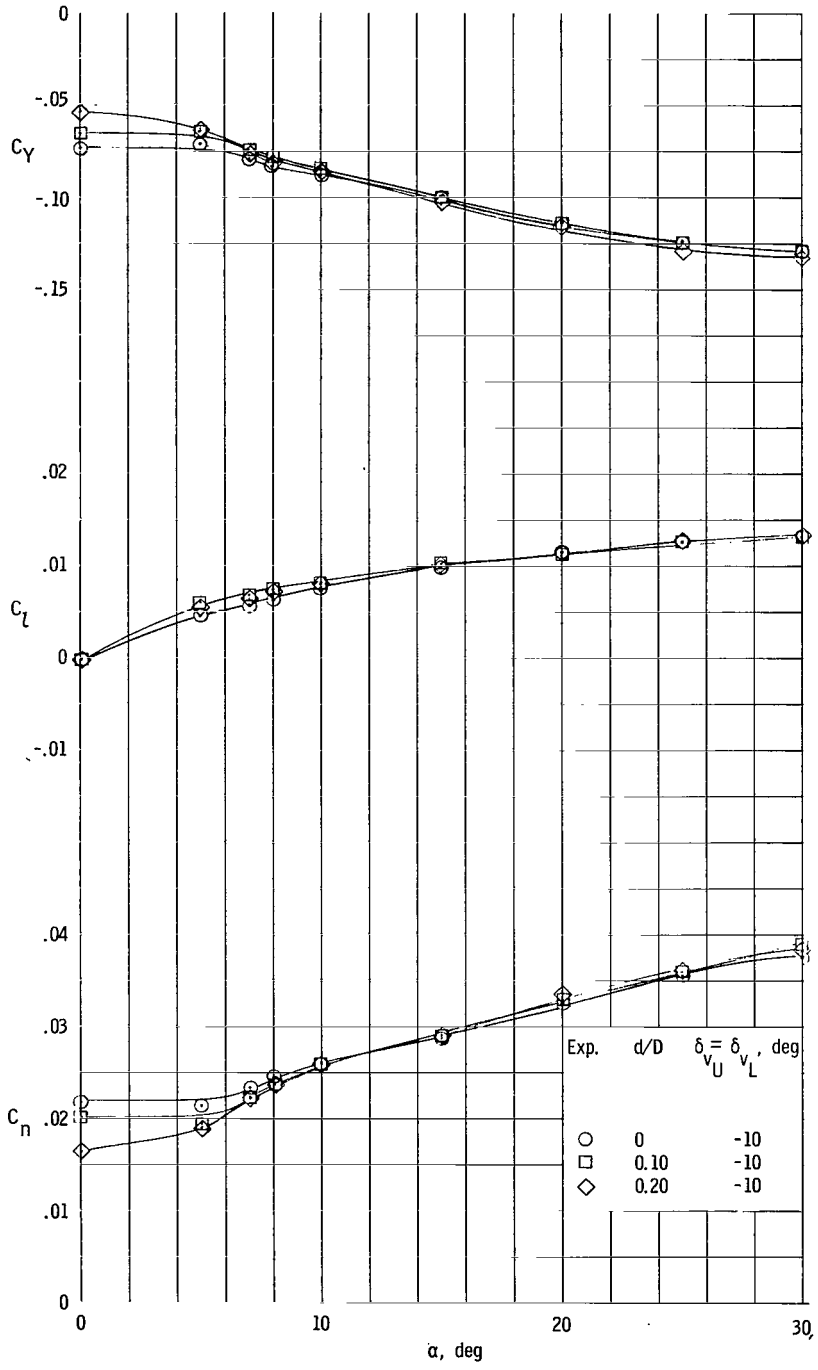

(c) Side-force, rolling-moment, and yawing-moment coefficients.

Figure 26.- Concluded.

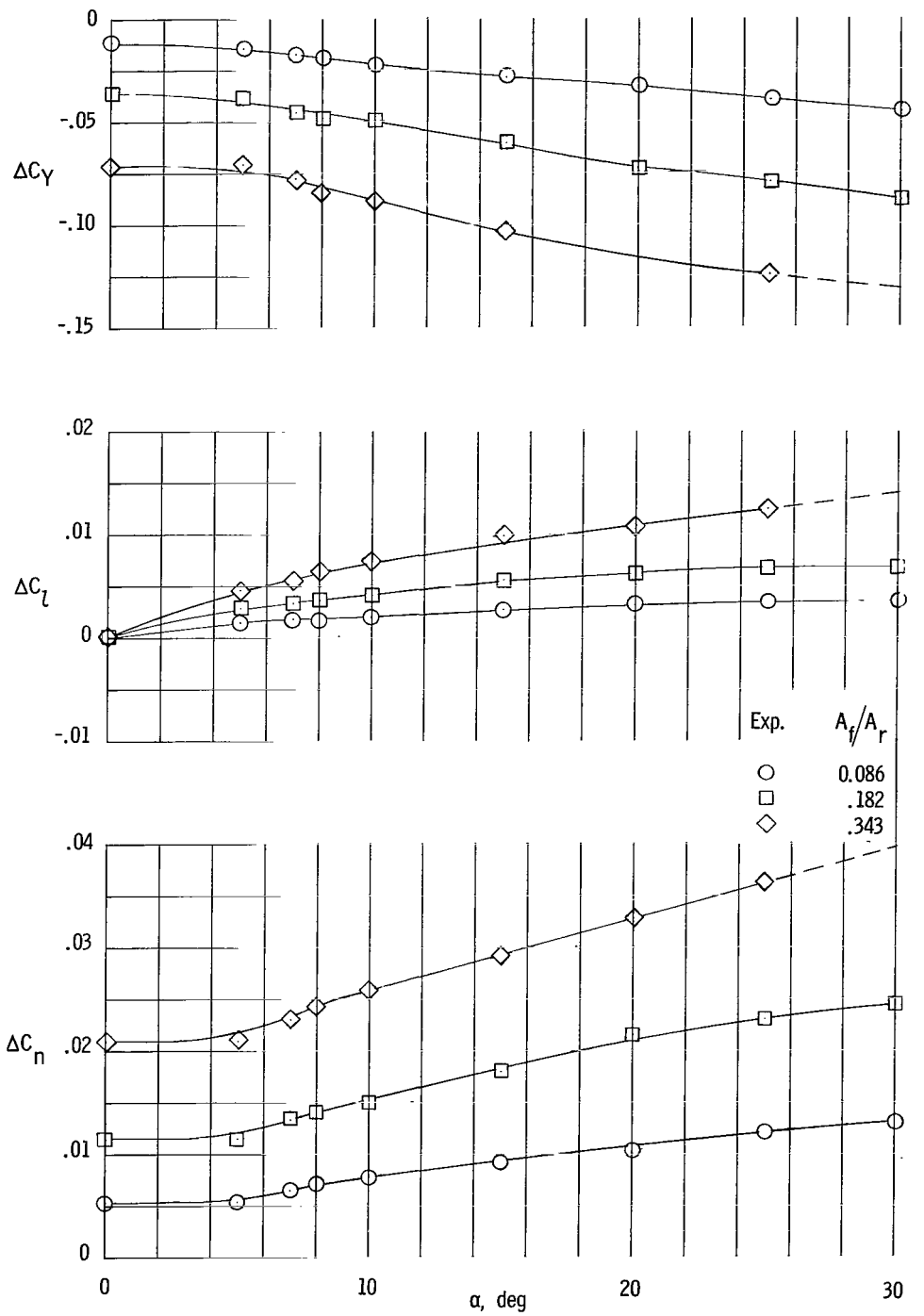

Figure 27.- Incremental lateral-directional characteristics of sharp 5^0 cone due to yaw control for various sharp L.E. controls. M = 6.9; $R = 2.8 \times 10^6$.

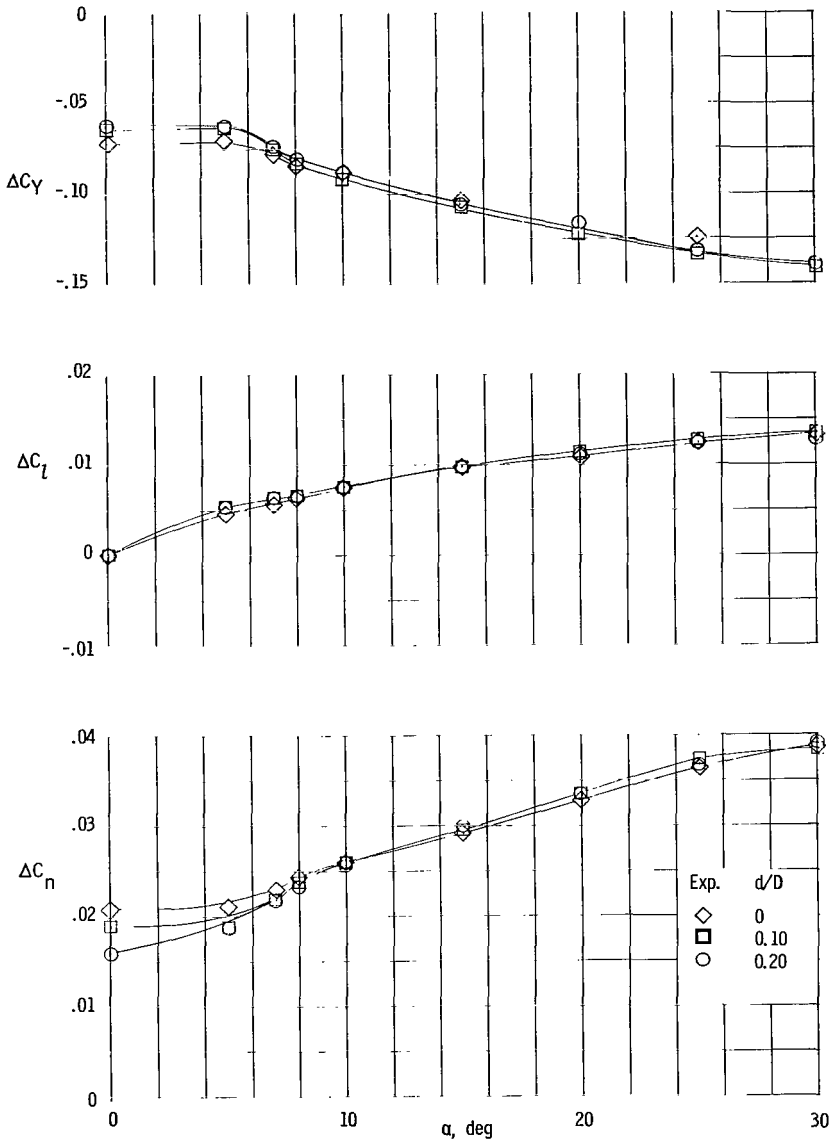

Figure 28.- Incremental lateral-directional characteristics of 5^0 cone due to yaw control for sharp L.E. controls and various nose bluntness ratios. $A_f/A_r = 0.343$.

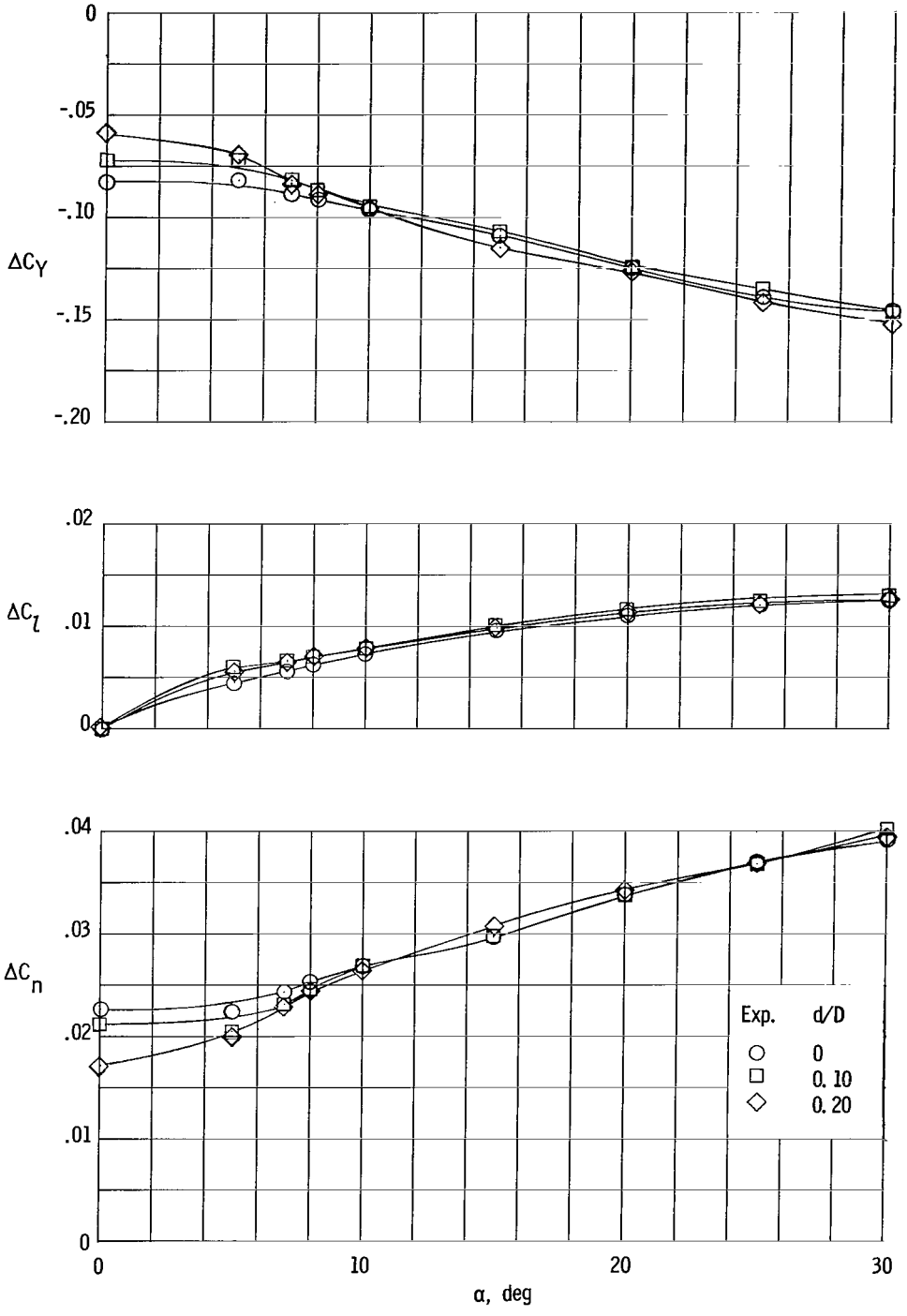

Figure 29.- Incremental lateral-directional characteristics of 5° cone due to yaw control for blunt L.E. controls and various nose bluntness ratios. $A_f/A_r = 0.359$.

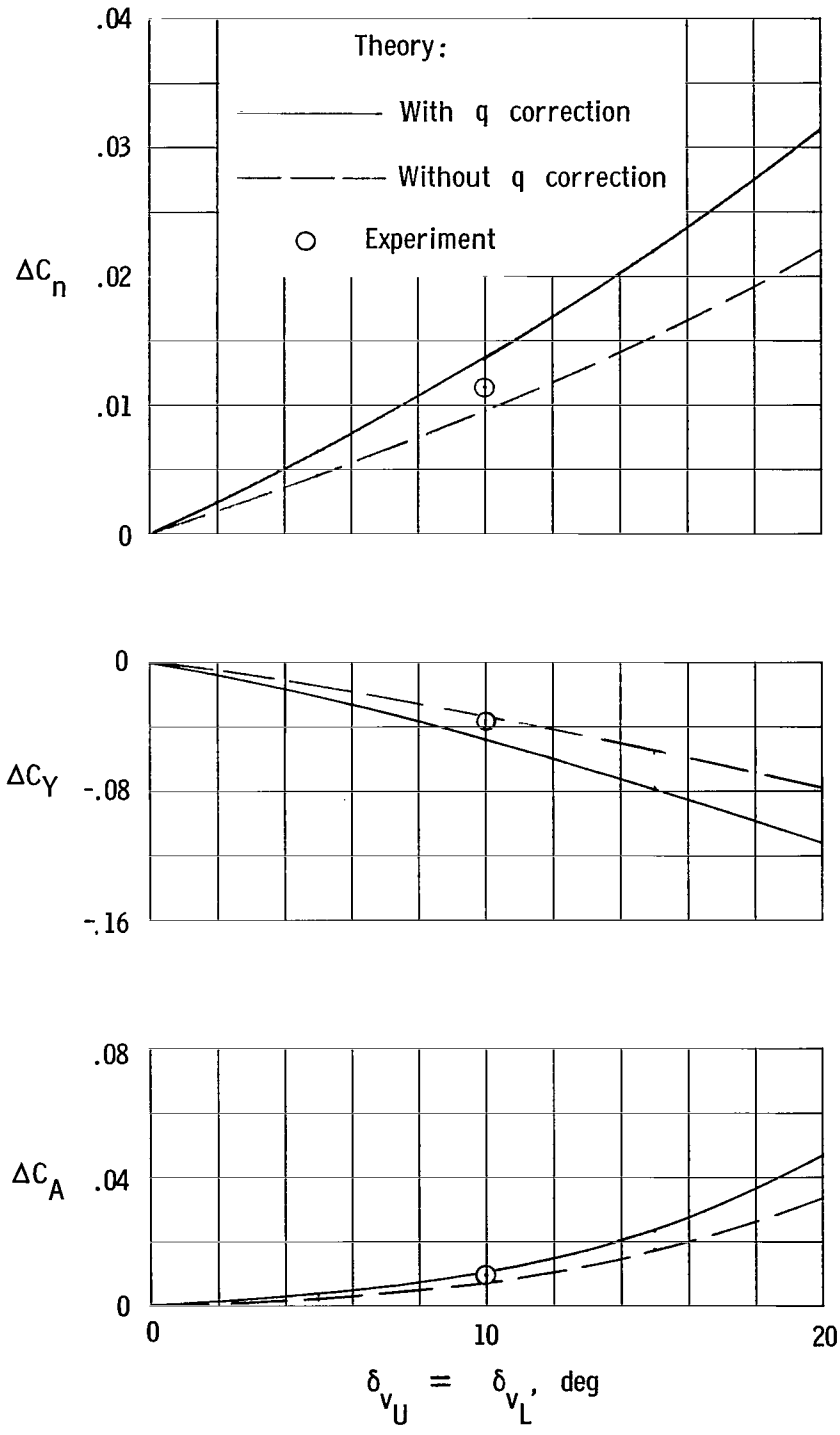

Figure 30.- Comparison of experimental and theoretical incremental yaw control characteristics. $\alpha = 0^0$; $A_f/A_r = 0.182$; $d/D = 0$.

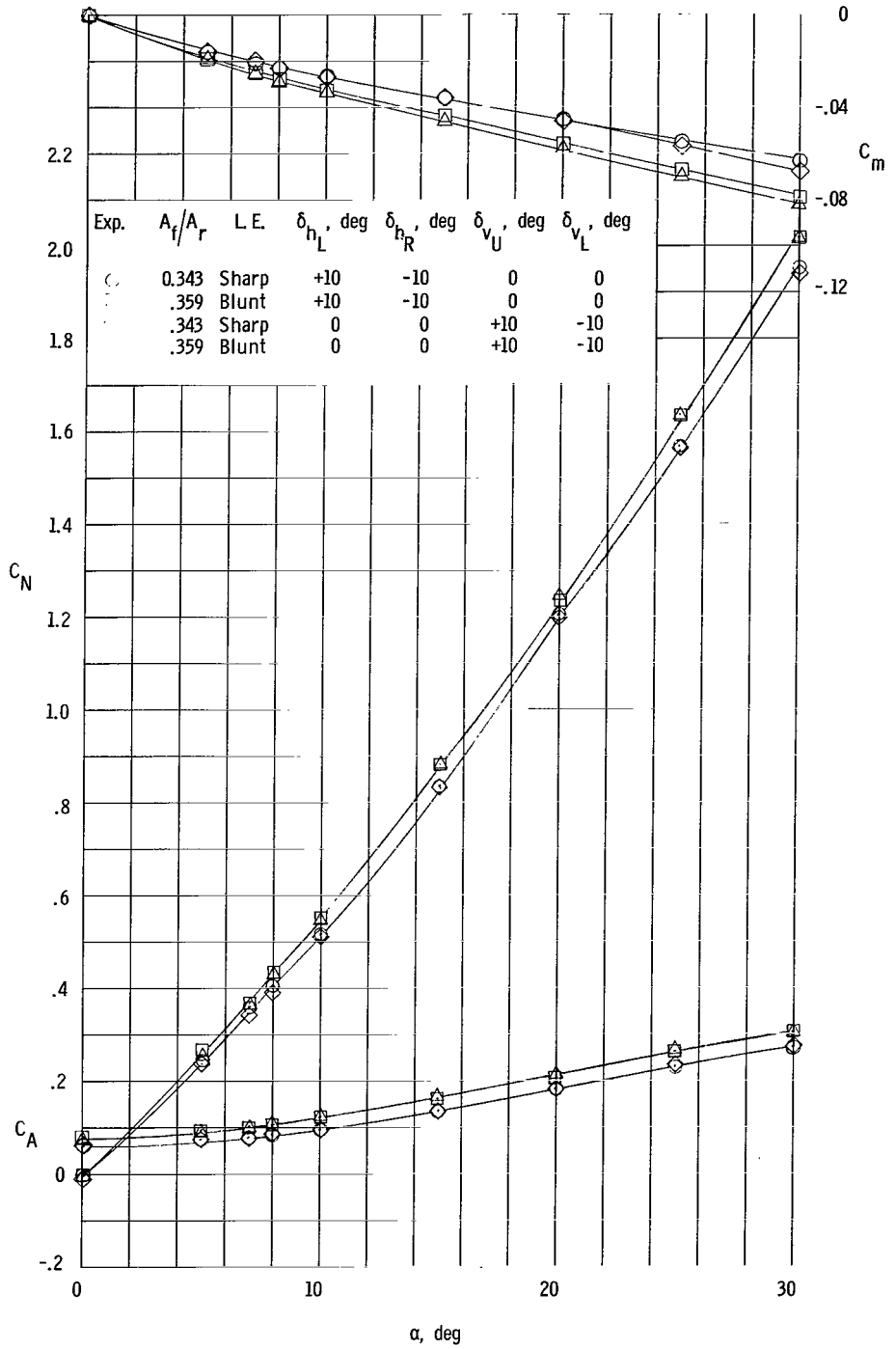

(a) Pitching-moment, normal-force, and axial-force coefficients.

Figure 31.- Longitudinal, lateral, and directional characteristics of sharp 5^0 cone having roll control and sharp and blunt L.E. controls.

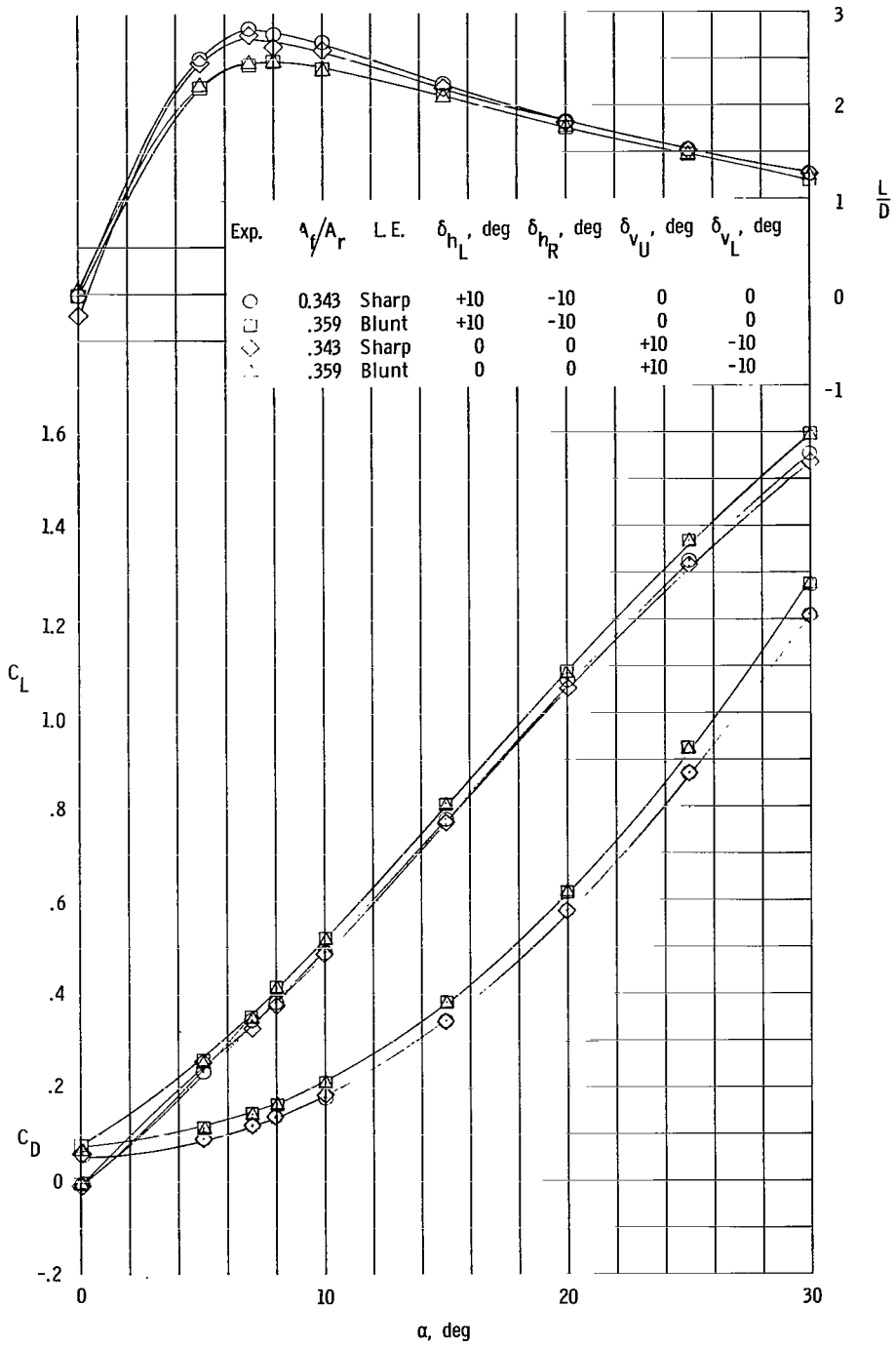

(b) Lift and drag coefficients and lift-drag ratio.

Figure 31.- Continued.

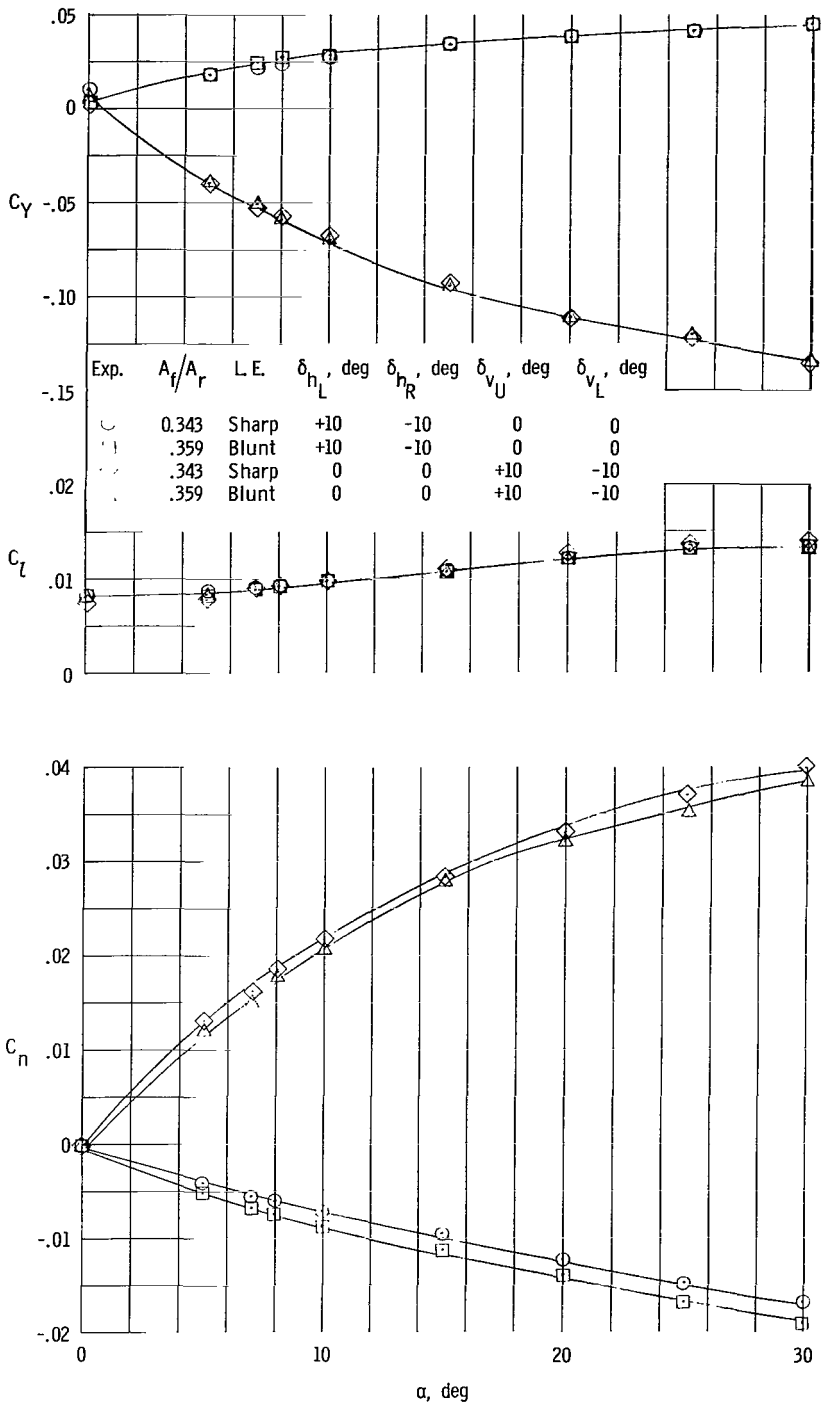

(c) Side-force, rolling-moment, and yawing-moment coefficients.

Figure 31.- Concluded.

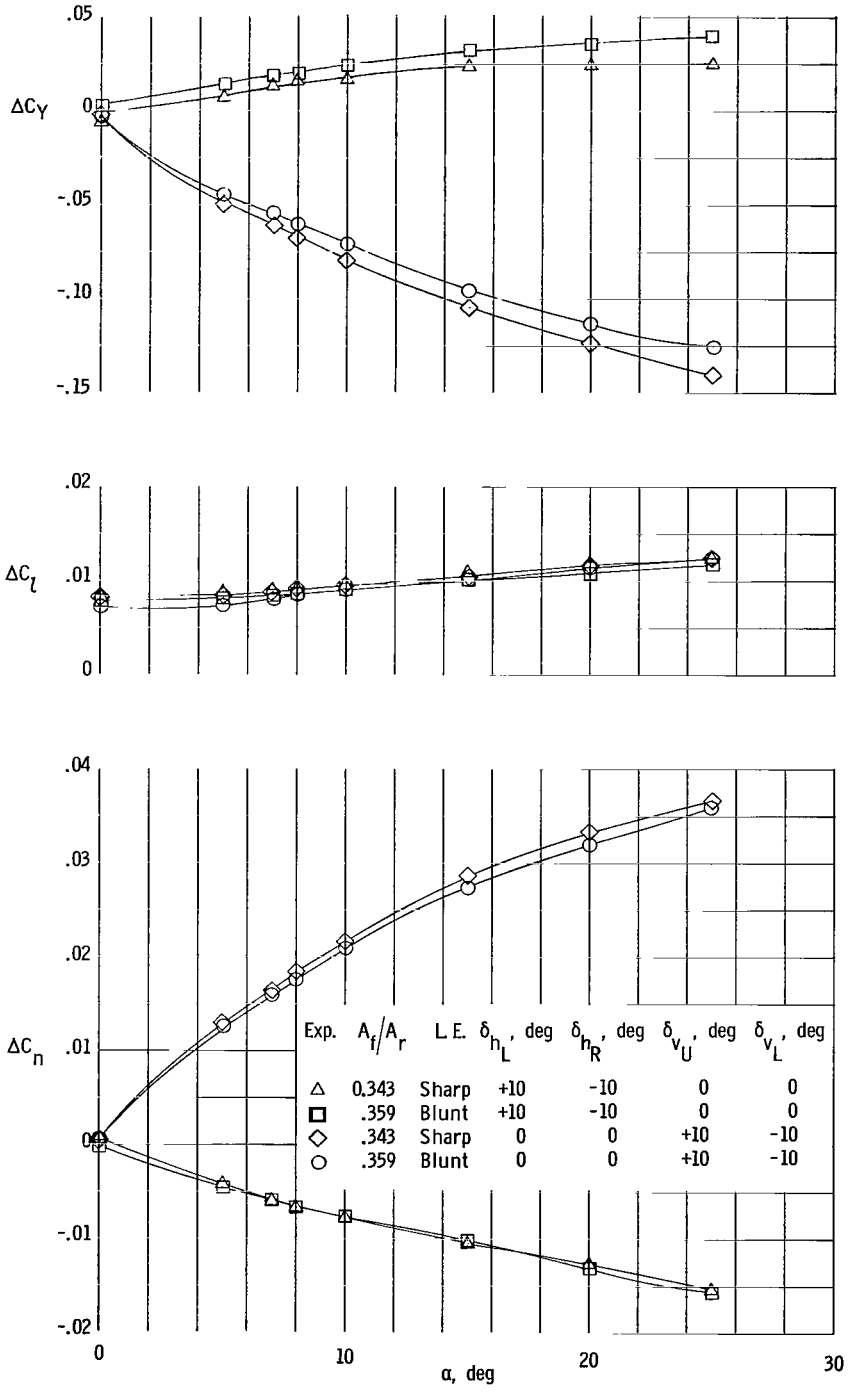

Figure 32.- Incremental lateral-directional characteristics of sharp 5° cone having roll control and sharp and blunt L.E. controls.

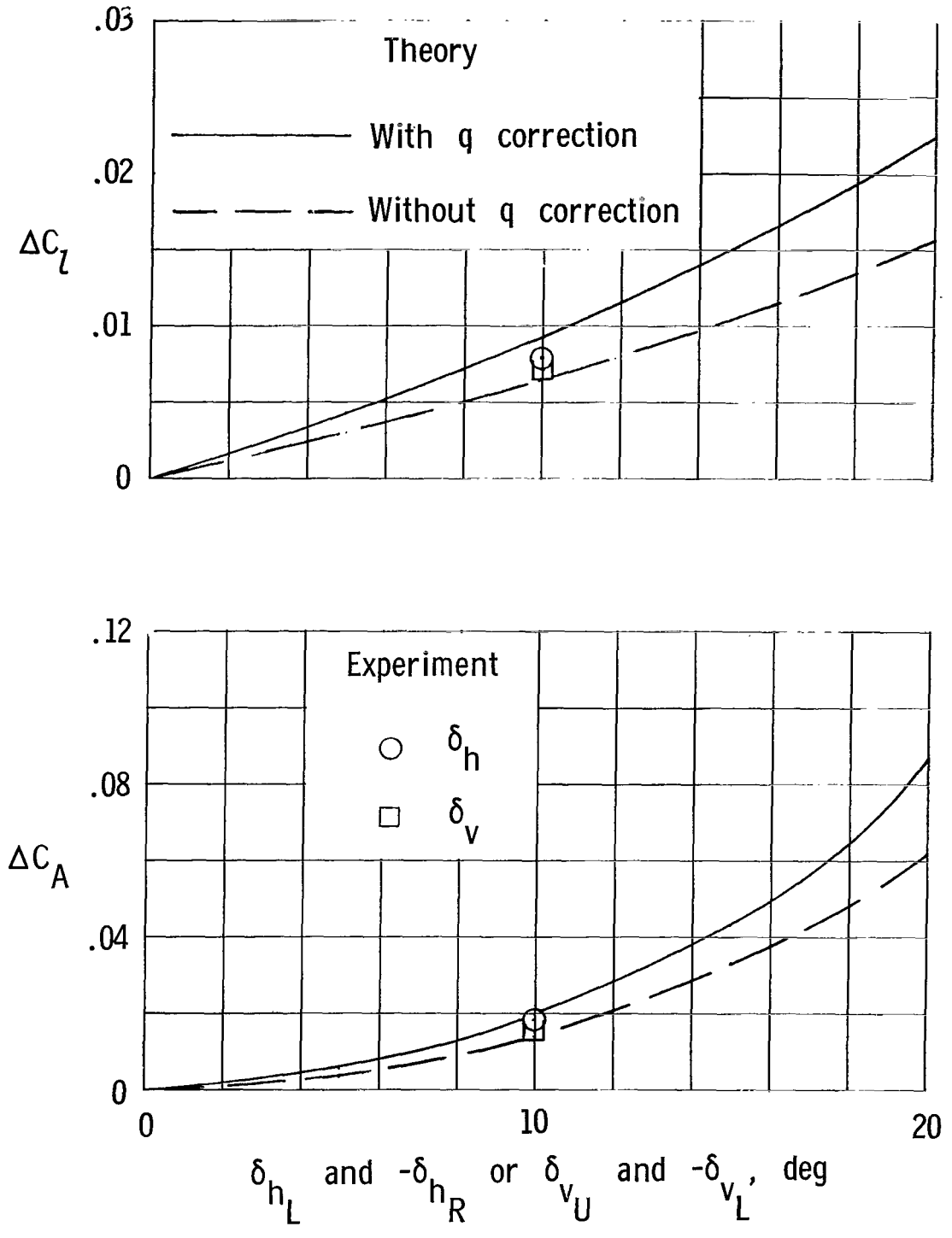

Figure 33.- Comparison of experimental and theoretical incremental roll control characteristics. $\alpha = 0^0$; $A_f/A_r = 0.343$; $d/D = 0$.

"The aeronautical and space activities of the United States shall be conducted so as to contribute . . . to the expansion of human knowledge of phenomena in the atmosphere and space. The Administration shall provide for the widest practicable and appropriate dissemination of information concerning its activities and the results thereof."

—NATIONAL AERONAUTICS AND SPACE ACT OF 1958

NASA SCIENTIFIC AND TECHNICAL PUBLICATIONS

TECHNICAL REPORTS: Scientific and technical information considered important, complete, and a lasting contribution to existing knowledge.

TECHNICAL NOTES: Information less broad in scope but nevertheless of importance as a contribution to existing knowledge.

TECHNICAL MEMORANDUMS: Information receiving limited distribution because of preliminary data, security classification, or other reasons.

CONTRACTOR REPORTS: Technical information generated in connection with a NASA contract or grant and released under NASA auspices.

TECHNICAL TRANSLATIONS: Information published in a foreign language considered to merit NASA distribution in English.

TECHNICAL REPRINTS: Information derived from NASA activities and initially published in the form of journal articles.

SPECIAL PUBLICATIONS: Information derived from or of value to NASA activities but not necessarily reporting the results of individual NASA-programmed scientific efforts. Publications include conference proceedings, monographs, data compilations, handbooks, sourcebooks, and special bibliographies.

Details on the availability of these publications may be obtained from:

SCIENTIFIC AND TECHNICAL INFORMATION DIVISION

NATIONAL AERONAUTICS AND SPACE ADMINISTRATION

Washington, D.C. 20546